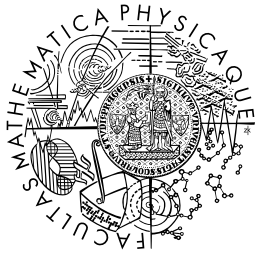

FACULTY
OF MATHEMATICS
AND PHYSICS
Charles University

DOCTORAL THESIS

Morteza Kerachian

Selected problems in relativistic cosmology

Institute of Theoretical Physics

Supervisor of the doctoral thesis: Prof. RNDr. Jiří Bičák, DrSc., dr. h. c.
Study programme: Physics
Study branch: Theoretical Physics, Astronomy and Astrophysics

Prague 2020

I declare that I carried out this doctoral thesis independently, and only with the cited sources, literature and other professional sources. It has not been used to obtain another or the same degree.

I understand that my work relates to the rights and obligations under the Act No. 121/2000 Sb., the Copyright Act, as amended, in particular the fact that the Charles University has the right to conclude a license agreement on the use of this work as a school work pursuant to Section 60 subsection 1 of the Copyright Act.

In ..... date ....

Author's signature

Foremost, I would like to thank to my supervisor Prof. RNDr. Jiří Bičák, DrSc., dr. h. c. for his guidance, supports and many useful advices throughout my studies.

Next, I would like to gratefully acknowledge Dr. Georgios Lukes-Gerakopoulos and Dr. Giovanni Acquaviva for their immense help, support, patients, guidance, and their collaboration during my research.

I would like to thank RNDr. Otakar Svítek, Ph.D. and Dr. Tayebeh Tahamtan for their help and useful advices.

Last but not least, I would like to thank my wife, my parents, and my brother for their uninterrupted help.

Title: Selected problems in relativistic cosmology

Author: Morteza Kerachian

Department: Institute of Theoretical Physics

Supervisor: Prof. RNDr. Jiří Bičák, DrSc., dr. h. c., Institute of Theoretical Physics

Abstract: In this work, we studied three selected problems in FRW spacetime. In the first part, we analysed the motion of a test particle in the homogeneous and isotropic universe. We presented a framework in which one can derive the uniformly accelerated trajectory and geodesic motion if a scale factor for a given spacetime is provided as a function of coordinate time. By applying the confomal time transformation, we were able to convert second order differential equations of motion in FRW spacetime to first order differential equations. From this, we managed to obtain a formalism to derive the uniformly accelerated trajectory of a test particle in spatially curved FRW spacetime. The second part of this work is devoted to dynamical cosmology. In particular, we analyse the cases of barotropic fluids and non-minimally coupled scalar field in spatially curved FRW spacetime. First, we set up the dynamical systems for an unspecified EoS of a barotropic fluid case and an unspecified positive potential for a non-minimal coupled scalar field case. For both of these systems, we determined well-defined dynamical variables valid for all curvatures. In the framework of these general setups we discovered several characteristic features of the systems, such as invariant subsets, symmetries, critical points and their physical interpretations. Finally, in the second part of both of these works, we provided some examples to illustrate how these general setups can be used.

Keywords: Gravitation, Cosmology, Barotropic fluid, Non-minimal coupling; Dynamical systems.

Contents

Introduction

The aim of this thesis is to study selected problems in the isotropic and homogeneous universe. On one hand, we studied the dynamics of a test particle moving in an expanding universe; namely, we presented a novel formalism to obtain the trajectory of a moving particle that has either uniform acceleration or uniform velocity. On the other hand, we analysed the dynamics of barotropic fluid and non-minimally coupled scalar field in spatially curved FRW spacetime.

The materials given in this work can be divided into two parts; the introductory part and the part based on my research. The introductory part is split into three chapters, i.e. Chapters 1, 3, and 4; and the Chapters 2, 5, and 6 are based on the papers Kerachian [2020], Kerachian et al. [2020], and Kerachian et al. [2019] respectively.

This work is organized as follows. Chapter 1 provides a brief introduction to modern cosmology by providing notions, equations, and definitions in this field. In Chapter 2, we study the motion of a test particle uniformly accelerated in an expanding universe. Chapter 3 provides the necessary background regarding the theory of dynamical systems. We present the basic definitions and theorem in this context. In Chapter 4 we give instructions on how dynamical system analysis should be applied on a cosmological model along with an explicit example. Chapter 5 analyses the dynamics of classes of barotropic fluids, while Chapter 6 covers dynamics of classes of non-minimally coupled scalar field are discussed. This work ends with concluding remarks.

0.1 Conventions and Formulas

In this thesis, we define some of general conventions and formulas that we adopt throughout this work. The metric tensor signature is assumed to be $(-,+,+,+)$. We work in natural units where the speed of light c is set to one. We considered coupling constants $\kappa = 8\,\pi\,G/c^4 = 1$. Throughout this work, the Greek indices μ, ν, $\sigma, ...$ run from 0 to 3 unless stated otherwise. Boldfaced quantities refer to vectors in a general $\mathbb{R}^n$ space.

In this work, some formulas without explicit definition are given. These formulas are:

- The Christoffel symbol Γ is

$$\Gamma^{\sigma}_{\mu\nu} = \frac{1}{2}\, g^{\sigma\delta}\left(g_{\nu\delta,\mu} + g_{\mu\delta,\nu} - g_{\mu\nu,\delta}\right), \tag{1}$$

  where $g_{\mu\nu}$ is the metric tensor.

- The Ricci tensor $R_{\mu\nu}$ is

$$R_{\mu\nu} = \Gamma^{\sigma}_{\mu\nu,\sigma} - \Gamma^{\sigma}_{\sigma\nu,\mu} + \Gamma^{\sigma}_{\mu\nu}\,\Gamma^{\delta}_{\delta\sigma} - \Gamma^{\sigma}_{\delta\mu}\,\Gamma^{\delta}_{\sigma\mu}. \tag{2}$$

- The Ricci scalar is

$$R = g^{\mu\nu}\,R_{\mu\nu}. \tag{3}$$

1. An introduction to cosmology

Cosmology is the branch of physics that seeks to understand the origin, the evolution, the dynamics, the structure formation of the universe along with its ultimate fate. Cosmology as a field of science was established from the Copernican principle and was followed by Newtonian laws. Thanks to Albert Einstein's theory of general relativity, the modern cosmology have flourished. This field, then, was improved by major observation discoveries in the 1920s: Edwin Hubble uncovered that our universe is expanding. Subsequently, all these efforts led to speculations regarding the origin of the universe and presented the big bang theory as a leading cosmological paradigm. In 1990s observations from Type Ia supernovae concluded that the expansion of our universe is accelerating. This finding implies that there should be a hidden energy density in the universe that expresses itself as some kind of negative pressure, which is known as the dark energy.

In this chapter, we assume that readers are sufficiently knowledgeable about the basics of general relativity. Moreover, the chapter derives from the following well known text books such as Griffiths and Podolský [2009], Weinberg [2008], and Faraoni [2004] to describe elements of current cosmological trend.

The layout of this chapter is as follows. In Sec. 1.1 we will introduce cosmological principles and the basic material needed in studying modern cosmology. In Sec. 1.2 the Einstein universe will be introduced as a model describing static universe. In order to visualize the known cosmological models, in Sec. 1.3,the conformal transformation will be applied. The big bang theory and the dark side of the universe, i.e. dark matter and dark energy, will be discussed in Sec. 1.4. In the rest of this chapter, we will study possible candidates to solve the accelerated expansion of the universe: ΛCDM model, quintessence, and non-minimal coupling scalar field in Secs. 1.5, 1.6, and 1.7 respectively.

1.1 Introduction to FRW cosmology

On a sufficiently large scales the universe appears to be homogeneous and isotropic. Namely, the space is invariant under spatial translations and rotations. This means that, there is not any preferred direction or privileged point in three dimensional space of the universe. This assumption, which implies that the universe is highly symmetric, is in a good agreement with astronomical observations and it is represented by the Friedmann-Lemaître-Robertson-Walker (FLRW) paradigm.

Basically, the condition that indicates the cosmological principle, namely the isotropy and spatial homogeneity, is that the spacetime has a six-parameter group of isometries. This group of isometries acts transitively on spacelike 3-spaces. From the geometrical theorems, we know that a three-dimensional space has 6 isometries, at the most. Moreover, the curvature of these maximally symmetric spaces is constant. Therefore, the isotropic and spatially homogeneous spacetime has a foliation by a one-parameter family of 3-dimensional hypersurfaces Σ having constant spatial curvature. It can be proven that there exist only three types of such spaces, namely a 3-dimensional flat space, a 3-sphere, and a hyperbolic 3-space. Moreover, each of these hypersufaces Σ are labelled by t =Const., where

t is the coordinate time.

Therefore, in this paradigm, a four dimensional maximally spatially symmetric manifold, which is known as a Friedmann-Robertson-Walker (FRW) metric (or FLRW metric by including Lemaître), in pseudo-spherical coordinates reads

$$ds^2 = -dt^2 + a^2(t)\left(\frac{dr^2}{1-kr^2} + r^2 d\theta^2 + r^2 \sin^2(\theta) d\phi^2\right), \tag{1.1}$$

or

$$ds^2 = -dt^2 + a^2(t)\left(d\chi^2 + S_k^2(\chi)(d\theta^2 + \sin^2\theta d\phi^2)\right), \tag{1.2}$$

where

$$S_k(\chi) = \begin{cases} \sin\chi, & k=+1, \quad \text{closed}, \\ \chi, & k=0, \quad \text{flat}, \\ \sinh\chi, & k=-1, \quad \text{open}, \end{cases}$$

expresses the space curvature and $a(t)$ is the scale factor which describes the expansion of the universe. Even if these three metrics seem to be similar, they represent different types of geometries. The range of χ varies for different curvatures, χ lies in the range $\chi \in [0, \infty)$ for $k = 0, -1$ and $\chi \in [0, \pi]$ for $k = 1$; while the ranges of the coordinate time $t \in [0, \infty)$ and angles $\theta \in [0, \pi]$ and $\phi \in [0, 2\pi)$ are selected independently of the curvature.

To determine the unknown scale factor function $a(t)$ and as a consequence the evolution of the FRW space-time we need to apply the Einstein field equations (EFE). We already know from general relativity that any spacetime is defined by a metric $g_{\mu\nu}$ and the relation between the metric and matter distribution in spacetime is given by the Einstein equation, i.e.

$$G_{\mu\nu} = R_{\mu\nu} - \frac{1}{2} R g_{\mu\nu} = T_{\mu\nu}, \tag{1.3}$$

where $R_{\mu\nu}$ is Ricci tensor, R is Ricci scalar, and $T_{\mu\nu}$ is stress-energy tensor.

The next step is to determine the stress-energy tensor. From the assumption of homogeneity and isotropy, it can be shown that the matter inside the universe is in the form of perfect fluid for which the stress-energy momentum takes the form

$$T_{\mu\nu} = (\epsilon + P) u_\mu u_\nu + P g_{\mu\nu}. \tag{1.4}$$

Here the vector u^μ is the four-velocity of the fluid; ϵ is the energy density of matter and P is the isotropic pressure. We assume that both ϵ and P can be only the functions of time. For such a fluid, the energy conditions are

- The weak energy condition (WEC): For any timelike vectors t^μ, the condition
$$T_{\mu\nu}\, t^\mu\, t^\nu \geq 0, \tag{1.5}$$
should be satisfied. For the fluid (1.4) this condition reads
$$\epsilon \geq 0, \qquad \text{and} \qquad \epsilon + P \geq 0. \tag{1.6}$$

- The dominant energy condition (DEC): For any timelike vector t^μ, if the WEC is satisfied then $T^{\mu\nu}\, t_\mu$ is a null or timelike vector. Thus, for the (3.31) we get
$$\epsilon \geq \mid P \mid . \tag{1.7}$$

- The strong energy condition (SEC): For any timelike vector t^μ the condition

$$T_{\mu\nu}\, t^\mu\, t^\nu \geq -\frac{1}{2}T, \tag{1.8}$$

should be satisfied. This condition for the energy-momentum tensor (1.4) will be

$$\epsilon + P \geq 0, \qquad \text{and} \qquad \epsilon + 3\,P \geq 0. \tag{1.9}$$

- The null energy condition (NEC): For any null vector l^μ the condition

$$T_{\mu\nu}\, l^\mu\, l^\nu \geq 0, \tag{1.10}$$

should be satisfied. This means

$$\epsilon + P \geq 0, \tag{1.11}$$

for the energy-momentum tensor (1.4).

- The null dominant energy condition (NDEC): For any null vector l^μ, the NEC should be satisfied and $T^{\mu\nu}l_\mu$, is a null or timelike vector. This condition for the energy-momentum tensor (1.4) will be

$$\epsilon \geq \mid P \mid, \qquad \text{or} \qquad \epsilon = -P. \tag{1.12}$$

The next task is to derive the non-vanishing components of $G_{\mu\nu}$ from the metric (1.2) and equating it with the stress-energy tensor (1.4). Therefore, Einstein's equations (1.3) for the FRW spacetime reduce to

$$3\left(H^2 + \frac{k}{a^2}\right) = \epsilon, \tag{1.13}$$

$$2\dot{H} + 3H^2 + \frac{k}{a^2} = -P. \tag{1.14}$$

Here $H = \dot{a}/a$ is Hubble parameter and Eqs. (1.13) and (1.14) are known as the Friedmann equation and the Raychaudhuri equation respectively. Moreover, from a Bianchi identity one can derive the continuity equation which reads

$$\dot{\epsilon} + 3H(P + \epsilon) = 0. \tag{1.15}$$

The unknown scalar function $a(t)$ can be determined if the barotropic equation of state (EoS), i.e. $P = P(\epsilon)$, is given. Common EoS is a linear one of the form

$$P = w\epsilon, \tag{1.16}$$

where $0 \leq w \leq 1$. This linear EoS includes many special cases. For instance, a pressureless fluid or dust when $w = 0$, radiation when $w = 1/3$. Subsequently, from the linear EoS (1.16) and continuity equation (1.15) the energy density ϵ as a function of a will be

$$\epsilon = \frac{C}{a^{3(w+1)}}, \tag{1.17}$$

where C is a constant. The former equation reads

$$\epsilon \propto \begin{cases} a^{-3}, & \text{for dust-filled universe,} \\ a^{-4}, & \text{for radiation-like fluid.} \end{cases}$$

To derive the scale factor in terms of the coordinate time t, we should substitute Eq. (1.17) into the Friedmann equation (1.13), namely

$$\dot{a}^2 = \frac{C}{3} a^{-(1+3w)} - k, \tag{1.18}$$

then, by integrating the former relation one can get

$$a(\psi) = \left(\frac{C}{3}\sin^2\psi\right)^{1/(1+3w)}, \qquad t(\psi) = \frac{2\int a(\psi)d\psi}{1+3w}, \qquad k = +1, \tag{1.19}$$

$$a(t) = \left(\frac{\sqrt{3C}}{2}\gamma t\right)^{2/(3w+3)}, \qquad k = 0, \tag{1.20}$$

$$a(\psi) = \left(\frac{C}{3}\sinh^2\psi\right)^{1/(1+3w)}, \qquad t(\psi) = \frac{2\int a(\psi)d\psi}{1+3w}, \qquad k = -1, \tag{1.21}$$

where ψ is defined implicitly.

1.1.1 On the trajectories in a spacetime

In this section, we digress for a while to introduce specific trajectories in spacetime with the metric $g_{\mu\nu}$. In other words, we will introduce the necessary conditions for the timelike geodesics and uniformly accelerated trajectories (for more details see e.g. Poisson [2004]).

A curve in a spacetime is called a timelike geodesic if the proper time between two points a and b on the curve is extremum. If a curve γ is described by $x^\mu(\lambda)$ where the parameter λ is chosen arbitrary, then the proper time τ between points a and b is defined

$$\tau(a,b) = \int_a^b L(\frac{dx^\mu}{d\lambda}, x^\mu)\, d\lambda = \int_a^b \sqrt{-g_{\mu\nu}\frac{dx^\mu}{d\lambda}\,\frac{dx^\nu}{d\lambda}}\, d\lambda. \tag{1.22}$$

The extremum proper time is determined from the Euler-Lagrnage equations describing the particle's motions. After some manipulation one can get from Eq. (1.22)

$$\frac{d^2x^\mu}{d\,\lambda^2} + \Gamma^\mu_{\sigma\delta}\frac{dx^\sigma}{d\lambda}\,\frac{dx^\delta}{d\lambda} = \kappa\frac{dx^\mu}{d\lambda}, \tag{1.23}$$

where $\kappa = \frac{1}{L}\frac{dL}{d\lambda}$ and $\Gamma^\mu_{\sigma\delta}$ is the Christoffel symbol. If we pick a specific parameterization, i.e. $d\lambda = d\tau$ or $\lambda = c_1\tau + c_2$, which is called an affine class of parameters on the worldline, then κ vanishes and we get the geodesics equation in the more familiar form

$$\frac{d^2x^\mu}{d\,\tau^2} + \Gamma^\mu_{\sigma\delta}\frac{dx^\sigma}{d\tau}\,\frac{dx^\delta}{d\tau} = 0, \tag{1.24}$$

which is equivalent to $u^\mu_{;\nu}u^\nu = 0$. Here, the four-velocity $u^\mu = \frac{dx^\mu}{d\tau}$ is tangent to the geodesic. One can easily check that along an affinely parameterized timelike geodesic we get $u^\mu u_\mu = -1$. Thus, the motion of a test particle with very small

proper mass which moves in a gravitational field is represented by its worldline; this worldline is necessarily a timelike geodesic. However, if other forces act on the test particle, its worldline deviates form the geodesic one.

On the other hand, a trajectory of a uniformly accelerated test particle is given by (see e.g. Rohrlich [2020])

$$P^{\mu}_{\nu}\dot{a}^{\nu} = \dot{a}^{\mu} - (a^{\sigma}a_{\sigma})\,u^{\mu} = 0. \tag{1.25}$$

Here $P^{\mu}_{\nu} = \delta^{\mu}_{\nu} + u^{\mu}u_{\nu}$ is the projection tensor and the over dot means $u^{\nu}\nabla_{\nu}$, i.e. covariant derivative with respect to τ, and

$$a^{\mu} = u^{\nu}\nabla_{\nu}u^{\mu} = \frac{d^2x^{\mu}}{d\,\tau^2} + \Gamma^{\mu}_{\sigma\delta}\frac{dx^{\sigma}}{d\tau}\,\frac{dx^{\delta}}{d\tau}, \tag{1.26}$$

is the four-acceleration of a test particle. If we multiply Eq. (1.25) by a_{μ}, we get $\dot{a}^{\mu}a_{\mu} = 0$ which guarantees that

$$a_{\mu}a^{\mu} = \text{Constant}. \tag{1.27}$$

In other words, the magnitude of the four-acceleration is constant. Consequently, for a given accelerated trajectory if the condition (1.25) is satisfied the motion of the particle is uniformly accelerated.

In Minkowski spacetime, it is easy to check that the uniformly accelerated trajectory is a hyperbola (see e.g. Rindler [2012]). Although the conditions (1.24) and (1.25) seem to be simple, deriving the geodesic and the accelerated trajectory for the FRW spacetime is not an easy task. Kerachian [2020] derived a general formalism to determine the geodesic and accelerated trajectory of a test particle in the FRW spacetime.

1.2 The static universe

Historically, when Einstein presented his theory, it was assumed that we live in a static universe. From Eqs. (1.13) and (1.14) we can derive

$$\ddot{a} = -\frac{1}{6}(\epsilon + 3P)a, \tag{1.28}$$

which implies that in order to have a static universe $\dot{a} = 0$ and $\ddot{a} = 0$ or equivalently $P = -1/3\,\epsilon$, i.e. either pressure is negative or energy density. This statement violates the energy condition $\epsilon \geq P \geq 0$. Therefore, in 1917, Einstein modified his equations (1.3) by adding a constant called the cosmological constant Λ:

$$R_{\mu\nu} - \frac{1}{2}Rg_{\mu\nu} - \Lambda g_{\mu\nu} = T_{\mu\nu}. \tag{1.29}$$

Subsequently, the modifications of the Friedmann equation (1.13) and the Raychaudhuri equation (1.14) become

$$H^2 + \frac{k}{a^2} = \frac{\epsilon}{3} + \frac{\Lambda}{3}, \tag{1.30}$$

$$2\dot{H} + 3H^2 + \frac{k}{a^2} = \Lambda - P. \tag{1.31}$$

It can be derived from the former equations that for a desired static universe, i.e. $a = \tilde{a}$ =Const., the cosmological constant Λ and the spatial curvature k are strictly positive. Consequently, a spacetime representing the static universe is written as

$$ds^2 = -dt^2 + \tilde{a}^2 \left(d\chi^2 + \sin^2 \chi (d\theta^2 + \sin^2 \theta \, d\phi^2) \right). \tag{1.32}$$

This spacetime is known as the Einstein static universe.

Although, this spacetime represents the static universe, it is an unstable spacetime. Moreover, in the late 1920s, it was discovered that the universe is expanding and the use of the additional term in the Einstein field equation subsided. On the other hand, as we will see in Sec. 1.3, the global causal structure of other exact solutions of EFE can be studied simply from the Einstein static universe.

Before we proceed to the next section, here we shall briefly analyze the global structure of the Einstein universe. First, by using the time rescaling $t = \tilde{a}\tilde{\eta}$ and also $\chi = \tilde{\chi}$ the static universe metric takes the form

$$ds^2 = \tilde{a}^2 \left(-d\tilde{\eta}^2 + d\tilde{\chi}^2 + \sin^2 \tilde{\chi} (d\theta^2 + \sin^2 \theta \, d\phi^2) \right). \tag{1.33}$$

Recall that, since the Einstein universe is a specific case of the FRW spacetime with positive spatial curvature, the range of its coordinate are $\tilde{\eta} \in (-\infty, +\infty)$, $\tilde{\chi} \in [0, \pi]$, $\theta \in [0, \pi]$, and $\phi \in [0, 2\pi]$. Therefore, for any point having $\tilde{\eta}$ =Const. the spatially section is 3-sphere.

Therefore, Einstein universe can be visualized in 3-dimensions where $\theta = \pi/2$ as an interior of an infinite cylinder with radius π. Likewise, in 2-dimensions we suppress both $\theta = \pi/2$ and ϕ =Const.; in Fig. 1.1 the 2-dimension Penrose diagram for Einstein universe is plotted.

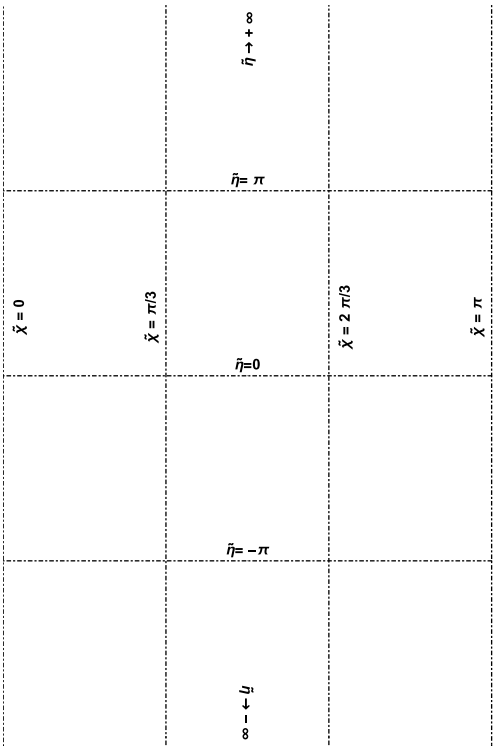

Figure 1.1: Penrose diagram for the Einstein universe where the θ and ϕ coordinates are suppressed.

1.3 Conformal structure

In this section we study the global structure of the FRW spacetime. To investigate this, we use the idea of a conformal transformation. In general, the conformal transformation is considered as a map between two spacetimes, i.e. $\mathcal{M}$ and $\tilde{\mathcal{M}}$ with metrics $g_{\mu\nu}$ and $\tilde{g}_{\mu\nu}$ respectively, that satisfy

$$\tilde{g}_{\mu\nu} = \Omega^2 g_{\mu\nu}. \tag{1.34}$$

Here we consider that $\mathcal{M}$ is a physical spacetime, $\tilde{\mathcal{M}}$ can be an unphysical spacetime with a boundary $\mathcal{I}$ (the boundary $\mathcal{I}$ is associated with the condition $\Omega = 0$.), and Ω is a smooth and strictly positive function. Therefore, the infinity of $\mathcal{M}$ is confined with the finite hypersurface $\mathcal{I}$. In other words, asymptotic properties of $\mathcal{M}$ and fields in $\mathcal{M}$ can be understood from studying $\mathcal{I}$ and the local behaviour of the fields at $\mathcal{I}$ (For more explanations we refer readers to the lecture given by Penrose in DeWitt and DeWitt [1964]).

To construct the conformal transformation for the FRW spacetime, it is enough to introduce the new temporal coordinate as a conformal time η. The relation between the new confomal time η and coordinate time t is

$$\eta = \int \frac{dt}{a(t)}. \tag{1.35}$$

Using this transformation, the transformed Friedmann metric (1.2) becomes

$$ds^2 = a^2(\eta)\left(-d\eta^2 + d\chi^2 + \sin^2(\chi)(d\theta^2 + \sin^2\theta d\phi^2)\right) \quad \text{for} \quad k = 1, \tag{1.36}$$

$$ds^2 = a^2(\eta)\left(-d\eta^2 + d\chi^2 + \chi^2(d\theta^2 + \sin^2\theta d\phi^2)\right) \quad \text{for} \quad k = 0, \tag{1.37}$$

$$ds^2 = a^2(\eta)\left(-d\eta^2 + d\chi^2 + \sinh^2(\chi)(d\theta^2 + \sin^2\theta d\phi^2)\right) \quad \text{for} \quad k = -1, \tag{1.38}$$

where $a(\eta) = a(t(\eta))$ and reads

$$a(\eta) = a_c\left(\sin(\frac{3w+1}{2}\eta)\right)^{\frac{2}{3w+1}} \quad \text{for} \quad k = 1, \tag{1.39}$$

$$a(\eta) = a_c\eta^{\frac{2}{3w+1}} \quad \text{for} \quad k = 0, \tag{1.40}$$

$$a(\eta) = a_c\left(\sinh(\frac{3w+1}{2}\eta)\right)^{\frac{2}{3w+1}} \quad \text{for} \quad k = -1. \tag{1.41}$$

In order to visualize the conformal spacetime, it is appropriate to plot Penrose diagram in which a given FRW spacetime relates to the part of the Einstein static universe. Namely, by applying the proper transformation from FRW spacetime to Einstein static universe (1.33), one should arrive at

$$ds^2_{Eins} = \Omega^2 ds_{FRW}. \tag{1.42}$$

It is easy to show that for the FRW spacetime with $k = +1$, by considering $\tilde{\eta} = \eta$ and $\tilde{\chi} = \chi$ the conformal factor becomes

$$\Omega = \frac{\tilde{a}}{a(\tilde{\eta})}, \tag{1.43}$$

where $a(\tilde{\eta})$ is given in (1.39). From the conformal factor (1.43) and the scale factor (1.39), it is clear that the infinity $\mathcal{I}$ which corresponds to $\Omega = 0$ or equivalently $a(\tilde{\eta}) = \infty$ does not exists. However, there are two singular points corresponding to $\Omega = \infty$, namely when $a(\tilde{\eta}) = 0$. These two singularities are called the initial singularity or the big bang when $\tilde{\eta} = 0$ and the final singularity when $\tilde{\eta} = \frac{2\pi}{3w+1}$. Therefore, any FRW spacetime with $k = 1$ is conformal to the part of the Einstein static universe (see Fig. 1.1) which is bounded between these two sections in which the universe expands from the initial singularity and reaches its maximum size a_c, this is followed by the re-collapses back to the final singularity.

In Fig. 1.2a the Penrose diagram for the radiation dominated FRW universe with $k = 1$ is plotted. As this figure shows, the initial singularity is located at $\tilde{\eta} = 0$ and the final singularity occurs at $\tilde{\eta} = \pi$ which are illustrated by the dotted dashed lines. The vertical dotted lines, on the other hand, show the η =Const. and the horizontal dotted lines represent $\tilde{\chi}$ =Const.. Moreover, the dashed line is the location of the maximum size $a = a_c$.

For the spatially flat FRW models, one has to apply the conformal transformations

$$\begin{aligned} \eta &= \frac{2\sin\tilde{\eta}}{\cos\tilde{\eta} + \cos\tilde{\chi}}, \\ \chi &= \frac{2\sin\tilde{\chi}}{\cos\tilde{\eta} + \cos\tilde{\chi}}, \end{aligned} \tag{1.44}$$

to get the conformal factor

$$\Omega = \frac{\tilde{a}}{a(\eta(\tilde{\eta},\tilde{\chi}))} \cos\left(\frac{\tilde{\eta}+\tilde{\chi}}{2}\right) \cos\left(\frac{\tilde{\eta}-\tilde{\chi}}{2}\right), \tag{1.45}$$

with $a(\eta(\tilde{\eta},\tilde{\chi}))$ given in (1.40). Therefore, we can see that the conformal infinity $\mathcal{I}$ occurs when $\tilde{\eta} + \tilde{\chi} = \pm\pi$, $\tilde{\eta} - \tilde{\chi} = \pm\pi$, and $a(\eta(\tilde{\eta},\tilde{\chi})) = \infty$. Moreover, the singularity takes place when $a(\eta(\tilde{\eta},\tilde{\chi})) = 0$ or equivalently $\tilde{\eta} = 0$. Since the scale factor 1.40 is a monotonic function of $\tilde{\eta}$, the Penrose diagram shape is independent of the choice of the fluid.

In fig. 1.2b the Penrose diagram for the spatially flat FRW spacetime is plotted. This spacetime is the part of the Einstein static universe which is confined between the initial singularity $\tilde{\eta} = 0$ and the $\tilde{\eta} + \tilde{\chi} = \pi$.

For the FRW spacetime with negative spatial curvature $k = -1$ by using the following conformal transformations

$$\begin{aligned} \eta &= \operatorname{arctanh}\left(\frac{\sin\tilde{\eta}}{\cos\tilde{\chi}}\right), \\ \chi &= \operatorname{arctanh}\left(\frac{\sin\tilde{\chi}}{\cos\tilde{\eta}}\right), \end{aligned} \tag{1.46}$$

we can derive the conformal factor

$$\Omega = \frac{\tilde{a}}{a(\eta(\tilde{\eta},\tilde{\chi}))} \sqrt{\sin(\tilde{\eta}+\tilde{\chi}-\frac{\pi}{2})\sin(\tilde{\eta}-\tilde{\chi}-\frac{\pi}{2})}, \tag{1.47}$$

where $a(\eta(\tilde{\eta},\tilde{\chi}))$ is given in (1.41). For this spacetime, the conformal infinity, i.e. $\Omega = 0$, occurs at $\tilde{\eta} + \tilde{\chi} = \pm\pi/2$ and $\tilde{\eta} - \tilde{\chi} = \pm\pi/2$ together with $a(\eta(\tilde{\eta},\tilde{\chi})) = \infty$.

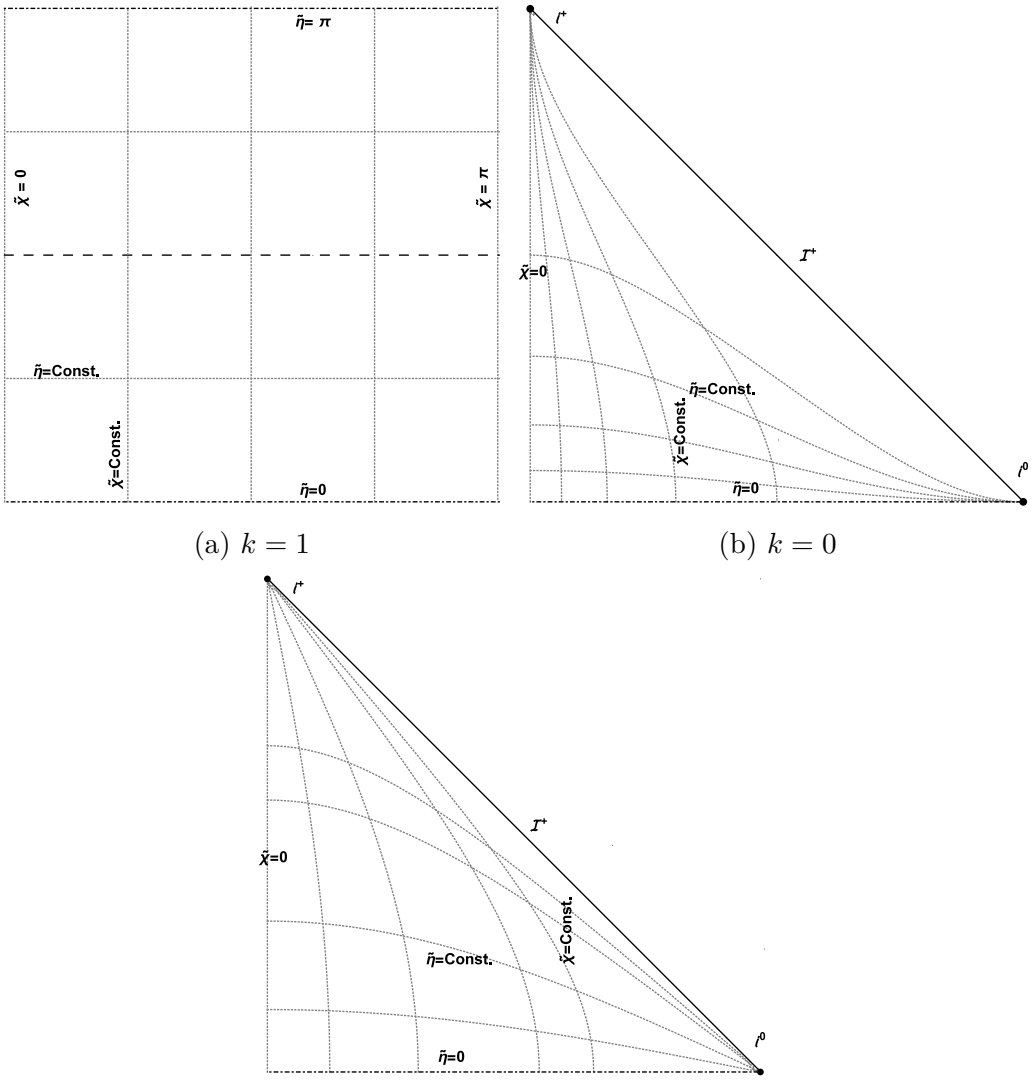

(a) $k = 1$ (b) $k = 0$

(c) $k = -1$

Figure 1.2: Penrose diagrams for the FRW spacetime when (a) $k = 1$, (b) $k = 0$, and (c) $k = -1$. The Penrose diagram for the positive spatial curvature corresponds to the FRW spacetime with radiation. However, the Penrose diagrams for $k = 0$ and $k = -1$ are the same for all the EoS (1.16) with $1 \leq w \leq 2$. In these figures, the dotted dashed lines show the singularities, dotted lines correspond to constant $\tilde{\eta}$ and $\tilde{\chi}$. Moreover, the $\mathcal{I}^+$ is called the future null infinity, i^+ is the future timelike infinity, and i^0 is the spacelike infinity.

There is also an initial singularity when $\tilde{\eta} = 0$. Similar to the flat cases, the shape of the Penrose diagram for the FRW spacetime with $k = -1$ is independent of the fluid choice.

Fig. 1.2c illustrates the Penrose diagram for the negative spatially curved FRW spacetime. This spacetime is the part of the Einstein static spacetime bounded by initial singularity $\tilde{\eta} = 0$ and the conformal infinity located at $\tilde{\eta} + \tilde{\chi} = \pm\pi/2$.

1.4 The dark side of the universe

In Sec. 1.1 the FRW spacetime was presented. By solving the EFE for different types of $T^{\mu\nu}$, one can deduce different cases of evolution for the scale factor a, i.e. one can deduce whether a is a constant function of time t or decreasing, or increasing. However, we should find out which of these forms describes the real universe. This information can be extracted from the observational measurements.

We know that the universe is expanding, which led us to one of the most important concepts in the modern cosmology, namely the big bang. We already know that the scale factor is positive, i.e. $a > 0$, and we also know $\dot{a} > 0$ from the expansion of the universe. Consequently, if t_0 is considered as the present time, we can deduce that there exists a finite time $t_\star$ in the past, where $t_\star < t_0$, that satisfies $a(t_\star) = 0$. The time $t_\star$ is called the big bang.

Moreover, Eq. 1.28 implies that for the baryonic matter, for which holds that $\epsilon + 3P > 0$, the rate of the expansion should slow down since $\ddot{a} < 0$, i.e. due to the mutual gravitational effect. However, observations of Type Ia supernovae from two different surveys, the Supernova Cosmology Project Perlmutter et al. [1999] and the High-z Supernova Search Team Riess et al. [1998], discovered that the rate of the expansion is accelerating. Consequently, from Eq. (1.28) the accelerated expansion ($\ddot{a} > 0$) requires an energy density satisfying $\epsilon + 3P < 0$. Since we do not know the nature of such energy density, this unknown energy density is called dark energy.

Apart from dark energy, there exists another unknown matter in the universe which is called dark matter. During $1960-1980$ Vera Rubin and her team studied the rotation curves of spiral galaxies. They observed that the velocity of the stars in the spiral galaxies, independent of their position from the core of the galaxies, remains almost constant. These findings are inconsistent with the gravitation of the visible mass of the galaxies, i.e. the visible is not strong enough to hold the farther fast-moving stars from the center of a galaxy. Therefore, they concluded that there should be dark matter in the galaxies and clusters in order to hold them stable.

According to the data gathered by Planck Collaboration et al. [2020], the total energy density of the universe consist of: $\sim 68.5\%$ dark energy, $\sim 26.5\%$ cold dark matter[1], and $\sim 5\%$ baryonic matter.

There are three main approaches in order to understand the physics behind the dark energy: the constant vacuum energy or cosmological constant, non-constant vacuum energy or scalar fields, and modified gravities. In the rest of this chapter, we will succinctly introduce the ΛCDM model and the scalar fields.

[1]Dark matter particles are called cold if their velocities are much lower that speed of light, i.e. their velocities are non-relativistic.

1.5 ΛCDM model

In this section we will introduce the standard cosmological model. Namely, we will discuss the ΛCDM model. Λ is the cosmological constant and CDM stands for the cold dark matter, as a model that fits well with the observations such as the survey in Planck Collaboration et al. [2020].

Based on the observations, dark energy's EoS has $w_{de} = -1.03 \pm 0.03$. From Eqs. (1.30) and (1.31) together with (1.16) one can deduce that the cosmological constant acts like an exotic fluid with $\epsilon_\Lambda = \Lambda$, $P_\Lambda = -\Lambda$, and also $w_\Lambda = -1$. We have seen in Sec. 1.2 that adding the cosmological constant Λ, led us to the non-physical Einstein Static universe; however, it may be an appropriate cosmological model to describe the late time inflation.

From the view point of particle physics, the cosmological constant can be interpreted as a vacuum energy, namely the states of the lowest energy. Lets start with the action of a scalar field (see e.g. Carroll [2001])

$$S = -\int d^4x\sqrt{-g}\,[\frac{1}{2}g^{\mu\nu}\partial_\mu\psi\,\partial_\nu\psi + V(\psi)]. \tag{1.48}$$

It's energy momentum tensor is

$$T_{\mu\nu} = \frac{1}{2}\partial_\mu\psi\,\partial_\nu\psi - \frac{1}{2}(g^{\rho\sigma}\partial_\rho\psi\,\partial_\sigma\psi) - V(\psi)g_{\mu\nu}. \tag{1.49}$$

Classically, the lowest energy density is defined when kinetic energy does not contribute, in other words when $\partial_\mu\psi = 0$. This condition implies $T_{\mu\nu} = -V(\psi_0)g_{\mu\nu}$ where $V(\psi_0)$ is the minimum value of the $V(\psi)$ or

$$T_{\mu\nu} = -\epsilon_{vac}\,g_{\mu\nu}, \tag{1.50}$$

where $\epsilon_{vac} = V(\psi_0)$. From quantum mechanics we already know that the lowest energy state has an non-zero energy $E_0 = 1/2\,\hbar\,\omega$ and consequently $V(\psi_0) > 0$. Moreover, by considering the vacuum energy as a perfect fluid, the energy momentum tensor (1.4) implies that

$$P_{vac} = -\epsilon_{vac}, \tag{1.51}$$

and consequently

$$\epsilon_{vac} = \epsilon_\Lambda = \Lambda. \tag{1.52}$$

The former relation implies that both vacuum energy and cosmological constant Λ have the same impact on the EFE. Additionally, cosmological observations confirm that the value of the cosmological constant is of the order

$$\Lambda \simeq 10^{-52}m^{-2}, \tag{1.53}$$

however, there is a big discrepancy between the theoretical values of the vacuum energy and the one which is observed; this problem will be discussed in detail in Sec. 1.5.2.

So far, we have seen that the EoS of the dark energy has $w_{de} \approx -1$ and identified the origin of cosmological constant as the vacuum energy. We shall now present the fundamental assumptions of the cosmological constituents in the ΛCDM model:

- Dark energy which is the main constituents of the universe that acts like the vacuum energy.
- Cold dark matter is the non-relativistic pressureless matter that does not interact with the normal matter except gravitationally.
- The spatial curvature of the universe is small and negligible.

Under these assumptions the Friedmann equation (1.30) and the Raychaudhuri equation (1.31) for the ΛCDM model become

$$H^2 = \frac{\epsilon}{3} + \frac{\Lambda}{3}, \tag{1.54}$$

$$2\dot{H} + 3H^2 = \Lambda - P. \tag{1.55}$$

1.5.1 A brief introduction to de Sitter universe

In the ΛCDM model, if we consider that the universe is dominated mostly by dark energy, in other words when the contributions of matter (both dark matter and baryonic matter) is neglected ($\epsilon = 0$ and $P = 0$), we obtain the de Sitter universe (see de Sitter [1917]). This solution is a vacuum solution from the modified EFE (1.29). Actually, we can obtain only three vacuum solutions from (1.29). If we contract Eq. (1.29) with $T_{\mu\nu} = 0$, we get $R = 4\,\Lambda$. Thus, the spacetimes with $\Lambda = 0$, $\Lambda > 0$, and $\Lambda < 0$ are the Minkowski spacetime, de Sitter spacetime, and anti-de Sitter spacetime respectively.

From the Eqs.(1.54) and (1.55) with $\epsilon = P = 0$ and $\Lambda > 0$ one can obtain

$$a(t) \propto e^{H\,t}, \qquad \text{with} \qquad H = \sqrt{\frac{\Lambda}{3}}, \tag{1.56}$$

and the de Sitter metric will be

$$ds^2 = -dt^2 + \left(a_0\, e^{\sqrt{\Lambda/3}\,t}\right)^2 \left(d\chi^2 + \chi^2\left(d\theta^2 + \sin^2\theta d\phi^2\right)\right). \tag{1.57}$$

Since, in the de Sitter universe the scale factor grows exponentially, the $\ddot{a} = H^2 a$ is always positive which means that the de Sitter universe expands for all its history.

1.5.2 Cosmological constant problems

In the previous section we presented that the cosmological constant can be considered as the vacuum energy and based on the observations it has the value of the order

$$\Lambda \simeq 10^{-52} m^{-2} \simeq (10^{-12}\, GeV)^4. \tag{1.58}$$

On the other hand, it is possible to calculate the vacuum energy from quantum theory. As we will see in the following, there is a big difference between the theoretical values of the vacuum energy and the one which is observed. This conundrum is known as the cosmological constant problem (see e.g. Carroll [2001] and Bahamonde et al. [2018]).

Cosmological constant can consist of different contributions, such as the electroweak (EW) phase, quantum chromodynamics (QCD), and fluctuations at the Planck scale. The EW phase transition provides the value of the vacuum energy density of the order

$$\epsilon_{vac}^{EW} \simeq (200\, GeV)^4, \tag{1.59}$$

whereas the QCD phase transitions calculates the value

$$\epsilon_{vac}^{QCD} \simeq (0.3\, GeV)^4. \tag{1.60}$$

Moreover for the vacuum energy at the Planck scale the fluctuations has the value

$$\epsilon_{vac}^{Pl} \simeq (10^{-12}\, GeV)^4. \tag{1.61}$$

The observational value of the cosmological constant (1.58) is much smaller than the theoretical ones (1.59), (1.60), and (1.61); this discrepancy is not ameliorated even by introducing a bare cosmological constant ϵ_B and summing up all the known theoretical vacuum energy densities to achieve

$$\Lambda = \epsilon_B + \epsilon_{vac}^{EW} + \epsilon_{vac}^{QCD} + \epsilon_{vac}^{Pl} + ... \tag{1.62}$$

From quantum field theory there is not any theoretical way to determine such a bare cosmological constant to cancel out all the other vacuum energy densities in the right hand of (1.62) and provide the observed value for the left hand side; this constitutes another problem for cosmology which is called a problem of fine tuning.

In fact, these conundrums are not the only unsolved question in the ΛCDM model. Apart from how one could theoretically determine such a small value for the cosmological constant, we know that this extremely small value of the cosmological constant led the universe to have a transition from the radiation epoch to the dark matter domination era. If the cosmological constant had just slightly bigger value, the universe would have directly transited from radiation to dark energy epoch without forming the galaxies, clusters, or other cosmological structures. Additionally, due to this value of the cosmological constant, the transition from dark matter to dark energy have been taking place at current time; this is another conundrum and it is called the cosmic coincidence problem.

So far, we have seen that the ΛCDM model is the simplest candidate to explain the dark energy and fits well with the observational data; however, it suffers from some unsolved conundrums. In the following we will present alternative models in order to alleviate these problems.

1.6 Quintessence

In the previous section, the ΛCDM model introduced as the standard model to describe the accelerated expansion of the universe; however, this model faces some problems with the cosmological constant (Sec. 1.5.2). Therefore, the idea of the non-constant vacuum energy density came forward in the cosmological community, this idea is often called quintessence. It suggests that the reason why the vacuum energy density contribution is small, is that our universe is old. In order to construct the time-varying vacuum energy density, it is considered

that there exist one or more scalar fields in which the vacuum energy density is changing with time.

In the following, we consider the action of the scalar field which is minimally coupled to gravity

$$S = \int d^4x\sqrt{-g}\left(\frac{R}{2} + \mathcal{L}_\psi\right), \tag{1.63}$$

where $\mathcal{L}_\psi$ is the Lagrangian of a scalar field ψ given by

$$\mathcal{L}_\psi = -\frac{1}{2}\, g^{\mu\nu}\, \partial_\mu\psi\, \partial_\nu\psi - V(\psi), \tag{1.64}$$

where $V(\psi)$ is an unspecified positive potential. The field equations can be determined from variation of the action (1.63) with respect to $g_{\mu\nu}$

$$R_{\mu\nu} - \frac{1}{2}R\, g_{\mu\nu} = T^{\psi}_{\mu\nu}, \tag{1.65}$$

where $T^{\psi}_{\mu\nu}$ is the energy momentum tensor of the scalar field given by (1.49). Moreover, the Klein-Gordon equation is given by the variation with respect to ψ:

$$\nabla_\mu\, \nabla^\mu\, \psi - \frac{\partial V(\psi)}{\partial\psi} = 0. \tag{1.66}$$

In the context of FRW cosmology the EFE (1.65) gives

$$3\left(H^2 + \frac{k}{a^2}\right) = \frac{1}{2}\dot{\psi}^2 + V(\psi), \tag{1.67}$$

$$2\dot{H} + 3H^2 + \frac{k}{a^2} = -\frac{1}{2}\dot{\psi}^2 + V(\psi), \tag{1.68}$$

and the Klein-Gordon equation (1.66) becomes

$$\ddot{\psi} + 3H\dot{\psi} + V^{'}(\psi) = 0, \tag{1.69}$$

where the over-dot means derivation with respect to the coordinate time and prime means derivation with respect to the scalar field ψ.

From the Friedmann equation (1.67) and the Raychaudhuri equation (1.68) we can define the energy density and pressure of the scalar field as follows

$$\epsilon_\psi = \frac{1}{2}\dot{\psi}^2 + V(\psi), \tag{1.70}$$

$$P_\psi = \frac{1}{2}\dot{\psi}^2 - V(\psi), \tag{1.71}$$

therefore, the effective EoS parameter for the scalar field becomes

$$w_\psi = \frac{P_\psi}{\epsilon_\psi} = \frac{\frac{1}{2}\dot{\psi}^2 - V(\psi)}{\frac{1}{2}\dot{\psi}^2 + V(\psi)}. \tag{1.72}$$

From Eq. (1.72) we see that the w_ψ is the dynamical EoS parameter in range $[-1, 1]$, in other words if $1/2\,\dot{\psi}^2 \ll V(\psi)$ we get $w_\psi \approx -1$ and if $V(\psi) \ll 1/2\,\dot{\psi}^2$ we get $w_\psi \approx 1$. Moreover, the former case refers to the dark energy.

1.7 Non-minimally coupled scalar field

In the previous section, we rendered the minimally coupled scalar field as the simplest choice of the scalar field, i.e. where the direct coupling between the scalar field and the Ricci curvature was ignored. In 1968, a non-minimal coupling was presented by Chernikov and Tagirov [1968] and followed by Callan et al. [1970]. There are some areas in which the inclusion of such a coupling term, like $-1/2\,\xi R\psi^2$ where ξ is the dimensionless coupling constant, in the scalar field Lagrangian provides interesting outcome. For instance, the first loop correction generates $\xi \neq 0$ even if it does not exists in the classical action (see e.g. Birrell and Davies [1982]). Moreover, a renormalization of a classical theory with $\xi = 0$, shifts the classical theory to a one with $\xi \neq 0$; although the shift is not big, it has a great impact on the inflation scenario (for more details see Faraoni [2004]).

For the non-minimally coupling scalar field, we shall start with the action in the form

$$S = \int d^4x\sqrt{-g}\left(\frac{R}{2} + \mathcal{L}_\psi\right), \tag{1.73}$$

where $\mathcal{L}_\psi$ is the Lagrangian of a non-minimally coupled scalar field ψ:

$$\mathcal{L}_\psi = -\frac{1}{2}\left(g^{\mu\nu}\,\partial_\mu\psi\,\partial_\nu\psi + \xi R\psi^2\right) - V(\psi), \tag{1.74}$$

where $V(\psi)$ is a scalar field potential. Variation of the action (1.73) with respect to $g_{\mu\nu}$ gives the EFE as follows

$$R_{\mu\nu} - \frac{1}{2}R\,g_{\mu\nu} = T^{\psi}_{\mu\nu}. \tag{1.75}$$

Here the $T^{\psi}_{\mu\nu}$ is the energy momentum tensor for the non-minimally coupled scalar field and reads

$$\begin{aligned} T^{\psi}_{\mu\nu} = (1-2\,\xi)\nabla_\mu\psi\,\nabla_\nu\psi + \left(2\,\xi - \frac{1}{2}\right) g_{\mu\nu}\nabla^\alpha\psi\,\nabla_\alpha\psi - V(\psi)\,g_{\mu\nu} \\ +\xi\left(R_{\mu\nu} - \frac{1}{2}g_{\mu\nu}R\right)\,\psi^2 + 2\,\xi\psi\,(g_{\mu\nu}\,\nabla^\alpha\,\nabla_\alpha - \nabla_\mu\,\nabla_\nu)\,\psi. \end{aligned} \tag{1.76}$$

Moreover, variation with respect to the scalar field ψ provides the Klein-Gordon equation

$$\nabla_\mu\,\nabla^\mu\,\psi - \xi R\psi - \frac{\partial V(\psi)}{\partial\psi} = 0. \tag{1.77}$$

There are three special cases for the coupling constant value:

- $\xi = 1/6$ is the conformal coupling, namely the physics of ψ and the Klein-Gordon equation (1.77) is conformally invariant if the scalar field potential is vanishing or $V(\psi) = \lambda\psi^4$.
- $\xi = 0$ is the minimal coupling.
- $|\,\xi\,| >> 1$ is called the strong coupling.

Since we deal with the isotropic and homogeneous universe, the Friedmann and the Raychaudhuri equations for the non-minimally coupled scalar field in the FRW background are

$$3\left(H^2+\frac{k}{a^2}\right)=\epsilon_\psi, \tag{1.78}$$

$$\left(2\,\dot{H}+3\,H^2+\frac{k}{a^2}\right)=-P_\psi, \tag{1.79}$$

and the Klein-Gordon equation will be

$$\ddot{\psi}+3\,H\,\dot{\psi}+\partial_\psi V+6\,\xi\,\psi\,\left(\dot{H}+2\,H^2+\frac{k}{a^2}\right)=0. \tag{1.80}$$

Here the ϵ_ψ and P_ψ are

$$\epsilon_\psi=\frac{1}{2}\,\dot{\psi}^2+V(\psi)+3\,\xi\,\psi\,\left(2\,H\,\dot{\psi}+\psi\left(H^2+\frac{k}{a^2}\right)\right), \tag{1.81}$$

$$P_\psi=(1-4\,\xi)\,\frac{1}{2}\,\dot{\psi}^2-V(\psi)-\xi\left(4\,H\,\psi\,\dot{\psi}+2\,\psi\,\ddot{\psi}+\psi^2\,\left(2\,\dot{H}+3\,H^2+\frac{k}{a^2}\right)\right). \tag{1.82}$$

The effective EoS parameter w_ψ can then be derived from Eqs. (1.81) and (1.82). However, the w_ψ is very complicated and it is difficult to analyse it in a way similar to the effective EoS parameter of the minimal coupling (1.72). However, one can apply a dynamical system analysis, as we will see in Chapter 6, to study a model of a non-minimally coupled scalar field cosmology.

2. Uniformly accelerated traveler

This chapter is based on the paper Kerachian [2020] " Uniformly accelerated traveler in an FLRW universe", published in Physical Review D. Here, we presented the version from arXiv.

In Sec. 1.1.1, the definition of the uniformly accelerated trajectories and the geodesics were presented. However, as we mentioned there, computing the exact form of these trajectories are not an easy task. Therefore, in this article, we managed to present a novel method, by applying the conformal time transformation, to derive general analytic solutions both for the accelerated motion and for the geodesic motion in spatially curved FRW spacetime. The conformal time transformation reduces the FRW metric to the forms (1.36), (1.37), and (1.38), in which the coordinates η and χ share a common coefficient $a(\eta)$. This allows us to convert the second order differential equations (1.26) into a first order set of equations. Geodesics can be calculated from the accelerated trajectories when the norm of acceleration is vanishing. Furthermore in this work, we provided some examples for the spatially flat FRW models.

The formalism presented in this work can be applied in a similar way to the whole Anti-de Sitter spacetime.

In the last part of this work, we studied the return journey of a rocketeer in spatially flat FRW spacetime. It was suggested by Rindler [1960] that having uniform deceleration would be enough to have a return journey; however, we prove that this condition is not sufficient for all spacetimes.

This work can be considered as a generalization of the work done by Rindler [1960].

Uniformly accelerated traveler in an FLRW universe

Morteza Kerachian[1,*]

[1] *Institute of Theoretical Physics, Faculty of Mathematics and Physics, Charles University, CZ-180 00 Prague, Czech Republic*

This paper introduces an analytical treatment of accelerated and geodesic motion within the framework of the Friedmann -Lemaître-Robertson-Walker (FLRW) spacetime. By employing conformal time transformations we manage to convert second order differential equations of motion in FLRW spacetime to first order equations in the conformally transformed spacetime. This allows us to derive a general analytical solution in closed-form for accelerated motion in spatially curved FLRW spacetime. We provide few examples of this general solution. The last part of our work focuses on the return journey for a traveler exploring a FLRW universe. We derive certain conditions for a de Sitter universe that have to be satisfied in order to achieve a return journey.

PACS numbers:
Keywords: Gravitation, Cosmology; Dynamical systems

1. INTRODUCTION

The paradigm of a homogeneous expanding isotropic universe in the framework of General Relativity is realised via the Friedmann-Lemaître-Robertson-Walker (FLRW) model [1–4]. In this work we are going to investigate the accelerated motion of a test particle in FLRW. Such a test particle corresponds to a rocketeer traveling in an FRLW universe. The derivation and the interpretation of accelerated motion have suffered from ambiguous treatments which will be discussed later on[1].

The motion of a uniformly accelerated traveller in an expanding universe is described by a set of differential equations which are in general non-trivial coupled. This set of equations does not become less complicated even if a specific cosmological model is applied. Thus, an analytical derivation of the path of a rocketeer is highly challenging. Actually a goal of this work is to present a general formulation which allows an analytical treatment. In particular, this work has been inspired by [10] in which W. Rindler proposed a generalization of the hyperbolic motion in Minkowski spacetime to solve the corresponding set of equations. However, Rindler solved it only for the de Sitter spacetime [10].

Studying the accelerated motion of a rocketeer is useful for the future accelerated space probe. For our universe (with $\Omega_m \approx 0.27$, $\Omega_\Lambda \approx 0.73$ and nearly spatially flat) a space traveler could visit a galaxy which is observed today at a redshift of 1.7 on a one-way journey with proper acceleration equal to the terrestrial gravitational acceleration, in almost 100 years [11]. However, for galaxies at redshift less than 1.7, e.g. 0.65, it is not clear whether the traveller would succeed to return back home. Therefore, it might be appropriate to consider a traveller of intermittent accelerations to explore the universe [9]. In this study, we are going to address this issue from a different point of view, i.e. our rocketeer travels with uniform deceleration in order to achieve a return trip.

The formalism presented in this work reduces to the geodesic motion in a spatially curved FLRW spacetime in the limit of zero proper acceleration. Since geodesic in an expanding universe has vast applications in cosmology, astrophysics and quantum gravity, many attempts have been undertaken to solve the geodesic equations of motion (for more details see references $[12-39]$ of [12]). The first attempt to tackle this issue was initiated by Whiting [13]. Whiting derived the equations of motion for a free particle with Newtonian background and its relativistic generalization. In [14] geodesic in low-velocity regime has been studied. These efforts by [13, 14] for solving geodesic motion was not sufficient due to the number of shortcomings in calculation and interpretation. Latter on, Grøn & Elgarøy [15] derived a general solution for geodesics in the full general relativity framework. Moreover, Ref. [13] claimed that particle moving uniformly in an expanding universe will join the Hubble flow. This claim has been refuted in [16], in which it has been formally proven that particles following the geodesic motion in an eternally expanding universe do not asymptotically rejoin the Hubble flow. Recently, a method for deriving both timelike and spacelike geodesic distances in spatially flat FLRW spacetime with given initial-value or boundary-value constraints was presented in [12].

In this work, we use conformal time transformations in order to get a general analytical formulation. Thus, it is useful to provide a brief overview of what has been already done in FLRW with conformal transformations. Conformal transformation and its symmetries help us to grasp the notion of the causal structure of spacetime [17]. FLRW metric has vanishing Weyl tensor, therefore, all Friedmann cosmological models are conformally flat and their systematic description has been studied in detail in Ref. [18–20]. The nature of FLRW models in conformal coordinates has been studied in [21]. It has been demonstrated in [22] that transformation into conformal coordinates do not eliminate superluminal recession velocities for open or flat matter dominated FLRW cosmologies, and all of them possess superluminal expansion. Ref. [23] derived the scalar field and the electromagnetic field of a moving charged particle in de Sitter spacetime, when the particle is following geodesic trajectories or it is uniformly accelerated.

*Electronic address: kerachian.morteza@gmail.com

[1] For example, it has been debated whether analysing uniformly accelerated motion in an expanding universe could clarify the physics behind the expansion. Namely, the debate has been about if the expansion is a trick of coordinates or a physical phenomenon [5–9].

In order to achieve this, conformal transformation between de Sitter and Minkowski spacetime was applied.

The layout of this work is as follows; Sec. 2 provides the essential mathematical background in which the conformal time transformation is applied. In Sec. 3 a novel general formalism is presented. Namely, using the transformed FLRW spacetime enables us to solve the equations of motion of accelerated particle. In this way, second order differential equations reduce to first order differential equations which allow us to solve the trajectories for accelerated particle and free motion. In addition, this formalism specifies the four-velocities of particles. This extends previous results [12, 15] covering only geodesic motion. We prove that accelerated and geodesic motions in FLRW universe depend on the expansion factor and its integral for any specific FLRW model. In Sec. 4 we give some examples for known FLRW models that have an analytic solution. In cases where there is no analytical solutions, we use numerical integration to solve them. Furthermore, in Sec. 4.4 we provide solutions for both the uniformly accelerated and the geodesic motion in the global anti-de Sitter spacetime by implementing similar prescription as we did in Sec. 3. This accelerated trajectory is indeed the generalized form of the known uniformly accelerated observer in the anti-de Sitter spacetime [24–26]. In Sec. 5 we discuss the return journey. We show that, in order to achieve a return journey having uniformly deceleration is not sufficient condition for every spacetime. For a de Sitter spacetime we derive the boundary condition that must be satisfied to be able to fulfill the return journey. Concluding remarks are driven in Sec. 6.

2. MATHEMATICAL BACKGROUND

We begin by introducing the line element of the FLRW spacetime, which describes the metric of an expanding, homogeneous and isotropic universe

$$ds^2 = -c^2dt^2 + R^2(t)[d\chi^2 + S_k^2(\chi)(d\theta^2 + \sin^2\theta d\phi^2)], \quad (1)$$

where c is light speed (hereafter $c = 1$),

$$S_k(\chi) = \begin{cases} \sin\chi, & k = +1, \quad \text{closed}, \\ \chi, & k = 0, \quad \text{flat}, \\ \sinh\chi, & k = -1, \quad \text{open}, \end{cases}$$

expresses the space curvature and $R(t)$ is the scale factor which describes the expansion of the universe. t is the coordinate time $t \in [0,\infty)$; χ lies in the range $\chi \in [0,\infty)$ for $k = 0,-1$ and $\chi \in [0,\pi]$ for $k = 1$; while the angles $\theta \in [0,\pi]$ and $\phi \in [0,2\pi)$ independently of the curvature.

Let us assume a cosmological model with a cosmological constant Λ and a fluid with equation of state given by

$$P = P(\rho) = (\gamma - 1)\rho \quad (2)$$

where P is the pressure, ρ is the energy density and we assume that constant γ can take any values. Then, the Friedmann equation reads

$$\frac{\dot{R}^2(t)}{R^2(t)} = \frac{\Lambda}{3} - \frac{k}{R^2(t)} + \frac{C}{R^{3\gamma}(t)}, \quad (3)$$

where dot means derivation with respect to t and C is a constant proportional to the matter density (see e.g. [24]).

The four-acceleration of a particle is given by

$$a^\mu = u^\mu_{;\nu}u^\nu = \frac{du^\mu}{d\lambda} + \Gamma^\mu_{\nu\sigma}\frac{dx^\nu}{d\lambda}\frac{dx^\sigma}{d\lambda}, \quad (4)$$

where u^μ is the four-velocity and λ is the proper time. a^μ and u^μ satisfy the following constraints

$$u^\mu u_\mu = -1, \quad (5)$$

$$a^\mu a_\mu = A^2, \quad (6)$$

$$a^\mu u_\mu = 0, \quad (7)$$

where A is the norm of the acceleration. Having uniform acceleration means that A =const.

Solving Eq. (4) for a given acceleration (say for A =const) is almost analytically intractable (see e.g [10]). Here we introduce the conformal time transformation in order to tackle this problem. In particular, the conformal time η is such that

$$\eta = \int \frac{dt}{R(t)}. \quad (8)$$

Additionally, by putting $\tilde{\chi} = \chi$, the FLRW metric reads

$$ds^2 = \tilde{R}^2(\eta)[-d\eta^2 + d\tilde{\chi}^2 + S_k^2(\tilde{\chi})(d\theta^2 + \sin^2\theta d\phi^2)], \quad (9)$$

Notice that, $\tilde{R}(\eta) = R(t)$.

When we have cosmological models with $\Lambda = 0$ or $\Lambda \neq 0$ but without matter, it holds that (see e.g. [24])

$$\tilde{R}(\eta) = \begin{cases} \tilde{R}_c \sin^b(\frac{\eta}{b}), & k = +1, \\ \tilde{R}_c \eta^b, & k = 0, \\ \tilde{R}_c \sinh^b(\frac{\eta}{b}), & k = -1, \end{cases}$$

where $\tilde{R}_c$ is a constant length which determines the scale of the universe. The power coefficient b for $\Lambda = 0$ is $b = \frac{2}{3\gamma-2}$. The value of b distinguishes between different cosmological models. For example, if $b = 2$ then the universe is filled with dust;for stiff matter $b = \frac{1}{2}$; while $b = 1$ describes the radiation case. Moreover, for non-negative curvature when $\Lambda \neq 0$ and without matter, which is actually a de-Sitter cosmological model, then $b = -1$.

3. PATH OF PARTICLES IN FLRW SPACETIME

We would like first to present the general formulation for the motion of particles in the transformed FLRW spacetime (9) by considering only the radial motion. To do that, we shall define the four-velocity as follows [11]

$$u^\eta = \frac{d\eta}{d\lambda} = \frac{\cosh\zeta(\lambda)}{\tilde{R}(\eta)}, \quad u^{\tilde{\chi}} = \frac{d\tilde{\chi}}{d\lambda} = \frac{\sinh\zeta(\lambda)}{\tilde{R}(\eta)}, \quad (10)$$

where $\zeta(\lambda)$ is the rapidity, which will be determined later. Note that equations (10) automatically satisfy constraint (5).

The only needed non-vanishing Christoffel symbols for this case are

$$\Gamma^{\eta}_{\eta\eta} = \Gamma^{\eta}_{\tilde{\chi}\tilde{\chi}} = \Gamma^{\tilde{\chi}}_{\eta\tilde{\chi}} = \frac{1}{\tilde{R}(\eta)}\frac{d\tilde{R}(\eta)}{d\eta}. \tag{11}$$

The four-acceleration in the set of coordinates (9) can be written in the following way

$$a^{\eta} = \frac{du^{\eta}}{d\lambda} + \Gamma^{\eta}_{\eta\eta}(u^{\eta})^2 + \Gamma^{\eta}_{\tilde{\chi}\tilde{\chi}}(u^{\tilde{\chi}})^2, \tag{12}$$

$$a^{\tilde{\chi}} = \frac{du^{\tilde{\chi}}}{d\lambda} + 2\Gamma^{\tilde{\chi}}_{\eta\tilde{\chi}}u^{\eta}u^{\tilde{\chi}}. \tag{13}$$

From now on, since all used Christoffel symbols have equal value, we shall denote them by Γ.

By differentiating the first term in the right-hand side of Eq. (12) and by using Eq. (10) we obtain

$$\frac{du^{\eta}}{d\lambda} = \frac{\sinh\zeta(\lambda)}{\tilde{R}(\eta)}\frac{d\zeta(\lambda)}{d\lambda} - \frac{\cosh\zeta(\lambda)}{\tilde{R}(\eta)^2}\frac{d\tilde{R}(\eta)}{d\lambda}. \tag{14}$$

Since the $\frac{d\tilde{R}(\eta)}{d\lambda}$ can be written in terms of η

$$\frac{d\tilde{R}(\eta)}{d\lambda} = \frac{d\eta}{d\lambda}\frac{d\tilde{R}(\eta)}{d\eta} = u^{\eta}\frac{d\tilde{R}(\eta)}{d\eta}, \tag{15}$$

by substituting it into Eq. (14) together with Eqs. (10) and (11) we arrive to

$$\frac{du^{\eta}}{d\lambda} = u^{\tilde{\chi}}\frac{d\zeta(\lambda)}{d\lambda} - (u^{\eta})^2\Gamma. \tag{16}$$

Thus

$$a^{\eta} = u^{\tilde{\chi}}\frac{d\zeta(\lambda)}{d\lambda} + (u^{\tilde{\chi}})^2\Gamma = u^{\tilde{\chi}}(\frac{d\zeta(\lambda)}{d\lambda} + \Gamma u^{\tilde{\chi}}). \tag{17}$$

Similar calculation can be undertaken for $a^{\tilde{\chi}}$ where

$$\frac{du^{\tilde{\chi}}}{d\lambda} = u^{\eta}\frac{d\zeta(\lambda)}{d\lambda} - u^{\eta}u^{\tilde{\chi}}\Gamma, \tag{18}$$

which finally gives

$$a^{\tilde{\chi}} = u^{\eta}\frac{d\zeta(\lambda)}{d\lambda} + u^{\eta}u^{\tilde{\chi}}\Gamma = u^{\eta}(\frac{d\zeta(\lambda)}{d\lambda} + \Gamma u^{\tilde{\chi}}). \tag{19}$$

We denote

$$A = \frac{d\zeta(\lambda)}{d\lambda} + \Gamma u^{\tilde{\chi}}, \tag{20}$$

where A, is the norm of acceleration as mentioned earlier in Eq. (6). As a result, the four-acceleration becomes

$$a^{\eta} = Au^{\tilde{\chi}}, \qquad a^{\tilde{\chi}} = Au^{\eta}. \tag{21}$$

Note that Eq. (21) satisfies also the constraints (6) and (7).

In the transformed FLRW metric (9) the coordinates η and $\tilde{\chi}$ share a common coefficient, i.e. the $R(\tilde{\eta})$. If we constraint the motion only on the radial direction through this transformation we get a solvable set of equations from Eq. (4). This allows us to analyze the radial motion of the rocketeer in the FLRW spacetime.

3.1. Accelerated Radial Motion

It is convenient to express the equation of motion of the rocketeer in terms of η. Therefore, from the four-velocity (10), we get

$$\frac{d\tilde{\chi}}{d\eta} = \frac{d\tilde{\chi}/d\lambda}{d\eta/d\lambda} = \tanh\zeta(\lambda). \tag{22}$$

To find the unknown rapidity $\zeta(\lambda)$ we need to use Eq. (20) and reparametrize it in terms of η

$$A - u^{\eta}\frac{d\tilde{\zeta}(\eta)}{d\eta} - \Gamma u^{\tilde{\chi}} = 0, \tag{23}$$

where $\tilde{\zeta}(\eta) = \tilde{\zeta}(\eta(\lambda)) = \zeta(\lambda)$ and A =const..

Integrating Eq. (23) with respect to η, we obtain

$$\tilde{\zeta}(\eta) = \operatorname{arcsinh}(A\tilde{\mathscr{R}}(\eta) + \frac{\upsilon}{\tilde{R}(\eta)}), \tag{24}$$

where

$$\tilde{\mathscr{R}}(\eta) = \frac{\int^{\eta}\tilde{R}(\tilde{\eta})^2 d\tilde{\eta}}{\tilde{R}(\eta)}, \tag{25}$$

and υ is an integration constant which is related to the initial velocity of particle. Consequently,

$$\tilde{\chi} = A\int \frac{\tilde{\mathscr{R}}(\eta)}{\sqrt{(A\tilde{\mathscr{R}}(\eta) + \frac{\upsilon}{\tilde{R}(\eta)})^2 + 1}}d\eta + \upsilon\int \frac{1/\tilde{R}(\eta)}{\sqrt{(A\tilde{\mathscr{R}}(\eta) + \frac{\upsilon}{\tilde{R}(\eta)})^2 + 1}}d\eta. \tag{26}$$

Now, we go back to the coordinates of the original FLRW metric (1). This is achieved by using the inverse transformation of Eq. (8), i.e. $\tilde{R}(\eta)d\eta = dt$, and by recalling that $R(t) = \tilde{R}(\eta)$. Thus, we obtain for Eq. (24)

$$\hat{\zeta}(t) = \operatorname{arcsinh}(A\mathscr{R}(t) + \frac{\upsilon}{R(t)}), \tag{27}$$

where

$$\mathscr{R}(t) = \frac{\int^{t} R(t')dt'}{R(t)}. \tag{28}$$

Using Eq. (27) enables us to derive the four-velocity in standard FLRW spacetime as follows

$$u^{t} = \frac{dt}{d\lambda} = \cosh\hat{\zeta}(t), \quad u^{\chi} = \frac{d\chi}{d\lambda} = \frac{\sinh\hat{\zeta}(t)}{R(t)}. \tag{29}$$

Finally, the trajectory of uniform acceleration motion is given by

$$\chi = A\int \frac{1}{R(t)}\frac{\mathscr{R}(t)}{\sqrt{(A\mathscr{R}(t) + \frac{\upsilon}{R(t)})^2 + 1}}dt + \upsilon\int \frac{1}{R(t)^2}\frac{1}{\sqrt{(A\mathscr{R}(t) + \frac{\upsilon}{R(t)})^2 + 1}}dt, \tag{30}$$

By specifying the evolution of the scale factor $R(t)$ Eq. (30) provides the accelerated radial path of the rocketeer in the standard FLRW coordinate.

3.2. Some characteristic types of motion

a. Purely accelerated motion. When one ignores the integration constant υ (i.e. $\upsilon = 0$) in trajectories (26) and (30) the motion is called *purely accelerated*. In the conformally transformed coordinates the trajectory is given by

$$\tilde{\chi}_a = A \int \frac{\tilde{\mathscr{R}}(\eta)}{\sqrt{A^2 \tilde{\mathscr{R}}(\eta)^2 + 1}} d\eta, \tag{31}$$

and in the original FLRW coordinates we get

$$\chi_a = A \int \frac{1}{R(t)} \frac{\mathscr{R}(t)}{\sqrt{A^2 \mathscr{R}(t)^2 + 1}} dt, \tag{32}$$

where index a in both Eqs. (31) and (32) refers to the *purely accelerated motion*.

b. Geodesic motion. To get the trajectory for the geodesic motion one has to substitute $A = 0$ into the Eqs. (24), (26) and (30). Thus, the rapidity function $\tilde{\zeta}(\eta)$ becomes

$$\tilde{\zeta}(\eta) = \operatorname{arcsinh}\left(\frac{\upsilon}{\tilde{R}(\eta)}\right). \tag{33}$$

Consequently, Eq. (26) will be

$$\tilde{\chi}_v = \int \frac{\upsilon}{\sqrt{\tilde{R}(\eta)^2 + \upsilon^2}} d\eta, \tag{34}$$

and for Eq. (30) we obtain

$$\chi_v = \int \frac{\upsilon}{R(t)} \frac{1}{\sqrt{R(t)^2 + \upsilon^2}} dt. \tag{35}$$

Here index v in Eqs. (34) and (35) denotes geodesic motion. For all υ values, $\upsilon^2 > 0$, which guarantees that Eq. (35) is a timelike geodesic [12].

Eqs. (34) and (35) are geodesics in any conformal time FLRW spacetime and FLRW spacetime respectively. Eq. (35) is the same as equation derived in [15] and recently in [12].

c. Null geodesics. We can see from Eq. (30) that for large acceleration A the particle's trajectory asymptotically reaches the null geodesic, that means

$$\lim_{A>>} \chi_a = \pm \int \frac{1}{R(t)} dt. \tag{36}$$

Moreover, this statement holds for large υ value, i.e.

$$\lim_{\upsilon>>} \chi_a = \pm \int \frac{1}{R(t)} dt. \tag{37}$$

d. Transformation conditions. For the flat spatial curvature FLRW spacetime the accelerated motion (31) can be transformed into geodesic motion (34) under certain conditions. In order to investigate this statement, we consider two different spacetimes having scale factors $\tilde{R}_m(\eta) = \mu \eta^m$ and $\tilde{R}_k(\eta) = \kappa \eta^k$. By substituting $\tilde{R}_m(\eta)$ and $\tilde{R}_k(\eta)$ into the Eqs. (34) and (31) respectively we get

$$\tilde{\chi}_v = \frac{\upsilon \, \eta^{1-m}}{\mu \, (m-1)} {}_2\mathrm{F}_1\left(\frac{1}{2}, \frac{m-1}{2m}; \frac{3m-1}{2m}; -\frac{\upsilon^2 \, \eta^{-2m}}{\mu^2}\right), \tag{38}$$

and

$$\tilde{\chi}_a = \frac{A \, \kappa \, \eta^{2+k}}{(2+k)\,(1+2k)} {}_2\mathrm{F}_1\left(\frac{1}{2}, \frac{2+k}{2+2k}; \frac{4+3k}{2+2k}; -\frac{A^2 \, \kappa^2 \, \eta^{2+2k}}{(1+2k)^2}\right), \tag{39}$$

where ${}_2\mathrm{F}_1(a, b; c; z)$ is the Gauss hypergeometric function. These two trajectories become equivalent if

$$\begin{cases} 1 + k = -m, \\ \frac{A\,\kappa}{1+2k} = \frac{\upsilon}{\mu}, \\ 1 + 2k \neq 0. \end{cases} \tag{40}$$

For instance, the uniformly accelerated trajectories in the de Sitter spacetime get transformed to the geodesic motion in the Minkowski spacetime and vice versa (See Sec. 4.3 for more details). Moreover, one can show that an observer with a suitable acceleration moving in a decelerating Friedmann universe, i.e. a dust field universe, has the same cosmological redshift as the observer in the ΛCDM model [27].

4. SOME EXAMPLES

In this section of section's 3 formalism is applied to specific FLRW universe models. The motion of a particle both in the original and in the transformed coordinates depends only on the scale factor and its integral (Eq. (28) and Eq. (25) respectively). Thus, specifying the expansion factor for each cosmological model enables us to determine the particles worldlines. In this section the behavior of the trajectories presented in paragraphs a and b of Sec. 3.2 is studied.

Recently, the solution of Friedmann Eq. (3) was presented for various FLRW models with $k = 0$ [28]. Namely, Chavanis has derived an analytical solution for $R(t)$ in a universe undergoing a various combination of eras, e.g. stiff matter era, dark matter era, and dark energy era due to the cosmological constant. From this study we use the form of the scale factor in the cosmological examples of Sec. 4 and Sec. 5.

Note that, although the transformation (8) is not, in general, conformally flat transformation (CFT) for spatially curved FLRW models, it is CFT for all the flat FLRW models. Thus, since the cosmological models appearing in Secs. 4.1 and 4.3 have zero spatial curvature, the transformation (8) is a CFT, i.e. it holds that

$$ds^2_{k=0} = \Omega^2 ds^2_{flat}, \tag{41}$$

where $\Omega = \tilde{R}(\eta)$.

It is clear that this formalism is able to reproduce the known hyperbolic motion in the Minkowski spacetime [29]. In a similar manner as in the Minkowski spacetime, the uniformly accelerated motion can be derived in the Einstein static universe, since for both spacetimes the scale factor $R(t) = 1$.

To provide visualization for our examples we are going to plot some trajectories in Penrose diagrams with coordinates η and χ given by the metric (9).

4.1. Flat FLRW spacetime without Λ

In this section we consider spatially flat FLRW spacetime with vanishing cosmological constant, i.e. $\Lambda = 0$, and a single fluid content provided by the EoS (2). From the Friedmann equation (3) one can obtain the scale factor

$$R(t) = R_c t^{\frac{2}{3\gamma}}, \tag{42}$$

where $R_c = \left(\frac{3}{2}\gamma\sqrt{C}\right)^{\frac{2}{3\gamma}}$. Substituting this scale facor into the equations Eqs. (32) and (35) we obtain

$$\chi_a = \frac{9At^{2-2/3\gamma}\gamma^2}{R_c\,(3\gamma+2)\,(6\gamma-2)} \; {}_2\mathrm{F}_1\left(\frac{1}{2}, 1-\frac{1}{3\gamma}; 2-\frac{1}{3\gamma}; -\left(\frac{3A\gamma t}{2+3\gamma}\right)^2\right), \tag{43}$$

and

$$\chi_v = \frac{3t^{1-2/3\gamma}}{R_c\,(3-2\gamma)} \; {}_2\mathrm{F}_1\left(\frac{1}{2}, \frac{3\gamma}{4}-\frac{1}{2}; \frac{3\gamma}{4}+\frac{1}{2}; -\left(\frac{R_c t^2/3\gamma}{\upsilon}\right)^2\right), \tag{44}$$

where a and v denote uniform acceleration and geodesic motion respectively. In conformal representation, where $\tilde{R}(\eta) = \tilde{R}_c\eta^b$ where $b = \frac{2}{3\gamma-2}$, we have

$$\tilde{\chi}_a = \frac{A\tilde{R}_c\,\eta^{2+b}}{(2+b)\,(1+2b)} \; {}_2\mathrm{F}_1\left(\frac{1}{2}, \frac{2+b}{2+2b}; \frac{4+3b}{2+2b}; -\frac{A^2\tilde{R}_c^2\,\eta^{2+2b}}{(1+2b)^2}\right) \tag{45}$$

and

$$\tilde{\chi}_v = \frac{\upsilon\,\eta^{1-b}}{\tilde{R}_c\,(b-1)} {}_2\mathrm{F}_1\left(\frac{1}{2}, \frac{b-1}{2b}; \frac{3b-1}{2b}; -\frac{\upsilon^2\eta^{-2b}}{\tilde{R}_c^2}\right). \tag{46}$$

The dynamical features of the above trajectories on a Penrose diagram are very similar for all the usual barotropic fluids, i.e. for fluids with $1 \le \gamma \le 2$. Thus, in Fig. 1 we plot just the case $\gamma = 1$, which shows different trajectories in a spatially flat FLRW universe with dust. Namely, Fig. 1 shows accelerated trajectories with zero υ and non zero υ (solid blue and dotted dashed red lines respectively), the geodesic trajectories (orange dashed lines) together with the null geodesic (black thick solid line). In the case of constant acceleration, the greater the acceleration the faster the rocketeer approaches the null geodesic behavior. We plot also one decelerating trajectory with non-zero υ, which exhibits a return journey: such trajectories will be discussed in Sec. 5. Regarding the geodesic motion the greater the initial velocity, the further the traveller can reach. Note that even if initially geodesic travellers overtake accelerated ones, eventually as expected the accelerated ones prevail. Additionally, this figure provides the asymptotic behavior of the trajectories as $t \to \infty$. One can see that, accelerated trajectories reach the future null infinity ,i.e. $\mathscr{I}^+$, whereas the geodesics motion ends up to timelike infinity, i.e. i^+.

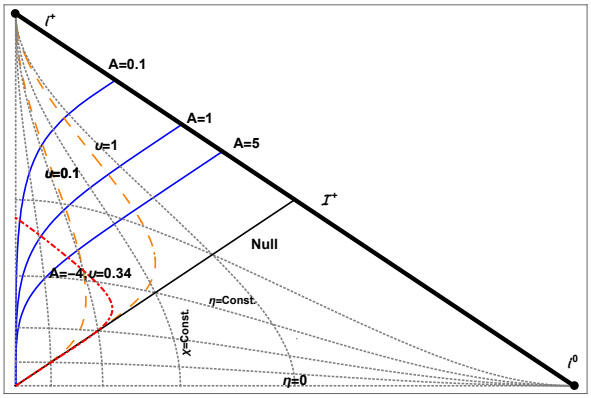

FIG. 1: Penrose diagram for the dust-filled universe. The thick black solid line denotes the photon trajectory. Solid lines have constant acceleration A and $\upsilon = 0$, while the dotted dashed lines have constant acceleration A and $\upsilon \neq 0$. Dashed curves are geodesics, i.e. $A = 0$.

4.2. Milne Universe

Vacuum FLRW model with $\Lambda = 0$ and $k = -1$ is known as Milne universe [30], where $R(t) = t$. For this spacetime particle's paths are

$$\chi_a = \ln\left(At + \sqrt{A^2t^2+4}\right) + \ln(C_5), \tag{47}$$

where C_5 is an integration constant. For a particle starting from $\chi_a = t = 0$ ($C_5 = \frac{1}{2}$), χ_a reduces to

$$\chi_a = \operatorname{arcsinh}(\frac{A}{2}t), \tag{48}$$

and χ_v becomes

$$\chi_v = -\operatorname{arctanh}(\frac{\upsilon}{\sqrt{t^2+\upsilon^2}}) + \operatorname{arctanh}(-\frac{\upsilon}{\sqrt{1+\upsilon^2}}). \tag{49}$$

For Milne universe we cannot use Eqs. (26) and (34) since transformation (8) is not CFT. In order to plot the above case in a Penrose diagram we have to use the transformation

$$t = \sqrt{T^2-R^2}, \qquad \chi = \operatorname{arctanh}(\frac{R}{T}), \tag{50}$$

between a Milne Universe and the Minkowski spacetime [29]. Using this transformation we get

$$(R_a + \frac{1}{A})^2 - T^2 = \frac{1}{A^2}, \tag{51}$$

and

$$R_v = \frac{\upsilon\,T}{\sqrt{1+\upsilon^2}}, \tag{52}$$

for the trajectories (48) and (49) respectively in the Minkowski spacetime.

It is known that Eqs. (51) and (52) describe hyperbolic and geodesic motion respectively in Minkowski spacetime. In Fig. 2 examples of these types of motion are depicted in the same manner as Fig. 1. The shaded region in this figure indicates the part of the Penrose diagram that does not belong to the Milne universe.

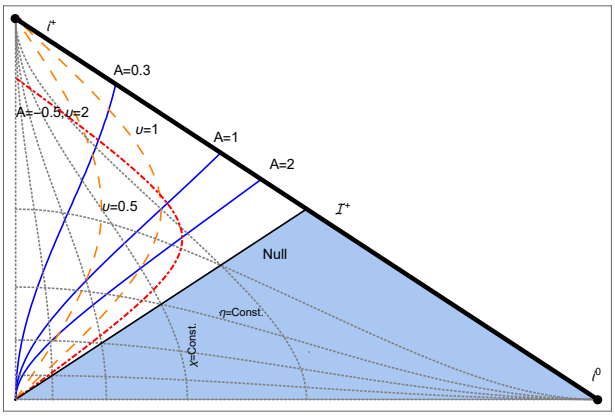

FIG. 2: Penrose diagram for the Milne universe. Curves have the same coloring as described in Fig. 1. Note that, the shaded part of the plot does not belong to the Milne universe.

4.3. de-Sitter Universe, $\gamma = 0$

Considering the dark energy dominated universe in the absence of any matter the scale factor is

$$R(t) = R_0 e^{\sqrt{\frac{\Lambda}{3}}t}, \tag{53}$$

where Λ is a cosmological constant [28]. This solution is known as the de Sitter solution.

Accelerated and geodesic motion in this particular spacetime are described by

$$\chi_a = -\frac{A}{\sqrt{\frac{\Lambda}{3}}R_0 e^{\sqrt{\frac{\Lambda}{3}}t}\sqrt{A^2+\frac{\Lambda}{3}}} + C_1, \tag{54}$$

$$\chi_v = -\sqrt{\frac{3}{\Lambda}}\frac{\sqrt{(R_0 e^{\sqrt{\frac{\Lambda}{3}}t})^2+\upsilon^2}}{\upsilon R_0 e^{\sqrt{\frac{\Lambda}{3}}t}}. \tag{55}$$

In conformal coordinates, where scale factor is $\tilde{R}(\eta) = -\sqrt{\frac{3}{\Lambda}}\frac{1}{\eta}$, we get

$$\tilde{\chi}_a = \frac{A}{\sqrt{A^2+\frac{\Lambda}{3}}}\eta, \tag{56}$$

$$\tilde{\chi}_v = -\sqrt{\frac{3}{\Lambda\upsilon^2}+\eta^2} + C_3. \tag{57}$$

It is clear from Eqs. (56) and (57) that the geodesic equation in conformally flat coordinates (Minkowski spacetime) get transformed to uniformly accelerated worldline in de Sitter spacetime, whereas the trajectory of a uniformly accelerated particle in Minkowski spacetime get transformed to geodesic in de Sitter spacetime (see Fig. 3). This result confirms previous works of Rindler[2] [10] and Bičák & Krtouš [23].

Fig. 3 shows the trajectories in the de Sitter spacetime. In this spacetime, all trajectories have the same description as in Fig 1, but some of them have different initial conditions. Namely, some of them do not pass through the origin $t = 0$. Another difference is that the de Sitter spacetime covers only the lower part of the Penrose diagram, since all trajectories end up at the $\mathscr{I}^+$. We continue plotting the trajectories even to the upper shaded region in order to provide a global view of the behavior of these trajectories.

4.4. Anti-de Sitter spacetime

In this section we consider a vacuum FLRW universe with a negative cosmological constant Λ and negative spatial curvature $k = -1$ namely Anti-de Sitter universe. This particular case of Anti-de Sitter universe has the scale factor

$$R(t) = \alpha\cos(\frac{t}{\alpha}) \tag{58}$$

where $\alpha = \sqrt{3/|\Lambda|}$. Thus, the accelerated and geodesic trajectories become

$$\chi_a = \ln\left(2\frac{A^2\alpha^2 + A\alpha\sqrt{A^2\alpha^2\sin^2(t/\alpha)+\cos^2(t/\alpha)}}{\cos(t/\alpha)}\right), \tag{59}$$

and

$$\chi_v = \operatorname{arctanh}\left(\frac{\upsilon\sin(t/\alpha)}{\sqrt{\alpha^2\cos^2(t/\alpha)+\upsilon^2}}\right). \tag{60}$$

In Fiq. 4 we illustrate these trajectories and we denote the different types of trajectories as we did in Fig. 1.

Note that this coordinate system does not cover the whole anti-de Sitter spacetime. In order to study the accelerated motion in the whole anti-de Sitter spacetime we use the following line element

$$ds^2 = -\cosh^2(r)dt^2 + \alpha^2\left(dr^2+\sinh^2(r)\left(d\theta^2+\sin^2\theta\, d\phi^2\right)\right), \tag{61}$$

[2] Note that, W.Rindler obtained only one special case of accelerated motion in de Sitter spacetime. Namely, he studied the case when a particle leaves the origin ($t = \chi = 0$) from rest, i.e. $u^t = 1$ and $u^\chi = 0$. One can rederive Rindelr's trajectory by putting $\upsilon = -\sqrt{\frac{3}{\Lambda}}A$ into the Eq. (30) together with $\chi_{(t=0)} = 0$.

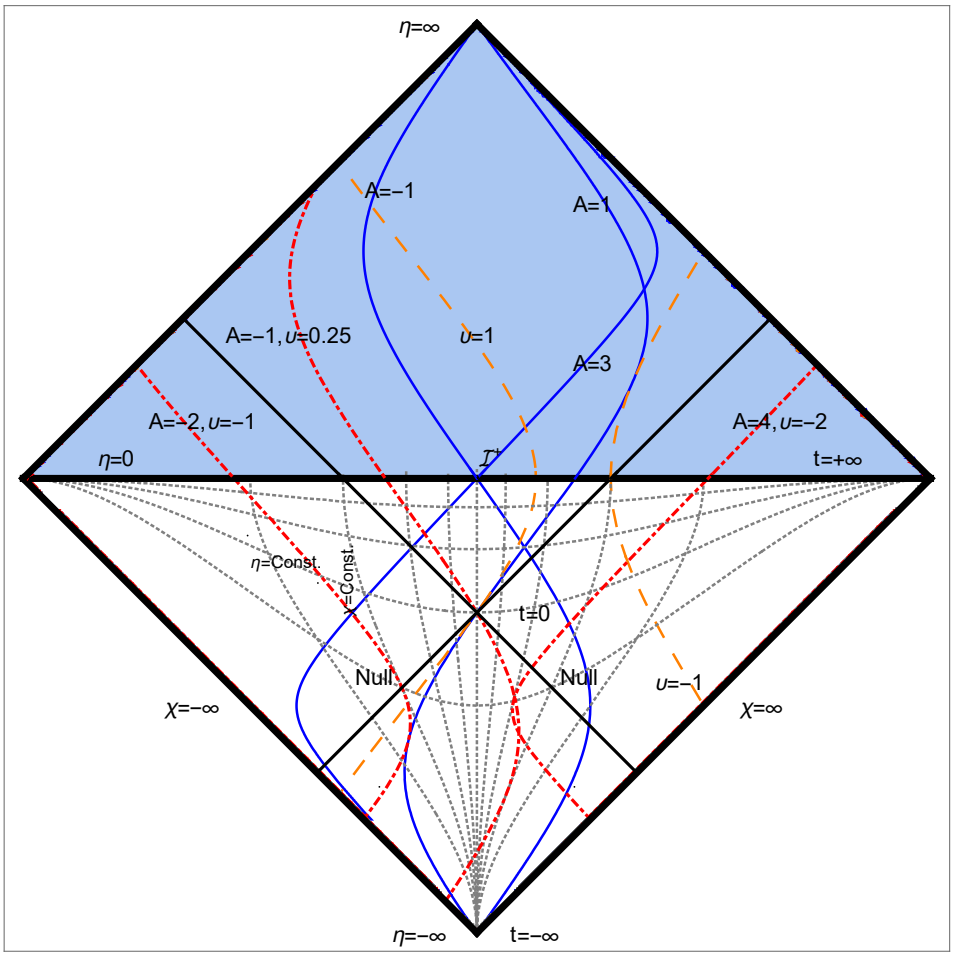

FIG. 3: Penrose diagram for de Sitter universe.The shaded part is not covered by the flat de Sitter universe.

where r is dimentionless. The accelerated and geodesic motions of this metric can not be studied from the formulation presented in Sec. 3. However, we can introduce a similar prescription to obtain those trajectories. Namely, we introduce the conformal coordinate χ by setting $\sinh(r) = \tan(\chi)$ together with $t = \alpha\,\eta$. Then, the metric (61) takes the form

$$ds^2 = \frac{\alpha^2}{\cos^2(\chi)}[-d\eta^2 + d\chi^2 + \sin^2(\chi)(d\theta^2 + \sin^2\theta\, d\phi^2)]. \tag{62}$$

It is clear that the anti-de Sitter spacetime time covers only half of the Einstein static universe, namely in the range $\chi \in [0, \pi/2)$.

Now, similarly to the formulation presented in Sec. 3, we introduce the radial four-velocity

$$u^\eta = \frac{d\eta}{d\lambda} = \frac{\cosh(\xi(\lambda))}{F(\chi)}, \quad u^\chi = \frac{d\chi}{d\lambda} = \frac{\sinh(\xi(\lambda))}{F(\chi)}, \tag{63}$$

where $F(\chi) = \dfrac{\alpha}{\cos(\chi)}$. This radial motion has the four-acceleration given by

$$a^\eta = Au^\chi, \quad a^\chi = Au^\eta, \tag{64}$$

where

$$A = \frac{d\xi(\lambda)}{d\lambda} + \Gamma u^\eta \tag{65}$$

and $\Gamma = \frac{1}{F(\chi)}\frac{dF(\chi)}{d\chi}$. Therefore, for the rapidity function $\xi(\chi) = \xi(\chi(\lambda)) = \xi(\lambda)$, which can be determined from Eq. (65), we get

$$\xi(\chi) = \text{arcCosh}\left(A\mathscr{F}(\chi) + \frac{\upsilon}{F(\chi)}\right), \tag{66}$$

where

$$\mathscr{F}(\chi) = \frac{\int F(\hat{\chi})^2 d\hat{\chi}}{F(\chi)}, \tag{67}$$

and υ is an initial velocity of the accelerated particle. Thus, from the four-velocity (63) and Eq. (66) we get

$$\eta = \int \coth(\xi(\chi))\, d\chi. \tag{68}$$

By substituting $\upsilon = 0$ into the Eq. (68), namely for the *purely accelerated motion*, after some manipulation we get the fol-

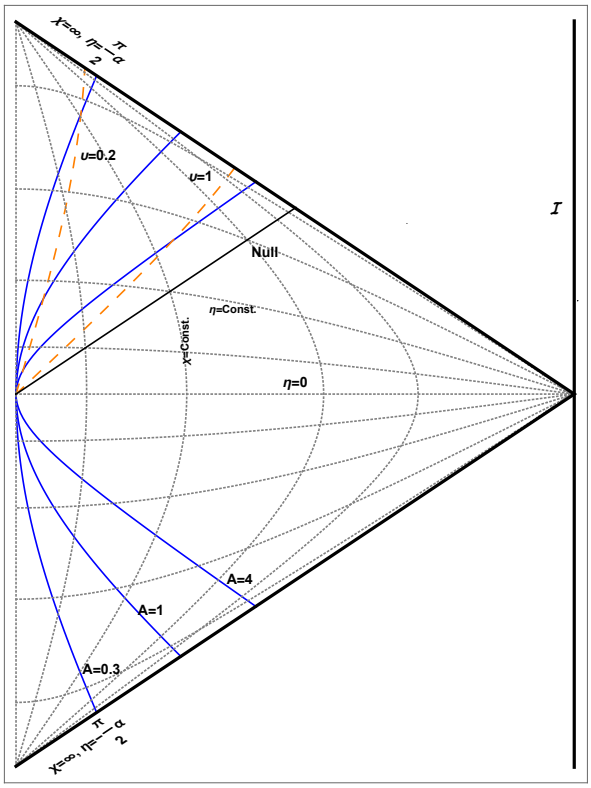

FIG. 4: Penrose diagram of the part of the anti-de Sitter spacetime as a particular case of the FLRW universe. Trajectories are collored in the same manner as Fig. 1.

lowing trajectory

$$\chi_a = \pi - \arccos\left(\frac{\sqrt{A^2\,\alpha^2-1}}{A\,\alpha}\,\frac{\tan(\Delta\eta)}{\sqrt{1+\tan^2(\Delta\eta)}}\right), \qquad (69)$$

where $A^2\,\alpha^2 > 1$ has to be satisfied, $\Delta\eta = \eta - \eta_0$ and the constant η_0 is an integration constant from integral appears in Eq. (68). Observers with an acceleration A travel radially in the range

$$\arcsin\left(\frac{1}{A\,\alpha}\right) < \chi_a < \frac{\pi}{2}.$$

At $\chi_a = \arcsin(1/(A\,\alpha))$ the χ component of the four-velocity vanishes and the radial moving observer turns to the stationary observer. Furthermore, Eq. (69) show that the maximum duration of the radial accelerated traveler in the anti-de sitter spacetime is $\Delta\eta = \pi/2$, since the trajectories reach the $\mathscr{I}$.

Moreover, by putting $A = 0$ into the Eq. (68) we derive the trajectories for geodesic motion

$$\chi_v = \arcsin\left(\frac{\sqrt{\upsilon^2-\alpha^2}}{\upsilon}\,\frac{\tan(\Delta\eta)}{\sqrt{1+\tan^2(\Delta\eta)}}\right), \qquad (70)$$

which holds under the condition that $\upsilon^2 > \alpha^2$ (for $\upsilon = \alpha$ the geodesic trajectory vanishes). Eq. (70) shows that, the observer moving with the constant υ moves in the range

$$0 < \chi_v < \arccos\left(\frac{\alpha}{\upsilon}\right).$$

When the observer reaches at $\chi_v = \arccos(\alpha/\upsilon)$ the u^χ becomes zero and therefore the radial moving observer becomes stationary. Similar to the accelerated motion, maximum duration of this motion is $\pi/2$.

Setting $\xi(\chi_0) = 0$ for any fixed $\chi = \chi_0$ reduces the accelerated radial motion to the family of the *timelike worldlines* representing uniformly accelerated observers studied in previous works [24–26]. Thus, the newly found radially moving accelerated observers have as a limiting case the already known stationary ones.

Fig. 5 shows these trajectories denoted in the same manner as in Fig. 1. As we discussed previously, worldlines of fixed χ represent uniformly accelerated observers. In this figure, trajectory number (1) shows that the stationary observer from $\eta \in (-\infty, 0]$. Then, at $\eta = 0$ it starts to accelerated radially with an acceleration $A = 3$ and goes toward $\mathscr{I}$(trajectory (4) has the similar behavior). Observer number (6) has a deceleration $A = -1.8$ from $\eta \in (-\pi/2, 0)$. Then, at $\eta = 0$ its u^χ vanishes and becomes stable. On the other hand, trajectories (5) and (7) which have the $\upsilon > 0$ start from $\eta = \chi = 0$ traveling with for $\Delta\eta = \pi/2$ with constant υ. Its radial component of four-velocity, i.e. u^χ is decreasing until at $\eta = 0$ it become zero. After this point, the observer becomes stationary. Observers (2) and (3) are at rest from $\eta \in (-\infty, -\pi/2]$ and then they move with negative υ towards O.

5. RETURN JOURNEY

In this section we are going to focus our study on analyzing the return journey of the rocketeer in spatially flat FLRW universe. In particular, we are going to study the behavior of the Eq. (30) or Eq. (26) in the spacetimes studied in the previous section. Actually, in order to fulfill the return journey, our rocketeer must begin to decelerate, i.e. $A_d < 0$, long enough time before it reaches the designated proper distance.

Assuming that, the spaceship is travelling with non-zero positive value υ, at $t = \lambda = \chi = 0$ the rocketeer applies a deceleration A_d. Thus, the rocketeer reaches the maximum comoving distance from the origin at the return point with coordinates $\{t_1, x_1\} > 0$ when $\hat{\xi}(t_1) = 0$ or equivalently $u^\chi(t_1) = 0$.

Therefore, depending on the form of scale factor, one can analyze the return journey of the rocketeer.

5.1. $R(t) = t^n$ spacetimes

In this section we analyze the return journey in the spacetime studied in sections 4.1- 4.2 , namely spacetimes having the scale factor like $R(t) = t^n$. In these particular spacetimes the rockeeter reaches the maximum comoving distance from the origin at

$$t_1 = \left(-\frac{\upsilon(n+1)}{A_d}\right)^{\frac{1}{n+1}}. \qquad (71)$$

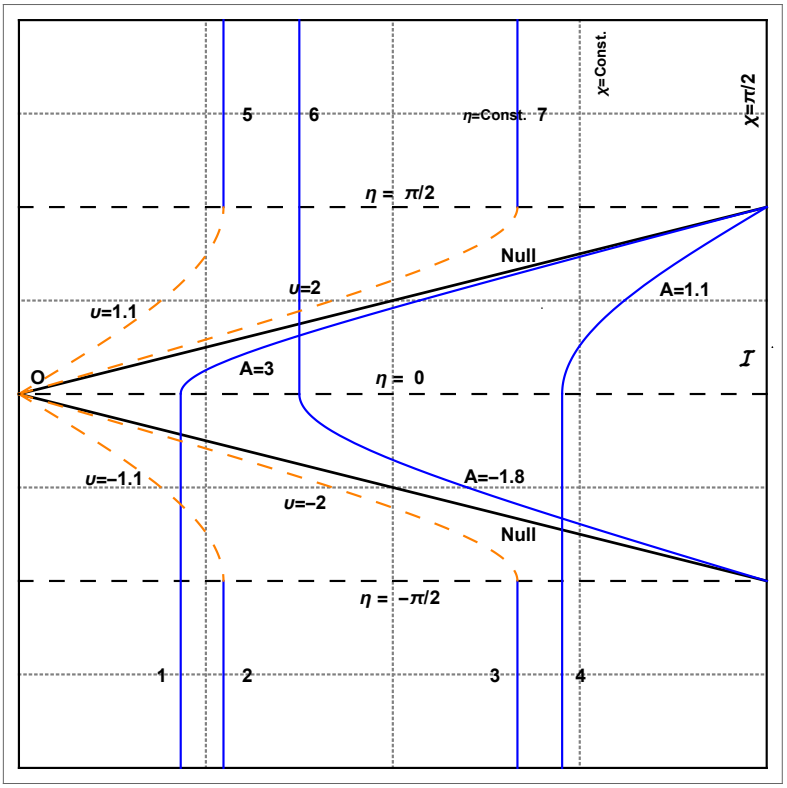

FIG. 5: The Penrose diagram for the global anti-de Sitter spacetime. See the text for more details.

Afterwards, the rocketeer returns towards the origin. As $t \to \infty$ the trajectory of the rocketeer asymptotically becomes

$$\lim_{t\to\infty} \chi = -\int \frac{1}{t^n} dt, \tag{72}$$

which means that there is a finite $t_2 > t_1$, when the rocketeer arrives back to the origin, $\chi = 0$. In Figs. (1)- (2), the dotted dash trajectories represent the return journeys in each spacetimes.

5.2. de-Sitter case

The return journey in the de Sitter spacetime has a different behavior with respect to the previous examples, since the scale factor (53) is given by a different function of time. In this specific spacetime, the rocketeer reaches the maximum comoving distance from the origin at

$$t_1 = \sqrt{\frac{3}{\Lambda}} \ln\left(-\sqrt{\frac{\Lambda}{3}}\frac{\upsilon}{A_d}\right). \tag{73}$$

Moreover, the total cosmic time t_2 needed to cover the return journey for a rocketeer that leaves the origin at $t = \lambda = 0$, is derived from Eq. (30) and it is given by

$$t_2 = \sqrt{\frac{3}{\Lambda}} \ln\left(-\frac{\sqrt{3\Lambda}\upsilon}{\sqrt{3\Lambda}\upsilon + 6A_d}\right). \tag{74}$$

Thus, from Eqs. (73) and (74) one can see that the return journey does not happen for all values of A_d and υ (see Fig. 6). Actually, to attain an actual return journey, the following relation

$$2A_d < -\sqrt{\frac{\Lambda}{3}}\upsilon < A_d, \tag{75}$$

has to be satisfied. In Fig. 6 we show several cases of return journeys in de Sitter spacetime for $\Lambda = 3$ and $A = -2$. The negative values of χ represents the opposite direction from the one that the rocketeer is supposed to explore.

Line 1. For $-\sqrt{\frac{\Lambda}{3}}\upsilon \geq A_d$, there isn't any return point for the particle and rocketeer will move toward the $-\chi$ direction.

Line 2. For $2A_d < -\sqrt{\frac{\Lambda}{3}}\upsilon < A_d$, there is a return point and the rocketeer is able to come back to the origin.

Line 3. For $-\sqrt{\frac{\Lambda}{3}}\upsilon = 2A_d$, there is a return point but the rocketeer will return back to origin in a infinite cosmic time.

Line 4. For $-\sqrt{\frac{\Lambda}{3}}\upsilon > 2A_d$, there is a return point but the rocketeer will never go back to the origin.

Thus, we have seen that in de Sitter spacetime, having the uniform deceleration motion is not sufficient for the rocketeer

to come back to the origin. One has to apply the deceleration which satisfies Eq. (75).

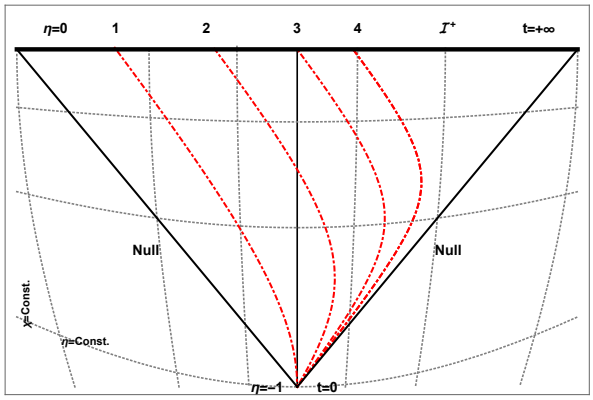

FIG. 6: Penrose diagram for the worldlines of return journeys in de Sitter spacetime. Here $\Lambda = 3$ and $A = -2$ and the spacetime is depicted only for $t \geq 0$.

6. CONCLUSIONS

In 1960, W.Rindler [10] proposed the problem of a "Hyperbolic Motion in Curved Spacetime" to study the accelerated motion in curved spacetime.

In particular, it was suggested that the accelerated motion is the best way of exploring our universe in a reasonably short time [9]. Taking the above suggestion into account, the motion of an accelerated traveller in an expanding universe has been studied in this work. This involves solving the non-trivial Eq. (4) for a given acceleration. To achieve this, we applied a conformal time transformation (8) to the generic FLRW universe. Using the method introduced in Sec. 3 has helped us to determine a generalized form of rapidity function (27), which leads us to derive the trajectory (30) of an accelerated traveler.

We have shown that the accelerated and the geodesic motion in an expanding universe are solely determined by the expansion factor and its integral (28). The scale factor is the solution of the Friedmann equation (3), which depends on the spatial curvature k, the cosmological constant Λ, and the equation of state $P = P(\rho)$. Although, we have chosen a specific form of the equation of state in Sec. 2, this formulation is independent of the choice of an equation of state. It depends only on whether the scale factor can be expressed analytically as a function of time or not.

Additionally, we have provided a similar formulation in the case of the anti-de Sitter spacetime for the uniformly accelerated and geodesic radial motion. The newly found radially accelerated trajectories are generalizations of the known uniformly accelerated stationary observers in the anti-de Sitter universe.

In the last part of our work we have focused on the return journey of the rocketeer. It had been suggested that having uniform deceleration would be enough in order to have an actual return journey [10]. Here we have proved that even if this condition is necessary, it is not sufficient for all spacetimes. In particular, among the cosmological models analyzed here, in the de Sitter case Eq. (75) must be satisfied for a return journey to be possible.

Acknowledgments

I am grateful to Georgios Loukes-Gerakopoulos, Giovanni Acquaviva and Jiří Bičák for valuable discussions on this work and useful comments on the manuscript.

[1] A. Friedmann. Über die krümmung des raumes. *Z. Physik*, 10:377–386, 1922.
[2] G. Lemaître. Expansion of the universe, a homogeneous universe of constant mass and increasing radius accounting for the radial velocity of extra-galactic nebulae. *Mon. Notices Royal Astron. Soc.*, 91:483–490, 1931.
[3] H. P. Robertson. Kinematics and world-structure. *Astrophys. J.*, 82:284, 1935.
[4] A.G. Walker. On milne's theory of world-structure. *Proc. London Math. Soc.*, 42:90, 1936.
[5] Marek A Abramowicz, Stanislaw Bajtlik, Jean-Pierre Lasota, and Audrey Moudens. Eppur si espande. *arXiv preprint astro-ph/0612155*, 2006.
[6] Marek A Abramowicz. Spacetime is not just space and time. *New Astronomy Reviews*, 51(10-12):799–802, 2008.
[7] Marek A Abramowicz, Stanislaw Bajtlik, Jean-Pierre Lasota, and Audrey Moudens. A short answer to critics of our article" eppur si espande"[arxiv: astro-ph/0612155]. *arXiv preprint arXiv:0812.3266*, 2008.
[8] Geraint F Lewis, Matthew J Francis, Luke A Barnes, Juliana Kwan, and J Berian James. Cosmological radar ranging in an expanding universe. *Monthly Notices of the Royal Astronomical Society*, 388(3):960–964, 2008.
[9] J. Kwan, G. F. Lewis, and J. B. James. The adventures of the rocketeer: accelerated motion under the influence of expanding space. *Publ. Astron. Soc. Aust.*, 27(1):15–22, 2010.
[10] W Rindler. Hyperbolic motion in curved space time. *Phys. Rev.*, 119(6):2082, 1960.
[11] J. S. Heyl. The long-term future of space travel. *Phys. Rev. D*, 72(10):107302, 2005.
[12] W. J. Cunningham, D. Rideout, J. Halverson, and D. Krioukov. Exact geodesic distances in flrw spacetimes. *Phys. Rev. D*, 96(10):103538, 2017.
[13] A. B. Whiting. The expansion of space: Free particle motion and the cosmological redshift. *Observatory*, 124:174, 2004.
[14] T. M. Davis, C. H. Lineweaver, and J. K. Webb. Solutions to the tethered galaxy problem in an expanding universe and the observation of receding blueshifted objects. *Am. J. Phys.*, 71(4):358–364, 2003.
[15] Ø. Grøn and Ø. Elgarøy. Is space expanding in the friedmann

universe models? *Am. J. Phys.*, 75(2):151–157, 2007.

[16] L. A. Barnes, M. J. Francis, J. B. James, and G. F. Lewis. Joining the hubble flow: implications for expanding space. *Mon. Notices Royal Astron. Soc.*, 373(1):382–390, 2006.

[17] S. W. Hawking and G. F. R. Ellis. *The large scale structure of space-time*. Cambridge university press, 1973.

[18] Ø. Grøn and S. Johannesen. Frw universe models in conformally flat-spacetime coordinates. i: General formalism. *Eur. Phys. J. C*, 126(3):28, 2011.

[19] Ø. Grøn and S. Johannesen. Frw universe models in conformally flat-spacetime coordinates ii: Universe models with negative and vanishing spatial curvature. *Eur. Phys. J. C*, 126(3):29, 2011.

[20] Ø. Grøn and S. Johannesen. Frw universe models in conformally flat-spacetime coordinates iii: Universe models with positive spatial curvature. *Eur. Phys. J. C*, 126(3):30, 2011.

[21] M. J. Chodorowski. A direct consequence of the expansion of space? *Mon. Notices Royal Astron. Soc.*, 378(1):239–244, 2007.

[22] G. F. Lewis, M. J. Francis, L. A. Barnes, and J. B. James. Coordinate confusion in conformal cosmology. *Mon. Notices Royal Astron. Soc.*, 381(1):L50–L54, 2007.

[23] J. Bičák and P. Krtouš. Accelerated sources in de sitter spacetime and the insufficiency of retarded fields. *Phys. Rev. D*, 64:124020, 2001.

[24] J. B. Griffiths and Jiří Podolský. *Exact space-times in Einstein's general relativity*. Cambridge University Press, 2009.

[25] J Podolskỳ. Accelerating black holes in anti-de sitter universe. *Czechoslovak journal of physics*, 52(1):1–10, 2002.

[26] Pavel Krtouš. Accelerated black holes in an anti-de sitter universe. *Physical Review D*, 72(12):124019, 2005.

[27] Antonio Feoli and Elmo Benedetto. Dark energy or local acceleration? *Gravitation and Cosmology*, 23(3):240–244, 2017.

[28] P. Chavanis. Cosmology with a stiff matter era. *Phys. Rev. D*, 92(10):103004, 2015.

[29] W. Rindler. *Essential relativity: special, general, and cosmological*. Springer Science & Business Media, 2012.

[30] E. A Milne. World structure and the expansion of the universe. *Nature*, 130:9, 1932.

3. Dynamical Systems

In this section, we are going to give a succinct introduction to dynamical system analysis. The dynamical system is a powerful mathematical instrument that has vast applications to different fields of science such as mathematics, physics, chemistry, biology, and medicine. Dynamics itself was proposed by Newton when he invented his laws of motion and universal gravitation. Namely, Newton was able to solve the motion of the earth around the sun which is known as the two-body problem. Later on, when physicists and mathematicians tried to solve the three-body problem, i.e., the motion of the earth, the moon and the sun, they found out this problem is too complicated to solve. Then in the late 1800s, Henry Poincaré made a breakthrough into this field. Basically, he suggested that one can study celestial mechanics by considering the qualitative behavior of the objects rather than quantitative. This was the first step to found the dynamical systems.

In the context of cosmology, the dynamical system analysis is also a useful technique for the qualitative study of the early and late time behavior of different cosmological models. Since the governing equations describing the evolution of cosmological models which are derived from the Einstein field equations (EFE) are an autonomous system of ordinary differential equations (ODE). This chapter follows mainly textbooks such as Wiggins [2003], Wainwright and Ellis [2005], Perko [2013] and the article written by Bahamonde et al. [2018] and the thesis of Tamanini [2014].

The layout of this chapter is as follows. In Sec. 3.1 basic ideas and theorems in dynamical system analysis together with fundamental definitions are provided. In Sec. 3.2 linear stability theory is presented. In Sec. 3.3 and Sec. 3.4 we will introduce the Lyapunov stability theorem and the centre manifold theorem as the methods when the linear stability theorem fails. Finally, in Sec. 3.5 we will provide an example to show how to apply these methods for a dynamical system.

3.1 Basic theorems

Principally, a well-established dynamical system is considered as an abstract system made up of a space, i.e., state space, together with a mathematical framework to explain the evolution of any particle in that space. This evolution is parameterized by τ which is considered mostly as time but it does not necessarily need to be a physical time. Moreover, the dynamical systems analysis is divided into two main parts:

- continuous dynamical systems where the evolution of the system is governed by the ODEs.
- time-discrete dynamical systems which are defined by a map or difference equations.

Note that, in studying the dynamical cosmology we are interested in the continuous dynamical systems.

To analyze a dynamical system, we choose the state space as $\mathbb{R}^n$ and a mathematical framework is given as a system of ODE of the form

$$\boldsymbol{\Omega}^{'} = \boldsymbol{f}(\boldsymbol{\Omega}), \tag{3.1}$$

where prime denotes differentiation with respect to the time τ and

$$\boldsymbol{\Omega} = (\Omega_1, \Omega_2, ..., \Omega_n) \in \mathbb{R}^n,$$

is a point in the state space. The ODE system (3.1) is called an autonomous system since the right-hand-side of (3.1) does not explicitly depend on time τ.

In order to find a solution for the ODE (3.1) which is valid for all $\tau \in \mathbb{R}$, we need to present three theorems.

Theorem 1 (Existence- Uniqueness)**.** *Consider the initial value problem*

$$\boldsymbol{\Omega}^{'} = \boldsymbol{f}(\boldsymbol{\Omega}), \qquad \boldsymbol{\Omega}(0) = \boldsymbol{a} \in \mathbb{R}^n, \tag{3.2}$$

if $\boldsymbol{f} : \mathbb{R}^n \to \mathbb{R}^n$ *is of class* $C^1(\mathbb{R}^n)$*, there exists an interval* $(-\delta, \delta)$ *and unique function* $\psi_{\boldsymbol{a}} : (-\delta, \delta) \to \mathbb{R}^n$ *such that*

$$\psi_{\boldsymbol{a}}^{'}(\tau) = \boldsymbol{f}(\psi_{\boldsymbol{a}}(\tau)), \qquad \psi_{\boldsymbol{a}}(0) = \boldsymbol{a}. \tag{3.3}$$

This theorem provides the existence of the solution only for the small interval $(-\delta, \delta)$ centred around $\tau = 0$; however, we are seeking for the solution that covers all $\tau \in \mathbb{R}$. The treatment comes from reapplying the above theorem to extend the interval. Resulting in the following theorem.

Theorem 2 (Maximality)**.** *For the ODE* $\boldsymbol{\Omega}^{'} = \boldsymbol{f}(\boldsymbol{\Omega})$ *where* $\boldsymbol{f} \in C^1(\mathbb{R}^n)$*, let* $\psi_{\boldsymbol{a}}(\tau)$ *be a unique solution of this ODE, which satisfies* $\psi_{\boldsymbol{a}}(0) = \boldsymbol{a}$*, together with* $(\tau_{\min}, \tau_{\max})$ *be a maximal range that* $\psi_{\boldsymbol{a}}(\tau)$ *is defined. If* $\tau_{\max}$ *is finite, then*

$$\lim_{\tau \to \tau_{\max}} \|\psi_{\boldsymbol{a}}(\tau)\| = +\infty. \tag{3.4}$$

Here $\|\|$ denotes the standard norm on $\mathbb{R}^n$.

This theorem is valid also for the left-hand side limit. A consequence of theorem 2 is the statement in the next corollary.

Corollary. Consider the ODE $\boldsymbol{\Omega}^{'} = \boldsymbol{f}(\boldsymbol{\Omega})$ where $\boldsymbol{f} \in C^1(\mathbb{R}^n)$, and let $D \subset \mathbb{R}^n$ be a compact set. If $\psi_{\boldsymbol{a}}(\tau)$, which is a maximally extended solution, lies in D, then this solution is defined for all $\tau \in \mathbb{R}$.

Theorem 3 (Extendibility)**.** *If* $\boldsymbol{f} : \mathbb{R}^n \to \mathbb{R}^n$ *is continuous, and there exists a constant* M *such that* $\|\boldsymbol{f}(\boldsymbol{\Omega})\| \leq M\|\boldsymbol{\Omega}\|$ *for all* $\boldsymbol{\Omega} \in \mathbb{R}^n$*, then any solutions of the ODE* $\boldsymbol{\Omega}^{'} = \boldsymbol{f}(\boldsymbol{\Omega})$ *is valid for all* $\tau \in \mathbb{R}$*.*

Therefore, according to these three theorems one can conclude that a solution for the ODE system $\boldsymbol{\Omega}^{'} = \boldsymbol{f}(\boldsymbol{\Omega})$ on $\mathbb{R}^n$ is a function $\psi : \mathbb{R} \to \mathbb{R}^n$ that satisfies:

$$\psi^{'}(\tau) = \boldsymbol{f}(\psi(\tau)), \tag{3.5}$$

for all $\tau \in \mathbb{R}$ in the domain of ψ.

Since we have the ODE's solutions for all times we can define a new concept in dynamical systems which is called a flow. The flow of the ODE is defined as a one-parameter family of maps $\{\phi_\tau\}_{\tau \in \mathbb{R}}$, of $\mathbb{R}^n \to \mathbb{R}^n$ such that

$$\phi_\tau(a) = \psi_a(\tau) \quad \text{for all} \quad a \in \mathbb{R}^n. \tag{3.6}$$

Consequently, from the (3.5) and (3.6) one can show that the vector field $\boldsymbol{f}$ is tangent to its associated orbit which can be considered as a velocity of the point in $\mathbb{R}^n$.

3.1.1 Basic definitions

In this section we are going to introduce some basic concepts and definitions in dynamical system theory.

Orbits: An orbit through each point of state space, i.e. $\mathbf{\Omega}_0$, for a given ODE and also its flow ϕ_τ is defined as

$$\gamma(\mathbf{\Omega}_0) = \{\mathbf{\Omega} \in \mathbb{R}^n \mid \mathbf{\Omega} = \phi_\tau(\mathbf{\Omega}_0)\,, \tau \in \mathbb{R}\}. \tag{3.7}$$

The most important concept in the dynamical system analysis is the notion of critical points. Mainly, we can characterize each points on the orbits as either critical points or ordinary points.

Critical point: A critical (or fixed or equilibrium) point $\mathbf{\Omega}_c \in \mathbb{R}^n$ is a point in the state space that satisfies

$$\boldsymbol{f}(\mathbf{\Omega}_c) = 0. \tag{3.8}$$

Namely, critical points are the zeros of the vector fields $\boldsymbol{f}$. Equivalently, in the context of flow, we can define the critical point as a point satisfying the condition $\phi_\tau(\mathbf{\Omega}_c) = \mathbf{\Omega}_c$ for all $\tau \in \mathbb{R}$. Moreover, from (3.7) one can see that the orbit through a critical point is the point itself, i.e. $\gamma(\mathbf{\Omega}_c) = \{\mathbf{\Omega}_c\}$.

Ordinary orbit: An orbit passing through an ordinary point is called the ordinary orbit. The ordinary orbit is the the smooth curve with the vector field $\boldsymbol{f}$ as a tangent. There are two important types of the ordinary orbits:

- Periodic orbit: for an orbit $\gamma(\mathbf{\Omega}_p)$ passing through an ordinary point $\mathbf{\Omega}_p$ exists a $T > 0$ such that $\phi_T(\mathbf{\Omega}_p) = \mathbf{\Omega}_p$. In other words, consider that the flow ϕ_τ has a periodic orbit with a period T, then the corresponding physical system shows an oscillatory behavior of period T.

- Recurrent orbit: is defined as an orbit $\gamma(\mathbf{\Omega}_r)$ such that for all neighborhoods of $\mathbf{\Omega}_r$, i.e. $N(\mathbf{\Omega}_r)$, and for all $T \in \mathbb{R}$, there exists $t > T$ in such a way that $\phi_t(\mathbf{\Omega}_r) = N(\mathbf{\Omega}_r)$. That means, if a flow ϕ_τ has a recurrent orbit, the physical system corresponding to that flow can return arbitrarily close to an earlier state.

Heteroclinic orbit: An orbit that connects distinct critical points is called a heteroclinic orbit.

Homoclinic orbit: Homoclinic orbit is an orbit that connects a critical point into itself.

Note that in heteroclinic and homoclinic orbits the critical points are not the part of the orbits. They can only be reached asymptotically, i.e. when $\tau \to \pm\infty$.

Invariant set: In the dynamical system analysis invariant sets play a key role in analyzing the systems. A set $S \subset \mathbb{R}^n$ is called an invariant set of flow ϕ_τ on $\mathbb{R}^n$ if for all $\mathbf{\Omega} \in S$ and for all $\tau \in \mathbb{R}$ we have $\phi_\tau(\Omega) \in S$. Moreover, an invariant set might have a lower dimensionality than the full parameter space. Namely, if a class of physical system is restricted, e.g. from a special property, it is described by a lower dimensional invariant set. In general, any orbits start in the invariant set remain in the invariant set as $\tau \to \pm\infty$.

So far, we have introduced some useful theorems and definitions in the theory of dynamical systems. However, finding the exact solution for the flow is equivalent to deriving the solution of the ODE which is almost impossible or rather

difficult for ODE's with $n \geq 2$. In particular, as Poincaré proposed, the aim of dynamical system analysis is to use the flow as a tool to derive the qualitative behavior of the whole family of the solutions of ODE. Therefore, by studying the vector field $\boldsymbol{f}$ we are able to determine the properties of the flow. In the next section, we will introduce a technique to do this.

3.2 Linear stability theory

To solve the dynamical system in a qualitative way, we need to know how the vector field $\boldsymbol{f}$ or equivalently the orbits behave in the vicinity of the critical points. In fact, for analyze this behavior we implement the linearization of the ODE at critical points as a first approximation method. Before we proceed to the linear stability theorem, we briefly introduce the linear ODEs in $\mathbb{R}^n$.

3.2.1 Linear ODEs

Suppose we have a linear ODE $\boldsymbol{\Omega}' = A\boldsymbol{\Omega}$ on $\mathbb{R}^n$ with the eigenvalues of A and its associated generalized eigenvectors. Three different subspaces of $\mathbb{R}^n$ can be defined as

$$\text{the stable subspace} \qquad E^s = \text{span}(\boldsymbol{e}_1, ..., \boldsymbol{e}_s), \tag{3.9}$$

$$\text{the unstable subspace} \qquad E^u = \text{span}(\boldsymbol{e}_{s+1}, ..., \boldsymbol{e}_{s+u}), \tag{3.10}$$

$$\text{the centre subspace} \qquad E^c = \text{span}(\boldsymbol{e}_{s+u+1}, ..., \boldsymbol{e}_{s+u+c}), \tag{3.11}$$

where the union of these three subspace create the $\mathbb{R}^n$, namely

$$E^s \oplus E^u \oplus E^c = \mathbb{R}^n. \tag{3.12}$$

Here, the stable subspace refers to those generalized eigenvectors $(\boldsymbol{e}_1, ..., \boldsymbol{e}_s)$ whose associated eigenvalues have the negative real parts, the unstable subspace refers to those generalized eigenvectors $(\boldsymbol{e}_{s+1}, ..., \boldsymbol{e}_{s+u})$ whose corresponding eigenvalues have the positive real parts. And the centre subspace means that the eigenvalues have the vanishing real part from the eigenvectors $(\boldsymbol{e}_{s+u+1}, ..., \boldsymbol{e}_{s+u+c})$.

Additionally, a general solution $\boldsymbol{\Omega}_s$ for a given linear dynamical system $\boldsymbol{\Omega}' = A\boldsymbol{\Omega}$ with an initial condition $\boldsymbol{\Omega}_s(\tau_0) = \boldsymbol{\Omega}_0$ is

$$\boldsymbol{\Omega}_s(\tau) = \boldsymbol{\Omega}_0 \, e^{A\,(\tau - \tau_0)}, \tag{3.13}$$

where

$$e^{A\,(\tau-\tau_0)} = \sum_{N=0}^{\infty} \frac{A^N (\tau - \tau_0)^N}{N!}. \tag{3.14}$$

Note that from solution (3.13) and the subspaces of $\mathbb{R}^n$ we conclude that

$$\boldsymbol{\Omega}_0 \in E^s \quad \textit{implies} \quad \lim_{\tau \to +\infty} \boldsymbol{\Omega}_s(\tau) = \boldsymbol{0}, \tag{3.15}$$

$$\boldsymbol{\Omega}_0 \in E^u \quad \textit{implies} \quad \lim_{\tau \to -\infty} \boldsymbol{\Omega}_s(\tau) = \boldsymbol{0}, \tag{3.16}$$

where $\boldsymbol{0}$ is the location of the critical point $\boldsymbol{\Omega}_c$. These statements claim that asymptotically all the orbits in the stable subspace converge to the critical point

whereas in the unstable subspace they diverge from the critical point. Moreover, if the state space consists of the stable subspace, i.e. $\mathbb{R}^n = E^s$, then all the orbits in the state space attract by the $\mathbf{0}$ as $\tau \to \infty$ which is called as a linear sink, while if the state space consists of unstable subspace, i.e. $\mathbb{R}^n = E^u$, all orbits in the state space repeal from the $\mathbf{0}$ as $\tau \to -\infty$, which is called as a linear source.

These results, which are obtained from the linear ODEs, are helpful to understand the notion of the linearization of the non-linear ODEs.

3.2.2 Non-linear ODEs

For a given non-linear ODE (3.1) on $\mathbb{R}^n$, where $\boldsymbol{f}$ is of class C^1, the linear approximation is given by the Taylor expansion for the vector field $\boldsymbol{f}$ around the critical point Ω_c up to the first order

$$\boldsymbol{f}(\boldsymbol{\Omega}) \simeq \boldsymbol{f}(\boldsymbol{\Omega}_c) + D\boldsymbol{f}(\boldsymbol{\Omega}_c)(\boldsymbol{\Omega} - \boldsymbol{\Omega}_c), \tag{3.17}$$

where

$$D\boldsymbol{f} = \frac{\partial \boldsymbol{f}_i}{\partial \boldsymbol{\Omega}_j} = \begin{pmatrix} \frac{\partial \boldsymbol{f}_1}{\partial \boldsymbol{\Omega}_1} & \frac{\partial \boldsymbol{f}_1}{\partial \boldsymbol{\Omega}_2} & \cdots & \frac{\partial \boldsymbol{f}_1}{\partial \boldsymbol{\Omega}_n} \\ \frac{\partial \boldsymbol{f}_2}{\partial \boldsymbol{\Omega}_1} & \frac{\partial \boldsymbol{f}_2}{\partial \boldsymbol{\Omega}_2} & \cdots & \frac{\partial \boldsymbol{f}_2}{\partial \boldsymbol{\Omega}_n} \\ \vdots & \vdots & \ddots & \vdots \\ \frac{\partial \boldsymbol{f}_n}{\partial \boldsymbol{\Omega}_1} & \frac{\partial \boldsymbol{f}_n}{\partial \boldsymbol{\Omega}_2} & \cdots & \frac{\partial \boldsymbol{f}_n}{\partial \boldsymbol{\Omega}_n} \end{pmatrix},$$

which is called the Jacobian matrix or the stability matrix of the function $\boldsymbol{f}$ at point $\boldsymbol{\Omega}_c$. The eigenvalues of $D\boldsymbol{f}$ and the associated generalized eigenvectors at each critical points are denoted by λ_i and $\boldsymbol{e}_i$ respectively. Since, the vector field vanishes at the critical point, i.e., $\boldsymbol{f}(\boldsymbol{\Omega}_c) = 0$, the Taylor expansion (3.17) reduces to

$$\boldsymbol{f}(\boldsymbol{\Omega}) \simeq D\boldsymbol{f}(\boldsymbol{\Omega}_c)(\boldsymbol{\Omega} - \boldsymbol{\Omega}_c). \tag{3.18}$$

If we reparametrize Eq.(3.18) by defining $\boldsymbol{U} = \boldsymbol{\Omega} - \boldsymbol{\Omega}_c$, namely moving the critical point to the center, the ODE (3.1) at the critical point $\boldsymbol{\Omega}_c$ becomes

$$\boldsymbol{U}' = D\boldsymbol{f}(\boldsymbol{\Omega}_c)\,\boldsymbol{U}. \tag{3.19}$$

Thus, the Eq. (3.19) is called the linearization of the ODE (3.1) at the equilibrium point $\boldsymbol{\Omega}_c$.

So far we have introduced the linearization of the ODE and we briefly introduced the linear ODEs. Actually, linear stability theorem provides a framework in which one can deduce, approximately, the stability behaviour of a critical point of the non-linear ODE from its linearization if the critical point is hyperbolic.

Hyperbolic critical point: A critical point $\boldsymbol{\Omega}_c$ for a given ODE (3.1) is a hyperbolic critical point if all eigenvalues of $D\boldsymbol{f}(\boldsymbol{\Omega}_c)$ have non-zero real part. (the critical point is called non-hyperbolic point if it's otherwise).

From this definition, we can now present the Hartman-Grobman theorem.

Theorem 4 (Hartman-Grobman)**.** *For an ODE $\boldsymbol{\Omega}' = \boldsymbol{f}(\boldsymbol{\Omega})$ on $\mathbb{R}^n$, if $\boldsymbol{f}$ is of class C^1,with flow ϕ_τ. If $\boldsymbol{\Omega}_c$ be a hyperbolic critical point, then there exists a neighbourhood N of the hyperbolic critical point such that the flow ϕ_τ is topologically equivalent to the flow of the linearization of ODE at $\boldsymbol{\Omega}_c$.*

Moreover, two flows ϕ_τ and $\tilde{\phi}_\tau$ on $\mathbb{R}^n$, are called topologically equivalent if there exists a homeomorphism $h : \mathbb{R}^n \to \mathbb{R}^n$, that maps orbits of ϕ_τ onto orbits of $\tilde{\phi}_\tau$, preserving the orientation.

Hyperbolic fixed points are divided into three categories. The critical point is called a local sink or stable point iff all the eigenvalues from $D\boldsymbol{f}(\boldsymbol{\Omega}_c)$ have negative real part, i.e., $\mathbf{Re}(\lambda_i) < 0$. On the other hand, the point is called the unstable or local source if $\mathbf{Re}(\lambda_i) > 0$. Moreover, if the eigenvalues of a given hyperbolic point have mixed sign in the real part, this point is called a saddle point.

Another important issue is to distinguish between the asymptotic behaviors of the orbits in the phase space. In other words, to see which orbits are attracted or repelled by a critical point $\boldsymbol{\Omega}_c$ as $\tau \to \infty$. To do this, we should generalize the idea of the subspaces introduced for a linear ODEs in Sec.3.2. Therefore, we shall define three differentiable manifolds as follows

$$\text{the stable manifold} \qquad W^s, \tag{3.20}$$

$$\text{the unstable manifold} \qquad W^u, \tag{3.21}$$

$$\text{the centre manifold} \qquad W^c. \tag{3.22}$$

At any critical point $\boldsymbol{\Omega}_c$ these manifolds are tangent to the corresponding subspaces of linearization at $\boldsymbol{\Omega}_c$, e.g., the W^s is tangent to E^s at the critical point $\boldsymbol{\Omega}_c$. Moreover, all the orbits in the stable manifold W^s are attracted by the $\boldsymbol{\Omega}_c$ as $\tau \to \infty$. While all the orbits in the unstable manifold W^u are attracted by the $\boldsymbol{\Omega}_c$ as $\tau \to -\infty$. However, the linear stability theory fails to predict the asymptotic behavior of the orbits in the centre manifold W^c.

3.3 Lyapunov stability theory

In the previous section, we have seen that from the linear stability theory we are not able to extract the stability properties of the orbits in the neighborhood of the non-hyperbolic critical points. Here we introduce a method which was introduced by Lyapunov to study the stability for all hyperbolic and non-hyperbolic points.

The Lyapunov method, on one hand, is a powerful method since it can be applied directly to the dynamical system. One the other hand, it's not an applicable method always since we need to determine a function, called a Lyapunov function, to study the stability.

The Lyapunov function V is defined as a continuous function in a neighbourhood of critical point $\boldsymbol{\Omega}_c$ and $V : \mathbb{R}^n \to \mathbb{R}$ be at least $\boldsymbol{C}^1$ function with the conditions

- $V(\boldsymbol{\Omega}_c) = 0$,
- $V(\boldsymbol{\Omega}) > 0$ in a neighborhood of $\boldsymbol{\Omega}_c$.

Then, the Lyapunov stability theorem claims that: if $\boldsymbol{\Omega}_c$ is a critical point for a ODE system $\boldsymbol{\Omega}' = \boldsymbol{f}(\Omega)$ with a Lyapunov function V then

- $\boldsymbol{\Omega}_c$ is stable iff $V' = \sum_{i=1}^{n} \frac{\partial V}{\partial \Omega_i} \Omega_i' = 1 \leq 0$ in a neighborhood of $\boldsymbol{\Omega}_c$,

- $\mathbf{\Omega}_c$ is asymptotically stable iff $V' < 0$ in a neighborhood of $\mathbf{\Omega}_c$,
- $\mathbf{\Omega}_c$ is unstable iff $V' \geq 0$ in a neighborhood of $\mathbf{\Omega}_c$.

In Lyapunov stability analysis the stable point is a point for which, for any neighborhood N_ϵ of $\mathbf{\Omega}_c$ there exists a neighborhood N_δ such that for $\mathbf{\Omega}_c \in N_\delta$ at τ_0 we get

$$\phi_\tau(\mathbf{\Omega}) \in N_\epsilon$$

for all $\tau > \tau_0$. Additionally, asymptotically stable refers to a critical point for which there exists a neighborhood N_δ such that for $\mathbf{\Omega}_c \in N_\delta$ we get

$$\lim_{\tau \to +\infty} \phi_\tau(\mathbf{\Omega}) = \mathbf{\Omega}_c.$$

Note that, the local sink presented in the linear stability theorem is an asymptotically stable point.

3.4 Centre manifold theorem

In this section we introduce another approach to describe the stability of non-hyperpolic critical point $\mathbf{\Omega}_c$. Although in the last section the Lyapunov theorem was introduced, this method is not an applicable method since in some cases it is almost impossible to guess the right Lyapunov function. To introduce the centre manifold theorem, we recall that in Sec. 3.2 we expand the vector field around the critical point $\mathbf{\Omega}_c$ up to the first order. To analyzing the centre manifold we use the Taylor expansion and keep the terms up to the second order, namely

$$\boldsymbol{U}' = D\boldsymbol{f}(\mathbf{\Omega}_c)\,\boldsymbol{U} + R(\boldsymbol{U}), \tag{3.23}$$

where $R(\boldsymbol{U}) = \mathcal{O}(|\ \boldsymbol{U}\ |^2)$.

To apply the centre manifold method, we should transform Eq. (3.23) to the desirable form. Therefore, one should first diagonalize the Jacobian matrix. It is know from elementary linear algebra that for a linear ODE $\boldsymbol{U}' = D\boldsymbol{f}(\mathbf{\Omega}_c)\,\boldsymbol{U}$ there exists a linear transformation T that transform the Jacobian matrix into block diagonal form

$$\begin{pmatrix} x' \\ y' \\ z' \end{pmatrix} = \begin{pmatrix} A_s & 0 & 0 \\ 0 & A_u & 0 \\ 0 & 0 & A_c \end{pmatrix} \begin{pmatrix} x \\ y \\ z \end{pmatrix}, \tag{3.24}$$

where

$$T^{-1}\boldsymbol{U} \equiv T^{-1} \begin{pmatrix} U_1 \\ U_2 \\ U_3 \end{pmatrix} = \begin{pmatrix} x \\ y \\ z \end{pmatrix},$$

where x, y, and z are vectors of certain dimensionality and A_s is an $s \times s$ matrix with the eigenvalues having negative real part, A_u is an $n \times n$ matrix which its eigenvalues have positive real part, and A_c is an $c \times c$ matrix with zero real part eigenvalues. Likewise, for a non-linear ODE, such as (3.23), we apply same linear transformation to obtain

$$\begin{aligned} x' &= A_s x + R_s(x, y, z), \\ y' &= A_u y + R_u(x, y, z), \\ z' &= A_c z + R_c(x, y, z), \end{aligned} \tag{3.25}$$

which are the appropriate form of the non-linear vector field for analyzing the centre manifold.

Before proceeding to the centre manifold analysis, we should consider whether in the dynamical system (3.25) the Jacobian of the non-hyperbolic critical point has both A_s and A_u non zero, the corresponding non-hyperbolic critical point represents as an unstable point and it is considered as a saddle point. However, the situation is different when either A_s or A_u is vanishing. Thus, the centre manifold analysis is implemented only in these two cases:

- For $E^u = \{\emptyset\}$, if the point is an attractor or a saddle as $\tau \to +\infty$.
- For $E^s = \{\emptyset\}$, if the point is a past attractor or a saddle as $\tau \to -\infty$.

In the following we will assume that the autonomous system has $E^u = \{\emptyset\}$. Then the case of $E^s = \{\emptyset\}$ is also treated in the similar way by performing the analysis as $\tau \to -\infty$.

Now, lets consider the dynamical system in the form

$$\begin{aligned} x' &= A_s x + R_s(x, z), \\ z' &= A_c z + R_c(x, z). \end{aligned} \tag{3.26}$$

where

$$\begin{aligned} R_s(0,0) &= 0, & DR_s(0,0) &= 0, \\ R_c(0,0) &= 0, & DR_c(0,0) &= 0. \end{aligned} \tag{3.27}$$

Definition: If an invariant manifold can be locally represented as

$$W^c(0) = \{(x, z) \in E^s \times E^c \mid x = \mathbf{h}(z), \mid z \mid < \delta, \mathbf{h}(0) = 0, D\,\mathbf{h}(0) = 0\}, \tag{3.28}$$

for a reasonably small δ, this invariant manifold is called a centre manifold. In other words, a centre manifold is described by a function $\mathbf{h} : E^c \mapsto E^s$. The conditions $\mathbf{h}(0) = 0$ and $D\,\mathbf{h}(0) = 0$ imply that the w^c is tangent to E^c at $u_3 = 0$.

By introducing these three theorems, we are able to analyse the stability of orbits in centre manifold (using z at this point is somehow obscured since z is the original coordinate for the vector field). Hereafter, we will use z instead of u since it is usually done in the literature.

Theorem 5 (Existence)**.** *there exists a* $\boldsymbol{C}^r$ *centre manifold which restricts the dynamics of the system* (3.26) *by the c-dimensional vector field as follows*

$$u' = A_c u + f(\boldsymbol{h}(u), u), \qquad u \in E^c. \tag{3.29}$$

Here we used the new notation u instead of z to emphasize that, in general, the restriction of the vector field to the center manifold is a vector field on a nonlinear surface.

Theorem 6 (Stability)**.** *i) If the zero solution of* (3.29) *is either stable, asymptotically stable, or unstable; the zero solution of* (3.26) *is also stable, asymptotically stable, and unstable respectively. ii) Consider that the solution of* (3.29) *is stable. Then, if* $(x(\tau), z(\tau))$ *is a solution of* (3.26) *with sufficiently small* $(x(0), z(0))$*, there exists a solution* $u(\tau)$ *from* (3.29) *that as* $\tau \to \infty$ *we get*

$$\begin{aligned} x(t) &= \boldsymbol{h}(u(\tau)) + \mathcal{O}(e^{-\gamma\tau}), \\ z(t) &= u(\tau) + \mathcal{O}(e^{-\gamma\tau}), \end{aligned} \tag{3.30}$$

where $\gamma > 0$ *is a constant.*

In order to compute the stability of a given non-hyperbolic critical point from centre manifold, we should first derive the function $\boldsymbol{h}(z)$ in advance. To do this we should follow these steps:

- Any point on $W^c(0)$ with the coordinates (x, z) should satisfy

$$x = \boldsymbol{h}(z). \tag{3.31}$$

- Derivative of (3.31) with respect to time should satisfy

$$x' = D\boldsymbol{h}(z)z'. \tag{3.32}$$

- Since any point on $W^c(0)$ has to obey the dynamical system (3.26), thus substituting

$$\begin{aligned} x' &= A_s\boldsymbol{h}(z) + R_s(\boldsymbol{h}(z), z), \\ z' &= A_c z + R_c(\boldsymbol{h}(z), z), \end{aligned} \tag{3.33}$$

  in to (3.32), gives

$$A_s\boldsymbol{h}(z) + R_s(\boldsymbol{h}(z), z) = D\boldsymbol{h}(z)[A_c z + R_c(\boldsymbol{h}(z), z)]. \tag{3.34}$$

- The latter equation can be re-arrange and written in the quasilinear partial different equation

$$\mathcal{N}(\boldsymbol{h}(z)) \equiv A_s\boldsymbol{h}(z) + R_s(\boldsymbol{h}(z), z) - D\boldsymbol{h}(z)[A_c z + R_c(\boldsymbol{h}(z), z)] = 0. \tag{3.35}$$

  This equation must be satisfied in order to be a centre manifold.

However, solving the equation (3.35) in some cases is rather more difficult than the original problem; But, there is a theorem which provides an approximation solution to calculate the function $h(z)$.

Theorem 7 (Approximation)**.** *Let $\phi : \mathbb{R}^c \to \mathbb{R}^s$ be a C^1 mapping with $\phi(0) = D\phi(0) = 0$ such that $\mathcal{N}(\phi(z)) = \mathcal{O}(\mid z \mid^q)$ az $z \to 0$ for some $q > 1$, then*

$$\mid \boldsymbol{h}(z) - \phi(z) \mid = \phi(\mid z \mid^q) \qquad\qquad as \quad z \to 0, \tag{3.36}$$

This theorem allows us to determine the center manifold to any desired degree of accuracy by solving (3.35) to the same degree of accuracy. Namely, this theorem suggests that to find the unknown function $\boldsymbol{h}(z)$ approximately, one can simply use the power series expansion of $h(z)$ and substitute it in (3.35), then calculate the $h(z)$ up to the desired order of accuracy. The following example makes it more clear.

3.5 An explicit example

In this section, we present an example of a dynamical system taken from Bahamonde et al. [2018].

3.5.1 Changing variables

We start the example from following autonomous system

$$\begin{aligned} u^{'} &= \frac{1}{8}[\gamma - 26 + 36v - (6\gamma + 4)u - (8\gamma + 1)u^3 \\ &\quad +(12\gamma - v + 3)u^2 + (v^2 - 2v)u + v^3 - 13v^3], \qquad (3.37) \\ v^{'} &= \frac{1}{8}[18 + \gamma - 20v - (6\gamma - 4)u - (8\gamma + 1)u^3 \\ &\quad +(12\gamma - v + 3)u^2 + 3v^2 + v^3 + (v^2 - 2v)u], \qquad (3.38) \end{aligned}$$

where γ is an arbitrary parameter. It can be verified that this dynamical system has a critical point located at $(u, v) = (1/2, 3/2)$. Therefore, the first step is to shift the critical point to the origin using the following transformation

$$U = u - \frac{1}{2}, \qquad V = v - \frac{3}{2}. \qquad (3.39)$$

With these new transformed variable the system becomes

$$U^{'} = \frac{1}{8}[-4U + 4V - U^3(8\gamma + 1) - U^2V + UV^2 + V^3 - 8V^2], \qquad (3.40)$$

$$V^{'} = \frac{1}{8}[-4V + 4U - U^3(8\gamma + 1) - U^2V + UV^2 + V^3 + 8V^2]. \qquad (3.41)$$

Although the critical point is at the center, the system (3.40)-(3.41) is not in the form of (3.26). At this point, we need to diagonalize the Jacobian matrix. In order to do this, we compute the Jacobian matrix at the origin

$$J\Big|_{U=0,V=0} = \frac{1}{2}\begin{pmatrix} -1 & 1 \\ 1 & -1 \end{pmatrix}. \qquad (3.42)$$

Then, by using the standard linear algebra method, we write

$$\frac{1}{2}\begin{pmatrix} -1 & 1 \\ 1 & -1 \end{pmatrix} = \begin{pmatrix} 1 & -1 \\ 1 & 1 \end{pmatrix}\begin{pmatrix} 0 & 0 \\ 0 & -1 \end{pmatrix}\begin{pmatrix} 1/2 & 1/2 \\ -1/2 & 1/2 \end{pmatrix} = T^{-1}DT, \qquad (3.43)$$

where D matrix is the diagonalized matrix, T matrix is the matrix of eigenvectors and T^{-1} is its inverse. To derive the transformed coordinates, we use

$$\begin{pmatrix} x \\ y \end{pmatrix} = T^{-1}\begin{pmatrix} U \\ V \end{pmatrix} = \begin{pmatrix} 1/2 & 1/2 \\ -1/2 & 1/2 \end{pmatrix}\begin{pmatrix} U \\ V \end{pmatrix}, \qquad (3.44)$$

or $U = x - y$ and $V = x + y$. By substituting this result into the dynamical system (3.40) and (3.41), we arrive at

$$x' = x^2y - \gamma(x - y)^3, \qquad (3.45)$$

$$y' = -y + (x + y)^2. \qquad (3.46)$$

Thus, by doing these transformations, the dynamical system is now in the form of (3.26) where $A_c = 0$, $A_s = -1$, $R_c(x, y) = x^2y - \gamma(x - y)^3$, and $R_s(x, y) = (x + y)^2$.

The dynamical system (3.45)-(3.46) is the desired form of the dynamical system; therefore, now we are able to apply either the Lyapunov stability or the centre manifold to analyse the stability of the non-hyperbolic critical point.

3.5.2 Lyapunov stability

In order to apply the Lyapunov method, one has to guess the appropriate form of the Lyapunov function. Therefore, we begin with the following Lyapunov function

$$V = \frac{1}{2}x^2 + \alpha y^4, \tag{3.47}$$

where α is a positive constant. It is clear that this function satisfies the first two conditions, namely $V(0,0) = 0$ and $V > 0$ in a neighborhood of the critical point. To analyse the stability, the $V^{'}$ at the critical point should be evaluated. Therefore

$$V^{'} = x^3 y + 4\alpha y^3((x+y)^2 - y) - \gamma x(x-y)^3. \tag{3.48}$$

This equation indicates that in the neighborhood of the origin, only the quartic terms dominate. Thus, this function might satisfy $V^{'} < 0$ for some values of α. Moreover, we can also change the coordinate to the polar coordinate, to see it more explicitly. By substituting $x = r\cos(\phi)$ and $y = \sin(\phi)$ we get

$$V^{'} = (-4\alpha \sin^4\phi - \gamma\cos\phi(\cos\phi - \sin\phi)^3 + \sin\phi\cos^3\phi)r^4 + \mathcal{O}(r^5). \tag{3.49}$$

This equation implies that for $\gamma > 0$ it is enough to choose a reasonably large α to ensure that $V^{'}$ is negative. On the other hand, for $\gamma \leq 0$ the Lyapunov function is not a suitable choice since $V^{'}$ will not be negative for all values of ϕ.

These calculation proves that the critical point is globally asymptotically stable for $\gamma > 0$.

3.5.3 Centre manifold

In this section we apply the centre manifold theorem to investigate the stability of the non-hyperbolic critical point for the dynamical system (3.45)-(3.46). To do this, we should substitute A_s, A_c, R_s and R_c that we found in Sec. (3.5.1) into the Eq. (3.35) as follows

$$\boldsymbol{h}'(x)[x^2\boldsymbol{h}(x) - \gamma(x - \boldsymbol{h}(x))^3] + \boldsymbol{h}(x) - (x + \boldsymbol{h}(x))^2 = 0. \tag{3.50}$$

Deriving the explicit for of the $\boldsymbol{h}(x)$ is almost impossible; however, from the approximation theorem one can use the power expansion of $\boldsymbol{h}(x)$ as

$$\boldsymbol{h}(x) = ax^2 + bx^3 + cx^4. \tag{3.51}$$

The next step is to substitute the former equation into the Eq. (3.50) which becomes

$$(a-1)x^3 + (b-2a)x^3 + (c - 3b - a^2 - 2\gamma a)x^4 = 0, \tag{3.52}$$

where we keep the terms up to the forth order. Since this equation has to be valid for all power of x, we can deduce that

$$a = 1, \qquad b = 2, \qquad c = 5 + 2\gamma, \tag{3.53}$$

and also

$$\boldsymbol{h}(x) = x^2 + 2x^3 + (5 + 2\gamma)x^4 \tag{3.54}$$

Moreover, function $\boldsymbol{h}(x)$ together with Eq.(3.29) enable us to analyze the dynamics of the system reduced to the centre manifold, which becomes

$$u' = -\gamma u^3 + (1+3\gamma)u^4 + \mathcal{O}(u^5). \tag{3.55}$$

Now the stability of the point can be verified from Eq. (3.55). Thus, one can see that this point is stable for $\gamma > 0$ and unstable for $\gamma \leq 0$. Fig. 3.1 illustrates the phase space for $\gamma > 0$,$\gamma < 0$, and $\gamma = 0$. Its is clear in Fig 3.1a that the orbits along the centre manifold, i.e. the orange line, are attracting from the critical point. However, Fig. 3.1b shows that orbits are repelling from the critical point along the centre manifold. For the case $\gamma = 0$ in Fig. 3.1c we see that orbits are attracted by one direction and repelled from another direction.

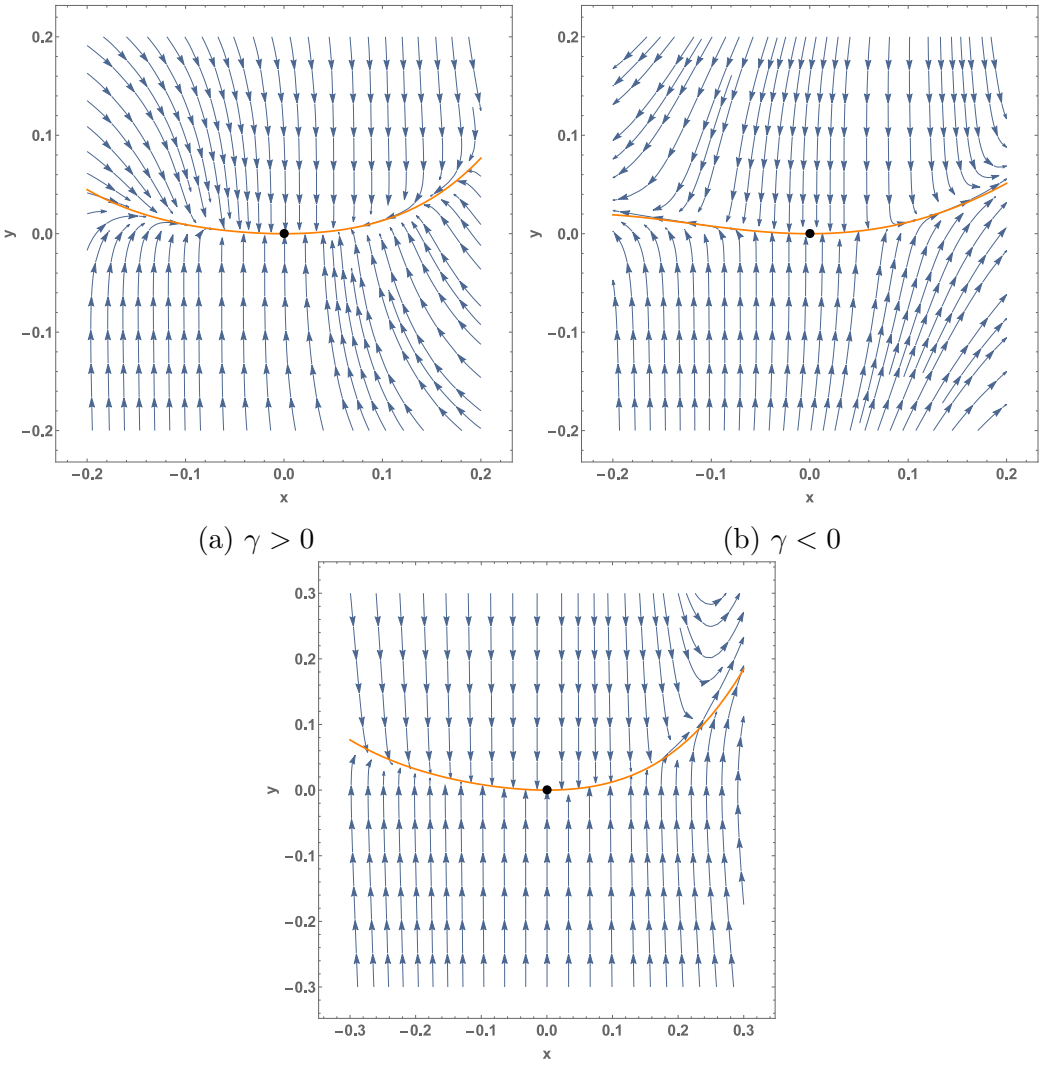

(a) $\gamma > 0$ (b) $\gamma < 0$

(c) $\gamma = 0$

Figure 3.1: Phase space portraits of the autonomous system (3.45)- (3.46) in the vicinity of the critical point for $\gamma > 0$, $\gamma < 0$, and $\gamma = 0$. The Orange line represent the centre manifold (3.54).

4. Dynamical cosmology

In the previous chapters, we presented succinct introductions to the modern cosmology and the dynamical systems analysis. In Chapter 1, we have seen that the governing equations describing the evolution of the universe are systems of ODEs. Hence, dynamical system analysis would be an elegant way to investigate the global behaviours of any cosmological model. By choosing the proper dynamical variables for a given cosmological model, one can derive its autonomous system. Then, we are able to analyse the features of the parameter space by determining and analysing the critical points, anomalies, and orbits in this space. This procedure provides a good insight on the global features of a cosmological model.

The layout of this chapter is as follows. Sec. 4.1 introduces the necessary steps that should be done in order to determine a dynamical cosmology system. This section drives from the text books Wainwright and Ellis [2005] and Coley [2013] and the article written by Wainwright and Lim [2005]. In Sec.4.2, we will implement the dynamical systems analysis to a specific cosmological model, namely the minimally coupled scalar field with an unspecified potential together with matter. The Sec. 4.3 is in fact a continuation of the Sec. 4.2 in which the form of potential is specified. These last two sections are given in this chapter in order to provide a pedagogical example showing how this dynamical analysis works. In these two sections, we mainly use the result of the work done by Copeland et al. [1998].

4.1 General framework

One of the reasons that we would like to apply dynamical systems analysis in the context of cosmology is that we want to describe the evolution of a cosmological model near the initial singularity as a source or past attractor of a dynamical system and late-time evolution as a sink or a future attractor of a dynamical system. From the governing equations in the FRW cosmology, namely the Friedmann, Raychaudhuri, and Kein-Gordon equations, one can not study these asymptotic behaviours since the physical variables tend to either diverge or vanish near the initial singularity or for late-time. Therefore, one needs to define a new set of variables, namely to normalize the physical variables, in order to achieve this goal. In the context of cosmology, the most appropriate normalization is to use the Hubble parameter as a normalization factor. One of the advantages of these new variables is that, in most cases, they are bounded. For instance, the Friedmann equation (1.13) for zero spatial curvature, in the new set of variables, takes the form

$$1 = \Omega_m = \frac{\epsilon}{3H^2}. \tag{4.1}$$

As we can see, the new variable Ω_m is dimensionless and it does not diverge or vanish at the initial singularity and for late-time. Therefore, in general, one should be able to rewrite the Friedmann equation in terms of the dimensionless variables, i.e.

$$1 = f(\Omega_1, \Omega_2, ..., \Omega_n), \tag{4.2}$$

where n refers to the number of dimensionless variables; moreover, a set of dimensionless variables creates a n-dimensional variable space. In order to create a well-defined set of dimensionless variables, each Ω_n should be defined in such a way that, each physical variable can be identified with a single dimensionless variable. By doing this, dimensionless variables have a direct physical interpretation. Thus, in this way, we transform the old variables, i.e. physical variables such as energy density ϵ, cosmological constant Λ, scalar field ψ, scalar potential $V(\psi)$, etc., to the new variables, i.e. Ω_ϵ, Ω_Λ, Ω_ψ, Ω_V, etc. This transformation is valid if the Jacobian determinant of the transformation is not singular (see e.g.Alho et al. [2016]).

Another property of this setup is that, in most cases, we can write one of these variables in terms of the other variables, i.e. as a constraint; thus, this constraint allows us to study the dynamics of the reduced system. For instance, let's consider the ΛCDM model where the matter part consists of radiation and dust. The Friedmann equation (1.54) for such a system will be

$$3H^2 = \epsilon_r + \epsilon_d + \Lambda, \tag{4.3}$$

where ϵ_r and ϵ_d refers to the energy density of radiation and dust. The Friedmann equation (4.3) in the dimensionless variables will be

$$1 = \Omega_r + \Omega_d + \Omega_\Lambda. \tag{4.4}$$

where $\Omega_r = \epsilon_r/3H^2$, $\Omega_d = \epsilon_d/3H^2$, and $\Omega_\Lambda = \Lambda/3H^2$. Since $0 < \epsilon_r$, $0 < \epsilon_d$, and $0 < \Lambda$, Friedmann equation (4.4) implies $0 < \Omega_r < 1$, $0 < \Omega_d < 1$, and $0 < \Omega_\Lambda < 1$, in other words they are bounded. Subsequently, one can obtain the constraint

$$0 < \Omega_r + \Omega_d = 1 - \Omega_\Lambda < 1, \tag{4.5}$$

and eliminate, for instance, Ω_Λ in the further analysis.

The next step is to investigate the evolution of the dimensionless variables. To do this, a new evolution parameter τ is defined as $d\tau = Hdt$. Therefore, the evolution of dimensionless variables can be written in the following form

$$\boldsymbol{\Omega}' = \boldsymbol{f}(\boldsymbol{\Omega}), \tag{4.6}$$

where $\boldsymbol{\Omega} = (\Omega_1, \Omega_2, ..., \Omega_n)$. This equation is similar to the system of ODEs, namely the autonomous systems introduced in Sec.3.1. Finally, the last step is to investigate the critical points of the autonomous system and their stabilities. Once we have found the critical points, we can look for their physical interpretation.

So far, we have presented the necessary steps that one has to follow in order to determine an autonomous system form the Friedmann equation, Raychaudhuri equation, and Klein-Gordon equation[1] together with investigation of the critical points. However, there are still some points that we would like to mention:

- In order to analyse the whole variable space, the dimensionless variables have to be bounded. However, there are some cases that some (or all) of

[1]The Raychaudhuri equation and Klein-Gordon equation are needed in order to write the autonomous systems in terms of new variables.

these variables are not bounded. In these cases, one can again define new bounded variables from dimensionless variables. For instance, in Kerachian et al. [2020], some of the dimensionless variables were not bounded. Therefore, we introduced the bounded variables from the unbounded variables.

- If the dimensionless variables are defined in such a way that physical variables are mixed, then one should be careful about the interpretation of a critical point.

- We have introduced the Hubble parameter as a normalization factor. For the cases that the spatial curvature is not vanishing, i.e. $k \neq 0$, one can define $D = \sqrt{H^2 + \mid k \mid /a^2}$ as a generalized normalization factor (see Kerachian et al. [2019] and Kerachian et al. [2020]). Subsequently, the evolution parameter is defined as $d\tau = Ddt$.

- One has to notice that, in general, there is not a unique prescription on how the dimensionless variable and the evolution parameter should be defined. What we have introduced here is the most common procedure in the dynamical cosmology analysis (See e.g. Ananda and Bruni [2006], Sami et al. [2012], and Szydłowski et al. [2014], for the different approaches).

4.2 Minimally coupled scalar field cosmology

In Sec. 1.6 we have introduced the Friedmann and the Raychaudhuri equations for a scalar field which is minimally coupled to gravity. Here we assume that the spatial curvature is zero $k = 0$ and also the matter sector is not vanishing and it has a linear EoS (1.16) as it was defined in Sec. 3.1. Moreover, we demand that the scalar field potential $V(\psi)$ is positive. Therefore, the Friedmann equation and the Raychaudhuri equation for this model read

$$3H^2 = \epsilon + \frac{1}{2}\dot{\psi}^2 + V(\psi), \tag{4.7}$$

$$2\dot{H} + 3H^2 = -w\epsilon - \frac{1}{2}\dot{\psi}^2 + V(\psi). \tag{4.8}$$

Recall that the the Klein-Gordon equation (1.69) is

$$\ddot{\psi} + 3H\dot{\psi} + V^{'}(\psi) = 0. \tag{4.9}$$

We shall define the effective energy density ϵ_e and pressure P_e as

$$\epsilon_e = \epsilon + \epsilon_\psi, \quad \text{and} \quad P_e = P + P_\psi, \tag{4.10}$$

where $\epsilon_\psi = \frac{1}{2}\dot{\psi}^2 + V(\psi)$ and $P_\psi = \frac{1}{2}\dot{\psi}^2 - V(\psi)$. Therefore, the effective EoS will be $w_e = P_e/\epsilon_e$. Introducing the effective EoS is crucial since this parameter can tell us whether the expansion of the universe is accelerating ($w_e < -1/3$) or decelerating ($w_e > -1/3$).

In order to apply the dynamical system, we rewrite the Friedmann equation (4.7) in the form

$$1 = \frac{\epsilon}{3H^2} + \frac{\dot{\psi}^2}{6H^2} + \frac{V(\psi)}{3H^2}. \tag{4.11}$$

Thus, the dynamical variables or dimensionless variables for this system are

$$\Omega_m = \frac{\epsilon}{3H^2}, \qquad \Omega_\psi = \frac{\dot{\psi}}{\sqrt{6}H}, \qquad \Omega_V = \sqrt{\frac{V(\psi)}{3}}\frac{1}{H}. \tag{4.12}$$

By using this new variable, for the effective EoS parameter we obtain

$$w_e = \Omega_\psi^2 - \Omega_V^2 + w(1 - \Omega_\psi^2 - \Omega_V^2). \tag{4.13}$$

Since we assume that the energy density and the potential should be strictly positive, each term in the right-hand side of the Eq. (4.11) is positive. Therefore, we can rewrite the Friedmann equation in the form

$$0 \leq \Omega_\psi^2 + \Omega_V^2 = 1 - \Omega_m \leq 1. \tag{4.14}$$

From the former relation, we can reduce the dimensionality of the variable space, since Ω_m can be written as a function of the other two variables. Subsequently, the autonomous system will be

$$\Omega'_\psi = \frac{\ddot{\psi}}{\sqrt{6}\,H^2} - \Omega_\psi \frac{\dot{H}}{H^2}, \tag{4.15}$$

$$\Omega'_V = \Omega_V \left(\sqrt{\frac{3}{2}}\,\Omega_{\partial V}\,\Omega_\psi - \frac{\dot{H}}{H^2}\right), \tag{4.16}$$

where prime means d/Hdt and $\Omega_{\partial V}$, which is yet another dimensionless variable, is defined as

$$\Omega_{\partial V} = \frac{\partial_\psi V}{V}. \tag{4.17}$$

Moreover, from the Raychaudhuri equation and Klein-Gordon equation we obtain

$$\frac{\dot{H}}{H^2} = \frac{3}{2}\left[(w-1)\,\Omega_\psi^2 + (w+1)\,(\Omega_V^2 - 1)\right], \tag{4.18}$$

$$\frac{\ddot{\psi}}{H^2} = -3\sqrt{6}\Omega_\psi - 3\Omega_V^2\,\Omega_{\partial V}. \tag{4.19}$$

Since, from Eq. (4.16) we defined another dynamical variable, i.e. $\Omega_{\partial V}(\psi)$, the autonomous system (4.15)-(4.16) is not closed (see e.g. Steinhardt et al. [1999] and De La Macorra and Piccinelli [2000]). Therefore, it is needed to derive an evolution equation governing the $\Omega_{\partial V}$. This equation is given by

$$\Omega'_{\partial V} = \sqrt{6}\;\Omega_{\partial V}^2\;\Omega_\psi\;(\Gamma - 1)\,, \tag{4.20}$$

where Γ is called the tracker parameter (Steinhardt et al. [1999]) and it is defined as

$$\Gamma = \frac{V\partial_\psi^2 V}{(\partial_\psi V)^2}. \tag{4.21}$$

Again, it seems that we derived another dynamical variable that the respective system is not closed. However, since both $\Omega_{\partial V}$ and Γ are functions of ψ, we can relate them to each other if $\psi(\Omega_{\partial V})$ exists (see e.g. Zhou [2008]). Namely, if the function $\Omega_{\partial V}(\psi)$ is invertible, then we can write $\psi(\Omega_{\partial V})$ and hence $\Gamma(\psi(\Omega_{\partial V}))$.

Note that the physical features of the universe do not dependent directly on the choice of $\Omega_{\partial V}$. In other words, different functions of the potential V does not change the phenomenological properties of the universe. This statement comes from the fact that the effective EoS parameter (4.13), the EoS parameter of the scalar field [2], and the relative energy density of the scalar field Ω_Ψ[3] are independent of $\Omega_{\partial V}$.

4.2.1 General features of the system

Global critical points. Before we specify the form of V, its is useful to determine the critical points of the autonomous system (4.15), (4.16), and (4.20). One can check that, for this system there is one global critical point located at

$$\{\Omega_m, \Omega_\psi, \Omega_V, \Omega_{\partial V}\} = \{1, 0, 0, \forall\}.$$

However, $\Omega_V = 0$ means that $V = 0$ and subsequently $\Omega_{\partial V} = 0$, which is not obvious from the autonomous system. This point refers to the case when the scalar field contributions vanishes and the universe is filled with barotropic matter.

Invariant subsets. One of the tools in analysing a dynamical system are the invariant subsets since they help us to characterize and understand the global properties of the phase space. From the autonomous system (4.15), (4.16), and (4.20) we can identify the invariant subsets. For this system, $\Omega_V = 0$ represents an invariant set.

One may choose $\Omega_{\partial V} = 0$ as an invariant subset. However, this choice of $\Omega_{\partial V}$ is a specific case of $\Omega_{\partial V} = \text{const.}$. This condition is equivalent to $\Gamma = 1$ and seems like an invariant subset due to Eq. (4.20). However, this is a more subtle case, because choosing a constant value of $\Omega_{\partial V}$ actually constraints the form of the potential to the exponential form $V = V_0\, e^{\Omega_{\partial V}\, \psi}$ (see, e.g., Kerachian et al. [2019]).

Symmetries. The dynamical system (4.15), (4.16), and (4.20) under the simultaneous transformation $\{\Omega_\psi, \Omega_V, \Omega_{\partial V}\} \to \{-\Omega_\psi, \Omega_V, -\Omega_{\partial V}\}$ remains invariant if $\Gamma(\Omega_{\partial V}) = \Gamma(-\Omega_{\partial V})$ satisfies.

Moreover, under the transformation $\{\Omega_\psi, \Omega_V, \Omega_{\partial V}\} \to \{\Omega_\psi, -\Omega_V, \Omega_{\partial V}\}$ the dynamical system is invariant. In other words, this transformation means that the sign of H is changing. This implies that the physical behaviour for the expanding universe $H > 0$ is the same as the contracting universe $H < 0$ if the time direction is reversed.

[2] In Sec. 1.6 we derived the EoS parameter for the minimal coupled scalar field, namely Eq.(1.72). If we substitute the new dynamical variables instead of ψ and V we obtain

$$w_\psi = \frac{P_\psi}{\epsilon_\psi} = \frac{\frac{1}{2}\dot{\psi}^2 - V(\psi)}{\frac{1}{2}\dot{\psi}^2 + V(\psi)} = \frac{\Omega_\psi^2 - \Omega_V^2}{\Omega_\psi^2 + \Omega_V^2}. \tag{4.22}$$

[3] The relative energy density of the scalar field is defined as $\Omega_\Psi = \frac{\epsilon_\psi}{3H^2} = \Omega_\psi^2 + \Omega_V^2$.

4.3 $\Gamma = 1$: Exponential potentials

By choosing a form of the potential $V(\psi)$, the system is completely specified; subsequently, the variable $\Omega_{\partial V}$ becomes redundant. One of the special cases is $\Gamma = 1$, which holds that $\Omega_{\partial V} = \text{const.}$; therefore, in this case the form of the potentials are

$$V = V_0 e^{\Omega_{\partial V}\psi}, \tag{4.23}$$

where $\Omega_{\partial V}$ is a constant and $V_0 > 0$. The autonomous systems for this spacial case are

$$\Omega'_\psi = -\frac{3}{2}\left[2\Omega_\psi + (w-1)\Omega_\psi^3 + \Omega_\psi\,(w+1)\,(\Omega_V^2 - 1) - \sqrt{\frac{2}{3}}\Omega_{\partial V}\Omega_V^2\right], \tag{4.24}$$

$$\Omega'_V = -\frac{3}{2}\Omega_V\left[(w-1)\Omega_\psi^2 + (w+1)\,(\Omega_V^2 - 1) + \sqrt{\frac{2}{3}}\Omega_{\partial V}\Omega_\psi\right]. \tag{4.25}$$

So far, we have introduced the dimensionless variables and the dynamical systems for the universe having a minimally coupled scalar field with exponential potentials together with regular matter. The next step is to determine the critical points of this system.

4.3.1 Critical points and their interpretation

In this section we are going to determine the critical points of the system with their physical interpretations. Table 4.1 and Table 4.2 summarizes all this information.

A matter dominated critical point:

The coordinate of this critical point is $\{\Omega_\psi, \Omega_V\} = \{0, 0\}$. This point (called O) has $\Omega_m = 1$ (from Eq. (4.14)) and describes a matter dominated universe with $w_e = w$. This point however is the global critical point introduce in Sec. (4.2.1) and it represents a saddle point since it has the eigenvalues

$$\{\lambda_i\} = \{\frac{3}{2}(w-1), \frac{3}{2}(w+1)\}, \tag{4.26}$$

where the $i = 1, 2$

Two stiff fluid like critical points:

These critical points are located at $\{\Omega_\psi, \Omega_V\} = \{\pm 1, 0\}$ together with $\Omega_m = 0$. At these points (called $A_\pm$), since Ω_V vanishes the universe is dominated by kinetic energy of the scalar field and the effective EoS parameter is $w_e = \Omega_\psi^2 = 1$. These points describe the stiff fluid with the scale factor $a \propto t^{1/3}$. The point A_+ which corresponds to the $\Omega_\psi = +1$ has the eigenvalues

$$\{\lambda_i^{A_+}\} = \{3(w-1), \sqrt{\frac{3}{2}}(\sqrt{6} - \Omega_{\partial V})\}. \tag{4.27}$$

Critical point	Ω_ψ	Ω_V	Ω_m	Existence	w_e
O	0	0	1	$\forall\,\Omega_{\partial V},\, w$	w
A_+	1	0	0	$\forall\,\Omega_{\partial V},\, w$	1
A_-	-1	0	0	$\forall\,\Omega_{\partial V},\, w$	1
B	$\sqrt{\frac{3}{2}}\frac{1+w}{\Omega_{\partial V}}$	$\sqrt{\frac{3(1-w)^2}{2\Omega_{\partial V}^2}}$	$1-\frac{3(1+w)}{\Omega_{\partial V}^2}$	$\Omega_{\partial V}^2 > 3(1+w)$	w
C	$\frac{\Omega_{\partial V}}{\sqrt{6}}$	$\sqrt{1-\frac{\Omega_{\partial V}^2}{6}}$	0	$\Omega_{\partial V}^2 < 6$	$\frac{\Omega_{\partial V}}{3}-1$

Table 4.1: The critical points of the dynamical system (4.24)- (4.25).

Critical point	Stability
O	Saddle
A_+	Unstable node for $\Omega_{\partial V} \leq \sqrt{6}$ Saddle point for $\Omega_{\partial V} > \sqrt{6}$
A_-	Unstable node for $\Omega_{\partial V} \geq -\sqrt{6}$ Saddle point for $\Omega_{\partial V} < -\sqrt{6}$
B	Stable node if $3\,(w+1)^2 < \Omega_{\partial V}^2 < \frac{24\,(w+1)^2}{9\,w+7}$ Stable spiral for $\Omega_{\partial V}^2 \geq \frac{24\,(w+1)^2}{9\,w+7}$
C	Stable if $\Omega_{\partial V} < -\sqrt{6}$ Saddle point if $3(1+w) \leq \Omega_{\partial V}^2 < 6$

Table 4.2: The stability of the critical points of the dynamical system (4.24)-(4.25).

This point is a saddle point if $\Omega_{\partial V} > \sqrt{6}$ and it is an unstable node or a source if $\Omega_{\partial V} < \sqrt{6}$.

However, the critical point A_- has the eigenvalues

$$\{\lambda_i^{A-}\} = \{-3(w-1), \sqrt{\frac{3}{2}}(\sqrt{6} + \Omega_{\partial V})\}. \tag{4.28}$$

This point represents a saddle point if $\Omega_{\partial V} < -\sqrt{6}$ and an unstable node if $\Omega_{\partial V} > -\sqrt{6}$.

One scaling solution critical point:

There is another critical point (called B) located at

$$\{\Omega_\psi, \Omega_V\} = \{\sqrt{\frac{3}{2}}\frac{1+w}{\Omega_{\partial V}}, \sqrt{\frac{3(1-w^2)}{2\Omega_{\partial V}^2}}\}.$$

At this point, neither the scalar field nor the regular matter dominate the universe entirely. That is why this point have been called the scaling solution by Wetterich [1988]; in other words, at the same time, we have both $0 < \Omega_\Psi < 1$ and $0 < 1 - \Omega_m < 1$, hence the universe evolution is influenced from both the regular matter and the scalar field. Moreover, point B exists if the condition $\Omega_{\partial V}^2 > 3(1+w)$ (since we have $0 < \Omega_\Psi < 1$) is satisfied. This point has the effective EoS parameter $w_e = w$ with eigenvalues

$$\{\lambda_i^B\} = \{\frac{3}{4\,\Omega_{\partial V}}\left((w-1)\,\Omega_{\partial V} - \Delta\right), \frac{3}{4\,\Omega_{\partial V}}\left((w-1)\,\Omega_{\partial V} + \Delta\right)\}, \tag{4.29}$$

where $\Delta = \sqrt{(w-1)\left[(7-9w)\,\Omega_{\partial V}^2 - 24\,(w+1)^2\right]}$. Point B represents a stable node if

$$3\,(w+1)^2 < \Omega_{\partial V}^2 < \frac{24\,(w+1)^2}{9\,w+7}$$

and a stable spiral if

$$\Omega_{\partial V}^2 \geq \frac{24\,(w+1)^2}{9\,w+7}.$$

One scalar field dominated critical point:

The last critical point (called C) of this system is located at $\{\Omega_\psi, \Omega_V\} = \{\Omega_{\partial V}/\sqrt{6}, \sqrt{1 - \Omega_{\partial V}^2/6}\}$. At this point $\Omega_m = 0$ and $\Omega_\Psi = 1$ which means that the universe is dominated by the scalar field. It exists for the range $\Omega_{\partial V}^2 < 6$ and has the effective EoS parameter $w_e = w_\psi = \Omega_{\partial V}/3 - 1$; the effective EoS implies that for $\Omega_{\partial V} < 2$ the universe undergoes an accelerated expansion. The eigenvalues of this point are

$$\{\lambda_i^C\} = \{\frac{\Omega_{\partial V}^2}{2} - 3, \Omega_{\partial V}^2 - 3(w+1)\}. \tag{4.30}$$

Point C is an attractor if $\Omega_{\partial V}^2 < 3(1+w)$ and saddle point if $3(1+w) \leq \Omega_{\partial V}^2 < 6$.

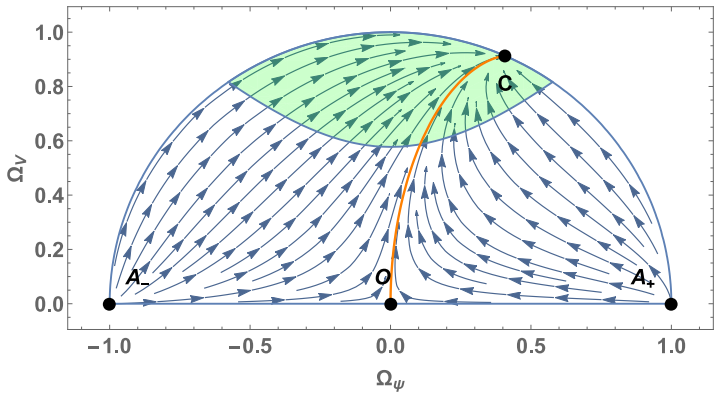

Figure 4.1: Variable space for $w = 0$ and $\Omega_{\partial V} = 1$. The orange lines denotes the separatrice of the system and the green shaded regions is the part of the parameter space where the universe is accelerating, i.e. $w_e < -1/3$. The points $A_\pm$ are the past attractors while the point C is the future attractor represent an accelerating expansion phase.

4.3.2 Parameter space portraits

In the previous section, we derived the critical points of the dynamical system (4.24)- (4.25) with their stability conditions and their interpretations. In this section, we would like to plot the parameter space portraits for different values of $\Omega_{\partial V}$. According to the Table 4.1 and Table 4.2, there are three regions for $\Omega_{\partial V}$ where the qualitative features of the parameter space remain similar; these regions are: $0 < \Omega^2_{\partial V} < 3(1+w)$, $3(1+w) < \Omega^2_{\partial V} < 6$, and $6 < \Omega^2_{\partial V} < \infty$. In the following (Figs. 4.1, 4.2, and 4.3), we plot the parameter spaces for these three regions with $w = 0$. Since we are interested in the late time accelerated expansion and also the transitions between matter dominated era to the dark energy epoch, choosing the matter EoS parameter $w = 0$ would be a suitable choice.

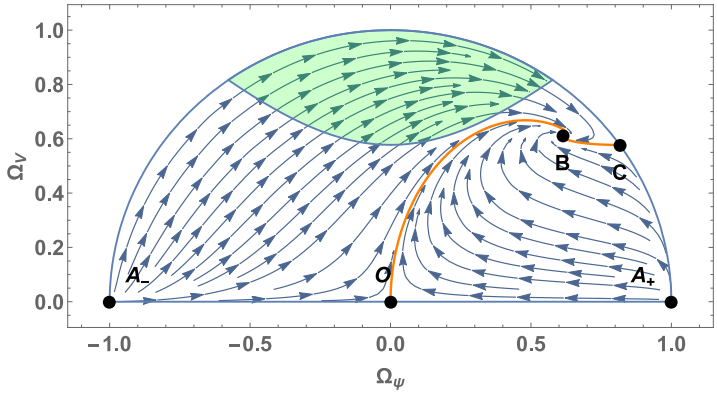

Figure 4.2: Variable space for $w = 0$ and $\Omega_{\partial V} = 2$. The orange lines denotes the separatrice of the system and the green shaded regions is the part of the parameter space where the universe is accelerating. Here, the points $A_\pm$ are the past attractors and the pont B is the future attractor.

The first region, i.e. $0 < \Omega^2_{\partial V} < 3(1 + w)$, is plotted in Fig. 4.1. This figure is divided into two subregions from the separatrice or the heteroclinic orbit connecting points O to C (the orange line). Both subregions start from the stiff

fluid dominated areas (points $A_{\pm}$), pass through a matter dominated phase in case they approach point O, and going toward the point C; where point C is the scalar field dominated area.

The second region is depicted in Fig. 4.2. Here the parameter space is divided into two subregions from two separatrices, i.e. the separatrices that connect the point O to the point B and point B to the point C. Both subregions start from stiff fluid (points $A_{\pm}$), pass through both a matter dominated phase (point O) and also scalar field dominated phase (point C), then going towards the scaling solution point B.

For the region $6 < \Omega_{\partial V}^2 < \infty$, the parameter phase space illustrates in Fig. 4.3. Here, the past attractor is only the point A_{-} and the other stiff fluid critical point A_{+} is a saddle point. Although there is a separatrix in this region, it does not split the parameter space into two distinct subregions. Same as the previous cases, here the matter dominated phase O is a saddle point; however, the scaling solution is the future attractor.

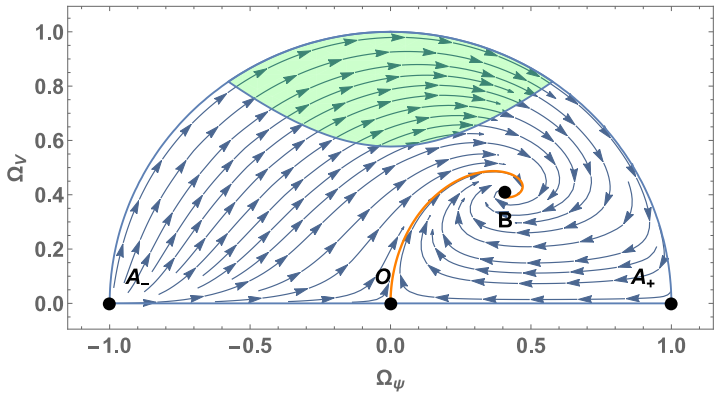

Figure 4.3: Variable space for $w = 0$ and $\Omega_{\partial V} = 3$. The orange lines shows the separatrice of the system and the green shaded regions is the part of the parameter space where the universe is accelerating. Here, the point A_{-} is the past attractor and the pont B is the future attractor.

So far, we have presented a minimally coupled scalar field having an exponential potential together with the regular matter. This model is one of the most interesting models in dynamical cosmology in the sense of simplicity. Namely, in this model, the three dimensional dynamical system reduces to the two dimensional dynamical system; the parameter space is compact and there are no anomalies. Moreover, the asymptotic features of the system can be determined from the behaviors of the critical points. Similar analysis by including both radiation and matter (dust and/or dark matter), by considering two barotropic fluids, has been done by Azreg-Aïnou [2013]. In our analysis, we considered only the case $V > 0$; however, the dynamical system of scalar field with negative exponential potentials was done by Heard and Wands [2002].

5. Dynamic of barotropic fluids

This chapter is based on the paper Kerachian et al. [2020] " Dynamics of classes of barotropic fluids in spatially curved FRW spacetimes", published in Physical Review D. Here, we presented the version from arXiv.

In the first part of this work, we studied the dynamics of a cosmological model with unspecified EoS, without the cosmological constant Λ, in the spatially curved FRW spacetime. From the Friedmann equation, we derived the dimensionless variables in such a way that the variables are well-defined and valid for all curvatures. Therefore, the autonomous systems were derived from the dimensionless variables for both positive and non-positive curvatures. We defined a tracker-like parameter Γ; this parameter enables us to encode the EoS. Subsequently, general features of the Γ together with the critical points of the system their cosmological interpretations analyzed. For this general setup, we identified that there are three critical lines in the system:

- two de Sitter critical lines for the case $k = 0$,
- one static universe critical line for the case $k \leq 0$.

In the second part of the paper, we provided two examples to show how this formalism can be used.

In the first example, we allied some conditions on Γ, such as causality condition, and consequently we could determine the EoS. This EoS represents a linear superposition of an exotic fluid with stiff matter. For large energy densities, the stiff matter part of EoS takes over; however, for low energy densities the other part, i.e. the exotic part, dominates.

In the second example, we analyzed the quadratic EoS in our framework. Since the quadratic EoS was analyzed previously by Ananda and Bruni [2006], we made a comparison with their findings.

Dynamics of classes of barotropic fluids in spatially curved FRW spacetimes

Morteza Kerachian,[1,*] Giovanni Acquaviva,[1,†] and Georgios Lukes-Gerakopoulos[2,‡]

[1] *Institute of Theoretical Physics, Faculty of Mathematics and Physics, Charles University, CZ-180 00 Prague, Czech Republic*

[2] *Astronomical Institute of the Academy of Sciences of the Czech Republic, Boční II 1401/1a, CZ-141 00 Prague, Czech Republic*

In this article we perform dynamical analysis of a broad class of barotropic fluids in the spatially curved Friedmann-Robertson-Walker (FRW) spacetime background without considering the cosmological constant. The first part of our study concerns the dynamics of a fluid with an unspecified barotropic equation of state (EoS) having as the only assumption the non-negativity of the fluid's energy density. After defining a new set of dimensionless variables and a new evolution parameter, we introduce the function Γ that encodes the EoS. In this general setup several features of the system are identified: critical points, invariant subsets and the characteristics of the function Γ, along with their cosmological interpretations. The second part of our work provides two examples with specific Γ functions. In the first example we provide a Γ function and then we exhibit how it can be trimmed down to a specific class of EoS through physical arguments, while in the second example we discuss the quadratic EoS studied in Phys.Rev. D **74**, 023523 (2006) by comparing our approach with their analysis.

PACS numbers:
Keywords: Gravitation, Cosmology; Dynamical systems

1. INTRODUCTION

On large scales, the Universe appears to be homogeneous and isotropic [1]: hence the Friedmann-Robertson-Walker (FRW) model still seems relevant in approximating its evolution. Moreover, considering a non-zero curvature of the spatial slices seems to be observationally relevant and might help in alleviating some tensions in cosmology [2, 3]. From the point of view of the source in Einstein's field equations, barotropic fluids are the first step in describing the matter content of the Universe. The above setting is a common starting point for studies trying to describe important cosmological aspects, such as the phenomenological behaviour of the dark sector. In such a setup one can, for instance, describe a multi-fluid source by a single phenomenological equation of state, such as in the case of Generalized Chaplygin Gas [4] or Logotropic fluids [5].

For a FRW cosmology with only a fluid component, the Friedmann equation and the Raychaudhuri equation are respectively given by

$$H^2 + \frac{k}{a^2} = \frac{\epsilon}{3}, \tag{1}$$

$$2\,\dot{H} + 3\,H^2 + \frac{k}{a^2} = -P\,, \tag{2}$$

while the continuity equation for the energy density is

$$\dot{\epsilon} + 3\,H(P+\epsilon) = 0\,, \tag{3}$$

where a is the scale factor, k is the spatial curvature, $H = \frac{\dot{a}}{a}$ is the Hubble expansion rate, $\dot{}$ denotes derivative with respect to the coordinate time, ϵ is the energy density and P is the pressure of the barotropic fluid. Once the EoS is given, *i.e.* $P = P(\epsilon)$, the system is closed and it is in principle possible to provide the scale factor as function of the energy density:

$$a = a_0 \exp\left(-\frac{1}{3}\int_{\epsilon_0}^{\epsilon} \frac{d\epsilon}{\epsilon + P(\epsilon)}\right), \tag{4}$$

where subscripts 0 denote integration constants resulting from integrating evolution equations, like the Raychaudhuri and the continuity equations. In this way the problem is reduced to solving a single second order ordinary differential equation (ODE) and it seems trivial. However, the integral in Eq. (4) is not necessarily easy to calculate and the resulting ODE might be difficult to treat. Of course, in order to address the problem in this manner, one has to know first the EoS.

In our study we analyse the dynamics of barotropic fluids in spatially curved FRW without specifying the EoS. The only assumption is that $\epsilon \geq 0$, while we do not impose any restrictions on the pressure P. Allowing pressure to attain negative values allows us to describe cosmological models driven by one fluid with a phenomenological EoS which can end with an accelerated expansion. During the evolution of the models such a fluid can have a standard behavior, *i.e.* the speed of sound $0 \leq c_s^2 \leq 1$, but also more exotic cases. Analysis of cosmological models including fluids with rather general EoS can be found in the literature. In [6, 7] the authors study the general properties of barotropic EoS: although a linear relation between energy density and pressure is implied, the proportionality parameter has a generic dependence on the scale factor. In [8] a dynamical analysis

*Electronic address: kerachian.morteza@gmail.com
†Electronic address: gioacqua@gmail.com
‡Electronic address: gglukes@gmail.com

of a generic real gas is performed in the parameter space spanned by the Hubble function H, the number density n and the temperature T of the gas. A quite general equation of state has been considered in [9] with the aim of studying future cosmological singularities. On the other hand, attempts to determine the form of EoS from observations can be found, for example, in [10] (see also [11] for a review).

A general functional form of dark energy has been considered in various settings: for instance, in [12] the cosmological consequences of a time-dependent Λ were discussed. A varying cosmological constant can be interpreted as a particle creation process, which has been discussed for example in [13], while an attempt to reconstruct dark matter/dark energy interaction through particle creation has been presented in [14].

The analysis that we carry out in the present paper takes inspiration from dynamical analysis of scalar fields in cosmology: in the simplest models describing a scalar field with an unspecified potential, general features regarding the dynamics of the system can be inferred by inspecting the properties of the so-called "tracker parameter", which depends on second derivatives of the potential (see [15]). Similarly, we will relate the global and asymptotic behaviour of entire classes of EoS to the properties of a function which depends on second derivatives of the pressure $P(\epsilon)$. An analogous study has been carried out in [16] for the generic functional form $P = P(H)$.

2. THE DYNAMICAL SYSTEM

In order to compose well-defined dimensionless variables which are valid for both $k > 0$ and $k \leq 0$ one can introduce the normalization $D^2 = H^2 + |k|/a^2$. Thus, we construct the new dimensionless variables as follows

$$\Omega_\epsilon = \frac{\epsilon}{3\,D^2} \quad , \quad \Omega_H = \frac{H}{D}\,, \tag{5}$$

$$\Omega_P = \frac{P}{D^2} \quad , \quad \Omega_{\partial P} = \frac{\partial P}{\partial \epsilon}\,, \tag{6}$$

$$\Gamma = \frac{\partial^2 P}{\partial \epsilon^2}\epsilon\,. \tag{7}$$

The Jacobian determinant of the above transformation is

$$\det J = -\frac{\Gamma}{3D^7}, \tag{8}$$

which implies that the transformation is singular when $\Gamma = 0$. We will discuss in detail the implications of this singularity in Sec. 4, here we just mention that when $\Gamma = 0$ then $\Omega_{\partial P}$ becomes redundant and the dimensionality of the system is reduced. Note also that the EoS is defined by the parameter Γ. Since we allow $\partial P/\partial\epsilon$ to be negative, we relax its interpretation as speed of sound and instead of denoting it as c_s^2 we have renamed it $\Omega_{\partial P}$.

In order to recast the evolution equations as an autonomous system, we take derivatives of the dimensionless variables with respect to the evolution parameter τ, related to the cosmic time by $d\tau = D\,dt$. This time parameter is well-defined throughout the whole cosmic evolution, in particular during possible recollapsing or bouncing scenarios where $H = 0$. The resulting system is given by

$$\Omega'_\epsilon = -\Omega_H \left[\Omega_p + \Omega_\epsilon \left(3 + 2\left(\frac{\dot H}{D^2} + \Omega_H^2 - 1\right)\right)\right], \tag{9}$$

$$\Omega'_H = \left(1 - \Omega_H^2\right)\left(\frac{\dot H}{D^2} + \Omega_H^2\right), \tag{10}$$

$$\Omega'_P = -\Omega_H \left[3\Omega_{\partial P}\left(\Omega_P + 3\Omega_\epsilon\right) + 2\Omega_P\left(\frac{\dot H}{D^2} + \Omega_H^2 - 1\right)\right], \tag{11}$$

$$\Omega'_{\partial P} = -\Omega_H \left(\frac{\Omega_P}{\Omega_\epsilon} + 3\right)\Gamma\,. \tag{12}$$

2.1. Positive curvature

When $k > 0$, the Friedmann equation can be expressed in terms of the variables Eqs. (5)-(7) in the following form:

$$\Omega_\epsilon = 1\,. \tag{13}$$

From Raychaudhuri equation we get

$$\frac{\dot H}{D^2} = -\frac{1}{2}\left(\Omega_P + 1\right) - \Omega_H^2\,. \tag{14}$$

2.2. Non-positive curvature

Applying the same definitions given by Eqs. (5)-(7) to the case of non-positive spatial curvature $k \leq 0$, one can reexpress the Friedmann constraint (1) as

$$\Omega_\epsilon = 2\,\Omega_H^2 - 1, \tag{15}$$

and the Raychaudhuri equation (2) as

$$\frac{\dot H}{D^2} = -\frac{1}{2}\left(\Omega_P + 1\right) + \left(1 - 2\Omega_H^2\right). \tag{16}$$

Since by definition $\Omega_H^2 \leq 1$ and by assumption $\epsilon \geq 0$, Eq. (15) implies that $0 \leq \Omega_\epsilon \leq 1$ and $\frac{1}{2} \leq \Omega_H^2 \leq 1$. However, as we will see, the system of evolution equations does not include automatically the requirement of positivity of energy and the trajectories might cross towards the negative energy regions: hence, we will have to select by hand the parts of variable space that we consider physically plausible.

3. CRITICAL POINTS AND THEIR INTERPRETATION

The critical elements of the system are those values of the variables such that $\mathbf{\Omega}' = 0$. Once the critical points are found, one can provide a cosmological interpretation in terms of the *deceleration parameter*

$$\begin{aligned} q &= -1 - \frac{\dot{H}}{H^2} \\ &= -1 - \Omega_H^{-2} \frac{\dot{H}}{D^2}\,, \end{aligned} \tag{17}$$

where we used the definition of Ω_H. From the Raychaudhuri Eq. (14) for positive curvature we see that, in order to have accelerated expansion, *i.e.* $q < 0$, one needs $\Omega_P < -1$. For the negative curvature case, by using Eq. (16), one has instead $\Omega_P < 1 - 2\,\Omega_H^2 = -\Omega_\epsilon$. Thus, of course, having negative pressure is a necessary but not sufficient condition for accelerated expansion.

3.1. Two de Sitter critical lines

The system presents two critical lines with a de Sitter behavior, with coordinates $\{\Omega_\epsilon, \Omega_H, \Omega_P, \Omega_{\partial P}\} = \{1, \pm 1, -3, \forall\}$. Note that since Γ has not yet been defined, these critical elements are independent of the EoS of the fluid. Specific choices of EoS can provide certain values for $\Omega_{\partial P}$, as we will show later on.

Taking into account the definitions of Ω_ϵ and Ω_P, for both of these lines one could claim that $P = -\epsilon$, which would imply that $\Omega_{\partial P} = -1$. However, this is not the case, since at this point the EoS is still kept unspecified. Actually, as we will see in Sec. 5, once an EoS is specified this critical point corresponds to the intersection between the function $P = P(\epsilon)$ and the $P = -\epsilon$ line.

The line with $\Omega_H = 1$ (called A_+) has the typical cosmological constant behaviour given by $q = -1$. The corresponding eigenvalues are

$$\{\lambda_i^{A_+}\} = \{-2, 0, -3\,(1 + \Omega_{\partial P})\}. \tag{18}$$

Thus, Eq. (18) implies that for $\Omega_{\partial P} < -1$ critical points along the line A_+ are saddles. If $\Omega_{\partial P} \geq -1$ the center manifold theorem does not provide the stability, thus we will discuss it through numerical examples for specific Γ.

The line with $\Omega_H = -1$ (called A_-) describes an exponentially shrinking universe with $q = -1$. The eigenvalues in this case are

$$\{\lambda_i^{A_-}\} = \{2, 0, 3\,(1 + \Omega_{\partial P})\}, \tag{19}$$

Eq. (19) implies that A_- is saddle for $\Omega_{\partial P} < -1$. Again, for $\Omega_{\partial P} \geq -1$ we will use numerical examples to discuss the stability for specific Γ.

3.2. Static universe critical line

For positive curvature, the coordinates $\{\Omega_\epsilon, \Omega_H, \Omega_P, \Omega_{\partial P}\} = \{1, 0, -1, \forall\}$ correspond to a critical line (called B) describing a static universe, i.e $a = \text{const.}$. These points have eigenvalues

$$\{\lambda_i^B\} = \{0, -\sqrt{1 + 3\Omega_{\partial P}}, \sqrt{1 + 3\Omega_{\partial P}}\}. \tag{20}$$

Regarding the stability, as long as $1 + 3\Omega_{\partial P} > 0$, B is saddle; for $1 + 3\Omega_{\partial P} < 0$ it is center; for $\Omega_{\partial P} = -1/3$ the corresponding point is degenerate and all eigenvalues are zero, hence the center manifold theory cannot say anything about its stability: however, from a numerical inspection we find that in this case the point is marginally unstable.[1]

4. GENERAL FEATURES OF Γ: INVARIANT SUBSETS AND CRITICAL POINTS

Since we have assumed that $P = P(\epsilon)$, the definition of Γ Eq. (7) implies that $\Gamma = \Gamma(\epsilon)$. But the energy density is not a dimensionless parameter of the system and since Γ should not depend on the geometry, the only valid option for its functional form is $\Gamma = \Gamma\left(\Omega_{\partial P}, \frac{\Omega_P}{\Omega_\epsilon}\right)$. In some cases (see Appendix A) one can express $\frac{\Omega_P}{\Omega_\epsilon}$ as a function of $\Omega_{\partial P}$ and hence $\Gamma = \Gamma(\Omega_{\partial P})$ or vice versa.

Eq. (12) of our dynamical system has been derived by combining the barotropicity of the effective fluid with the continuity equation (3), namely

$$\begin{aligned} \dot{\Omega}_{\partial P} &= \frac{\partial \Omega_{\partial P}}{\partial \epsilon}\,\dot{\epsilon} \\ &= -3\,H\,\left(1 + \frac{P}{\epsilon}\right)\,\left[\frac{\partial \Omega_{\partial P}}{\partial \epsilon}\,\epsilon\right]\,, \end{aligned} \tag{21}$$

where the last square bracket defines the parameter Γ. Eq. (21) is independent of our choice of dimensionless variables and it clearly indicates that any root of Γ will be a stationary point in time for $\Omega_{\partial P}$: this can happen either when $\epsilon = 0$ or whenever $\Omega_{\partial P}$ has an extremum with respect to the energy density, *i.e.* whenever $P(\epsilon)$ has an inflection point. Physically we expect $\epsilon = 0$ only asymptotically, either past or future depending whether the model is collapsing or expanding; the second case instead can happen for some finite energy density and at a finite time. Hence, any inflection point of the EoS for $\epsilon > 0$ will create an invariant subset in the parameter space of the dynamical system in the case that $\Gamma = \Gamma(\Omega_{\partial P})$.

---

[1] A critical line (denoted by $\bar{B}$) corresponding to a static universe exist also for the case of negative curvature. These points are located at $\{\Omega_\epsilon, \Omega_H, \Omega_P, \Omega_{\partial P}\} = \{-1, 0, 1, \forall\}$. This location, however, lies at $\Omega_\epsilon < 0$, which, as discussed in Sec. 2.2, is excluded from our study.

By choosing appropriately the form of the function Γ we can impose physically meaningful constraints on the evolution of the system. For instance, being $\Omega_{\partial P}$ a dynamical variable, one could require the causality condition $\Omega_{\partial P} \leq 1$ by imposing that $\Gamma(\Omega_{\partial P} = 1) = 0$ (see sec. 5.1). Such condition cannot be imposed at the level of equation of state, since this would not be part of the evolution equations of the system and it wouldn't stop the dynamical system from crossing the value $\Omega_{\partial P} = 1$. Something analogous can happen for any other condition which is not imposed at the level of evolution equations (see *e.g.* Sec. 4.2).

Critical lines $A_\pm$ and B are independent of the EoS since they exist for any $\Omega_{\partial P}$. However, once the function Γ is chosen, its roots $\tilde{\Omega}_{\partial P}$ introduce invariant subsets lying on $\{\Omega_H, \Omega_P\}$ planes and critical points lying in these planes[2]. These critical points are located at $\{\Omega_H, \Omega_P\} = \{\pm 1, 3\,\tilde{\Omega}_{\partial P}\}$, hence for each root of Γ there will be a pair of critical points $C_\pm$. Moreover, any new invariant subset might intersect the critical lines: we denote the resulting critical points with the same name as the respective critical lines throughout the text.

The scale factor in C_+ grows as $a \sim (t - t_0)^{\frac{2}{3\,(\tilde{\Omega}_{\partial P}+1)}}$, while in C_- the scale factor decreases as $a \sim (t_0 - t)^{\frac{2}{3\,(\tilde{\Omega}_{\partial P}+1)}}$. Moreover, the deceleration parameter at these points is $q = \frac{1}{2}(3\,\tilde{\Omega}_{\partial P} + 1)$. Therefore, according to this parameter these critical points describe an accelerated phase if $\tilde{\Omega}_{\partial P} < -\frac{1}{3}$ and a decelerated phase if $\tilde{\Omega}_{\partial P} > -\frac{1}{3}$.

On the invariant subset $\{\Omega_H, \Omega_P\}$ point C_+ has eigenvalues

$$\{\lambda_i^{C_+}\} = \{3\,(1 + \tilde{\Omega}_{\partial P}), 1 + 3\,\tilde{\Omega}_{\partial P}\}, \tag{22}$$

and C_- has

$$\{\lambda_i^{C_-}\} = \{-3\,(1 + \tilde{\Omega}_{\partial P}), -(1 + 3\,\tilde{\Omega}_{\partial P})\}. \tag{23}$$

From Eqs. (22) and (23) we see that for $-\frac{1}{3} < \tilde{\Omega}_{\partial P}$ point C_+ (C_-) represent a source (sink). For the case $-1 < \tilde{\Omega}_{\partial P} < -\frac{1}{3}$ instead $C_\pm$ are saddle. Finally, for $\tilde{\Omega}_{\partial P} < -1$ point C_+ (C_-) is a sink (source).

Since the stability of $A_\pm$, B (see Sec. 3) and $C_\pm$ depends on the value of $\tilde{\Omega}_{\partial P}$, we split our analysis into the following three ranges

- $-\frac{1}{3} < \tilde{\Omega}_{\partial P}$,
- $-1 < \tilde{\Omega}_{\partial P} < -\frac{1}{3}$,
- $\tilde{\Omega}_{\partial P} < -1$.

[2] It is not necessary to analyse the roots of Γ with respect to the combination Ω_P/Ω_ϵ, because having a constant ratio Ω_P/Ω_ϵ is equivalent to having a constant $\Omega_{\partial P}$ and hence the critical elements in the two cases can be related to each other.

The behaviour of these cases will be depicted for positive and non-positive curvatures, choosing one representative value of $\tilde{\Omega}_{\partial P}$ for each range, noting that the topology of the trajectories is independent of the specific value inside each range. Assuming further that the function Γ has only one root, there is only one pair of critical points $C_\pm$.

4.1. Positive curvature

For positive curvature the system has invariant subsets located at $\Omega_P = -3$ and $\Omega_P = 3\,\tilde{\Omega}_{\partial P}$. In order to study the behaviour at $\Omega_P = \pm\infty$ one can compactify Ω_P by using the transformation

$$X_P = \frac{\zeta \Omega_P}{\sqrt{1 + \zeta^2 \Omega_P^2}} \in [-1, 1], \tag{24}$$

where $\zeta > 0$ is just a constant rescaling parameter. This kind of compactification is well-defined and doesn't introduce any spurious element into the system (see *e.g.* Appendix B in [17]).

The evolution equation for this variable is

$$X_P' = \frac{\Omega_H}{\zeta}\sqrt{1 - X_P^2} \left(X_P + 3\,\zeta\,\sqrt{1 - X_P^2}\right)\left(X_P - 3\,\zeta\,\Omega_{\partial P}\,\sqrt{1 - X_P^2}\right), \tag{25}$$

which along with the Eq. (10) defines the compactified system.

a. Invariant subsets for $-\frac{1}{3} < \tilde{\Omega}_{\partial P}$. The corresponding invariant subsets divide the variable space into three disjoint regions. The portrait of the variable space is depicted in Fig.1a where the value $\tilde{\Omega}_{\partial P} = 1$ has been chosen. The sources of the system are C_+ and A_-, B is a saddle point, and A_+ and C_- are sinks.

- The region $3\,\tilde{\Omega}_{\partial P} \leq \Omega_P$ describes recollapsing models starting from expanding C_+ and going towards contracting C_-.
- The region bounded between $-3 \leq \Omega_P \leq 3\,\tilde{\Omega}_{\partial P}$ is divided into four subregions by separatrices. The separatrices meet at the static universe point B. The right subregion is characterized by trajectories starting from decelerating expansion in C_+ and going towards the de Sitter point A_+. The left subregion describes cosmologies which start from accelerated Anti-de Sitter A_- and end their collapse decelerating at C_-. The upper subregion describes recollapsing senarios starting from expanding C_+ and ending at the contracting C_-. The lower subregion describes bouncing models starting from the Anti-de Sitter A_- and ending at the expanding de Sitter A_+.

(a) $\tilde{\Omega}_{\partial P} = 1$

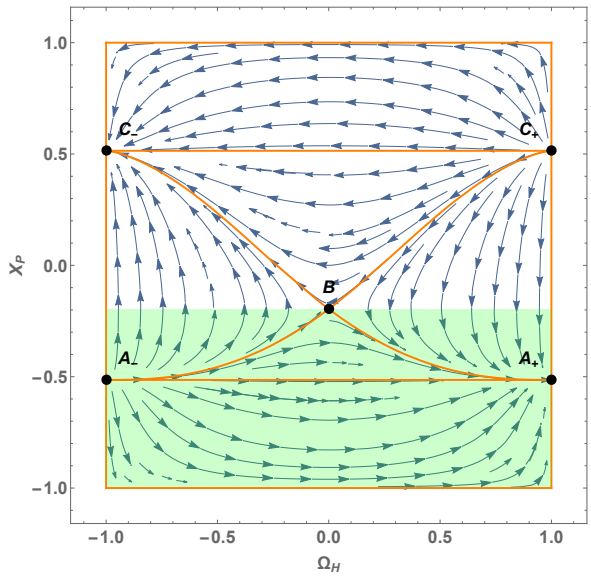

(b) $\tilde{\Omega}_{\partial P} = -\frac{1}{2}$

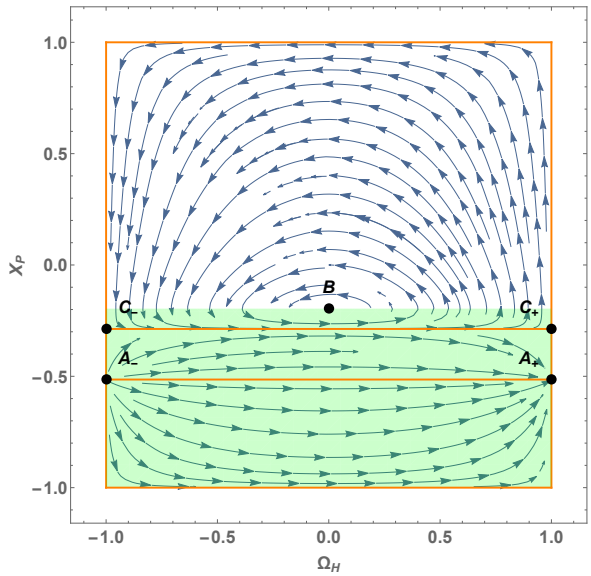

(c) $\tilde{\Omega}_{\partial P} = -2$

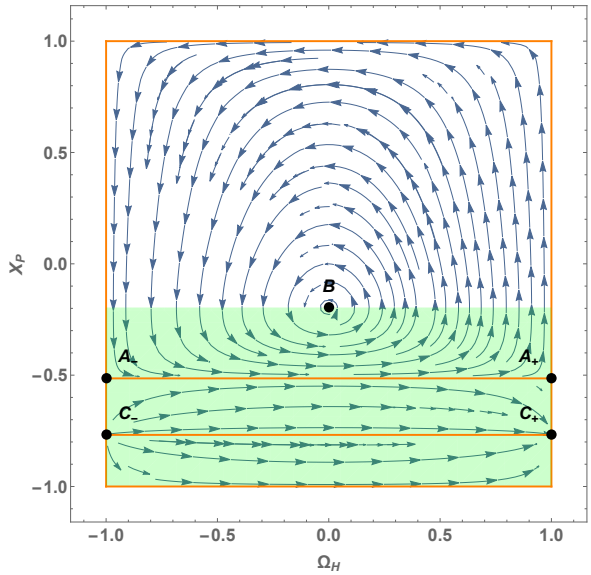

FIG. 1: Invariant subsets for positive spatial curvature and $\zeta = 0.2$ plotted for three representative values of $\tilde{\Omega}_{\partial P}$ in the ranges given in Sec. 4.1. The orange thick lines are the separatrices of the system and the green shaded regions denote the part of the variable space where the universe is accelerating.

- The last region lying in $\Omega_P \leq -3$ also describes bouncing models starting from the Anti-de Sitter A_- and going to the expanding de Sitter A_+.

b. Invariant subsets for $-1 < \tilde{\Omega}_{\partial P} < -\frac{1}{3}$. In this range, points A_- and A_+ still behave as source and sink respectively. Points $C_\pm$ become saddle points, while point B becomes a center. The variable space portrait is illustrated in Fig. 1b for $\tilde{\Omega}_{\partial P} = -\frac{1}{2}$. In this range the full invariant subset is divided into the three regions same as in the previous case.

- The region in the range $3\,\tilde{\Omega}_{\partial P} \leq \Omega_P$ is dominated by the presence of the center B. The trajectories in this region describe cyclic models which go through alternating accelerated and decelerated phases.

- The bounded region $-3 \leq \Omega_P \leq 3\,\tilde{\Omega}_{\partial P}$ describes bouncing universes starting from Anti-de Sitter A_- and going to expanding de Sitter A_+.

- The region for the case $\Omega_P \leq -3$ also represents bouncing universes starting from Anti-de Sitter A_- and going to the expanding de Sitter A_+.

c. Invariant subsets for $\tilde{\Omega}_{\partial P} < -1$. In this range, points $A_\pm$ become saddle points. Point B still describes center, while point C_- is a source and C_+ is a sink. The variable space dynamic for $\tilde{\Omega}_{\partial P} = -2$ is depicted in Fig. 1c. Similar to the previous cases the variable space is divided into three independent regions. These three regions are topologically the same as in the previous case. The only differences are that $A_\pm$ and $C_\pm$ have swapped stability properties and $C_\pm$ are located at lower values of Ω_P than $A_\pm$.

4.2. Non-positive curvature

There are additional critical points for the non-positive curvature once we consider $\Gamma(\tilde{\Omega}_{\partial P}) = 0$. These critical points are located at $\{\Omega_H, \Omega_P\} = \{\pm\frac{1}{\sqrt{2}}, 0\}$ and describe the Milne universe. At these points the deceleration parameter is $q = 0$ and the scale factor evolves as $a = \pm \mid k \mid (t + c_1)$ for $\Omega_H = \pm\frac{1}{\sqrt{2}}$ respectively.

A critical point with $\Omega_H = \frac{1}{\sqrt{2}}$, which we denote as D_+, has the eigenvalues

$$\{\lambda_i^{D_+}\} = \{\sqrt{2}, -\frac{\sqrt{2}}{2}\left(1 + 3\,\tilde{\Omega}_{\partial P}\right)\}, \tag{26}$$

in the invariant subset $\{\Omega_H, \Omega_P\}$. When $\Omega_H = -\frac{1}{\sqrt{2}}$, the critical point is denoted as D_- and has the eigenvalues

$$\{\lambda_i^{D_-}\} = \{-\sqrt{2}, \frac{\sqrt{2}}{2}\left(1 + 3\,\tilde{\Omega}_{\partial P}\right)\}. \tag{27}$$

Eqs. (26) and (27) imply that for $-\frac{1}{3} < \tilde{\Omega}_{\partial P}$ the critical points $D_\pm$ are saddles, while for $-\frac{1}{3} > \tilde{\Omega}_{\partial P}$, D_+ is a source and D_- is a sink.

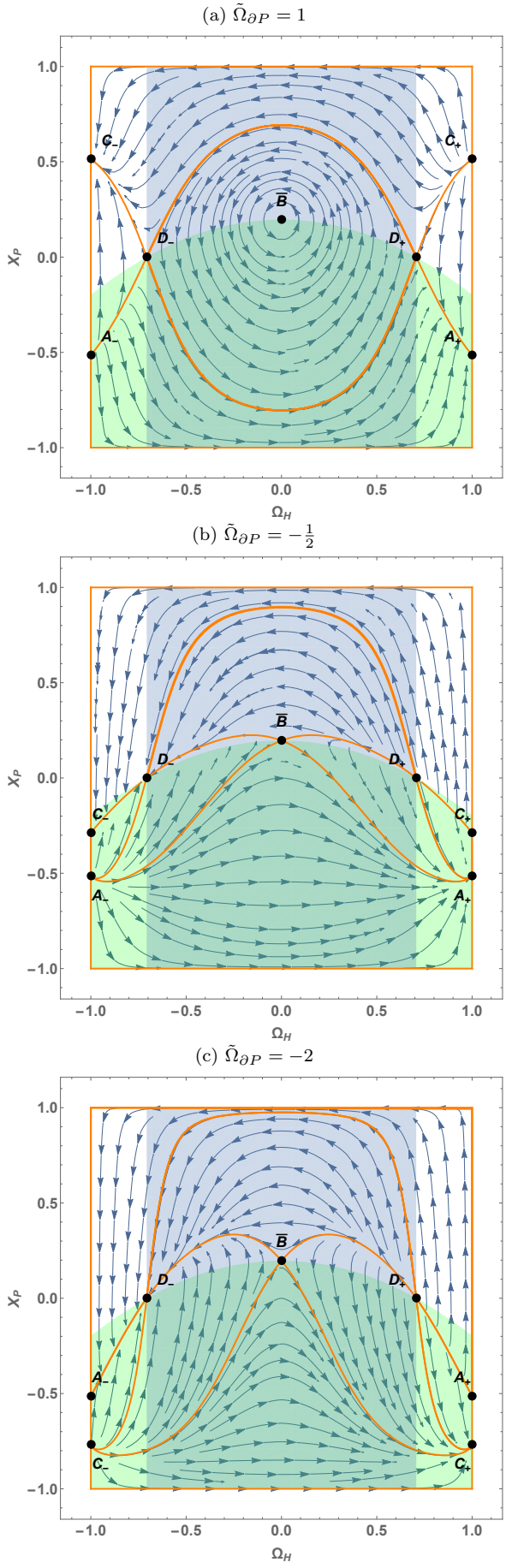

FIG. 2: Invariant subsets for negative spatial curvature and $\zeta = 0.2$ plotted for three representative values of $\tilde{\Omega}_{\partial P}$ in the ranges given in Sec. 4.2. The orange thick lines are the separatrices. The blue shaded areas are the regions excluded by our assumption that $\Omega_\epsilon > 0$. The green shaded region are the part of the variable space where we have accelerating universe.

As in the positive curvature case, one can compactify the variable space by applying the transformation (24) to obtain

$$X'_P = \frac{\Omega_H}{\zeta}\sqrt{1-X_P^2}\,(9\,\zeta^2\,\Omega_{\partial P}\,(1-2\,\Omega_H^2)\,(1-X_P^2)+ \zeta\,X_P\,\sqrt{1-X_P^2}\,(1-3\,\Omega_{\partial P}+2\,\Omega_H^2)+X_P^2)). \quad (28)$$

Our assumption of non-negative energy density causes the Friedman constraint to limit the physically admissible values of Ω_H as discussed in Sec. 2.2. This assumption is not imposed at the level of the evolution equations and hence some trajectories might cross to the forbidden area. The only trajectories lying entirely in the physical region are confined between the separatrices connecting the points $\{C_+, D_+, A_+\}$ for $\Omega_H > 0$ and $\{C_-, D_-, A_-\}$ for $\Omega_H < 0$, as can be seen in Fig. 2. In the following we will focus our discussion only in these physical regions.

a. Invariant subsets for $-\frac{1}{3} < \tilde{\Omega}_{\partial P}$. The points C_+ and A_- are sources, $D_\pm$ are saddle points while the points C_- and A_+ are sinks. Fig 2a shows the variable space dynamics for $\tilde{\Omega}_{\partial P} = 1$. For positive Ω_H, the trajectories start from C_+ and go towards the expanding de Sitter A_+. On the other hand, for negative Ω_H, the trajectories begin from the Anti-de Sitter universe A_- and go towards the contracting C_-. In both cases the trajectories can pass close to the saddle points D_+ and D_- respectively.

b. Invariant subsets for $-1 < \tilde{\Omega}_{\partial P} < -\frac{1}{3}$. The variable space is plotted in Fig. 2b for $\tilde{\Omega}_{\partial P} = -\frac{1}{2}$. In this case points D_+ and A_- represent sources, $C_\pm$ become saddle points and the sinks are A_+ and D_-. For $\Omega_H > 0$ the trajectories start from expanding Milne universe D_+ and going towards the expanding de Sitter A_+. On the other hand, for $\Omega_H < 0$, we see that the past attractor is now the Anti-de Sitter A_- and the trajectories move towards the collapsing Milne universe. In both cases some trajectories may approach transiently C_+ and C_- respectively.

c. Invariant subsets for $\tilde{\Omega}_{\partial P} < -1$. The variable space portrait for this case is illustrated in Fig. 2c where $\tilde{\Omega}_{\partial P} = -2$ is chosen. In contrast to the other cases, here $A_\pm$ become saddle points. Points D_+ and C_- represent sources and C_+ and D_- are sinks. For $\Omega_H > 0$ the trajectories start from expanding Milne universe and go towards the late attractor C_+. For $\Omega_H < 0$, the trajectories emerge from the past attractor C_- and end up at the contracting Milne universe D_-. In both cases, there are some trajectories passing transiently trough A_+ and A_- respectively.

5. EXAMPLES

In this section we close the system of equations following two approaches: first by choosing a specific form of the function Γ, and then by imposing instead a form of EoS from which Γ can be derived. As we will see, both

cases will have the simplest functional form of Γ, that is linear in $\Omega_{\partial P}$, i.e.

$$\Gamma = \alpha\,\Omega_{\partial P} + \beta, \tag{29}$$

where α and β are free parameters. One can find the functional form of the EoS by integrating Eq. (7). Namely, when $0 \neq \alpha \neq -1$

$$P = \frac{\alpha\Omega_{\partial P\star} + \beta}{\alpha\,(1+\alpha)\,\epsilon_\star^\alpha}\epsilon^{1+\alpha} - \frac{\beta}{\alpha}\epsilon + P_\star\,, \tag{30}$$

and

$$\Omega_{\partial P} = \frac{\partial P}{\partial \epsilon} = \frac{\alpha\Omega_{\partial P\star} + \beta}{\alpha\,\epsilon_\star^\alpha}\epsilon^{\alpha} - \frac{\beta}{\alpha}\,, \tag{31}$$

where $P_\star$, $\Omega_{\partial P\star}$, $\epsilon_\star$ are EoS integration constants.[3] Depending on the free parameters, the first term in eq. (30) can represent a generalized Chaplygin gas [4], while the second term includes a typical linear EoS; however in general both terms can describe more exotic fluids.

We can rewrite Eq. (30) as

$$\Omega_P = \frac{3}{1+\alpha}\,\Omega_\epsilon\,(\Omega_{\partial P} - \beta) + \Omega_{P_\star}\,, \tag{32}$$

where $\Omega_{P_\star} = \dfrac{P_\star}{D^2}$. Eq. (32) is a constraint between $\Omega_{P_\star}$ and the dynamical variables of our system and it implies that, even though this quantity appears as a new variable, we can retreat it during the evolution.

5.1. $\beta = -\alpha$: causality condition

In light of the discussion of Sec. 4, we impose the causality condition to this model by choosing $\beta = -\alpha$, which implies $\Gamma = \alpha(\Omega_{\partial P} - 1)$. The EoS (30) in this case reduces to

$$P = \frac{\Omega_{\partial P\star} - 1}{(1+\alpha)\,\epsilon_\star^\alpha}\epsilon^{1+\alpha} + \epsilon + P_\star\,. \tag{33}$$

Note that this represents a combination of a stiff EoS and an exotic fluid.

By demanding further that when the energy density tends to zero, the pressure does not diverge, Eq. (33) implies that $\alpha > -1$.[4]

The EoS (33) has an extremum at

$$\epsilon_e = \frac{\epsilon_\star}{(1-\Omega_{\partial P\star})^{1/\alpha}}\,, \tag{34}$$

which is maximum if $\alpha > 0$ and minimum if $\alpha < 0$. If one ignores an early inflationary epoch, then the pressure of the fluid should be positive for large energy densities. For low energy densities, to reproduce the effect of dark energy, one would expect negative pressure. Thus, the EoS we want has a minimum, i.e. $-1 < \alpha < 0$.

For $P = P_\star$ Eq. (33) implies that either

$$\Omega_{\partial P\star} = -\alpha$$

or $\epsilon_\star = 0$. The latter leads to the trivial EoS of the stiff fluid, since $-1 < \alpha < 0$. Thus, we choose the former. If further we make the reasonable demand that the pressure tends to zero along with the energy density, then

$$P_\star = 0\,,$$

which brings the constraint (32) to

$$\Omega_P = \frac{3}{1+\alpha}\,\Omega_\epsilon\,(\Omega_{\partial P} + \alpha)\,. \tag{35}$$

This, combined with the Friedmann constraint, reduces the system to two dimensions. Namely, due to the Friedmann constraints (13) or (15) one can disregard the Ω_ϵ evolution eq. (9), and due to the constraint (35) we can ignore the Ω_P evolution equation (11). Thus, the remaining dynamical variables are $\Omega_{\partial P}$ and Ω_H. Note that constraint (35) introduces an invariant subset at $\Omega_{\partial P} = -(1+2\alpha)$. As we want to preserve causality and also allow for positive $\Omega_{\partial P}$, we will focus our analysis in the compact region $\Omega_{\partial P} \in [-(1+2\alpha), 1]$.

The critical lines $A_\pm$ intersect the new invariant subset at

$$\{\Omega_H, \Omega_{\partial P}\} = \{\pm 1, -(1+2\alpha)\}\,, \tag{36}$$

while the critical line B intersects it at

$$\{\Omega_H, \Omega_{\partial P}\} = \{0, -\frac{1+4\alpha}{3}\}\,. \tag{37}$$

The critical points $D_\pm$ lie at

$$\{\Omega_H, \Omega_{\partial P}\} = \{\pm\frac{1}{\sqrt{2}}, 1\}\,. \tag{38}$$

Given the chosen form of Γ and the assumptions on the parameters made above, for the negative curvature we get a new pair of Milne-like critical points $E_\pm$ at

$$\{\Omega_H, \Omega_{\partial P}\} = \{\pm\frac{1}{\sqrt{2}}, -(1+2\,\alpha)\}\,. \tag{39}$$

In the invariant subset $\{\Omega_H, \Omega_{\partial P}\}$ critical point E_+ has eigenvalues

$$\{\lambda_i^{E_+}\} = \{\sqrt{2}, 3\,\sqrt{2}\,\alpha\}, \tag{40}$$

while critical point E_- has eigenvalues

$$\{\lambda_i^{E_+}\} = \{\sqrt{2}, 3\,\sqrt{2}\,\alpha\}, \tag{41}$$

[3] The two special cases $\alpha = 0$ and $\alpha = -1$ will not be discussed, since in the former case the EoS can violate causality, while in the latter case the pressure diverges as $\epsilon \to 0$.

[4] Note that, since we have assumed causality, it holds that $1 - \Omega_{\partial P\star} \geq 0$. Thus, $\dfrac{\Omega_{\partial P\star} - 1}{(1+\alpha)\,\epsilon_\star^\alpha} \leq 0$.

which shows that points $E_\pm$ represent saddle points in the range $-1 < \alpha < 0$. The critical points $C_\pm$ lie at

$$\{\Omega_H, \Omega_{\partial P}\} = \{\pm 1, 1\}\,. \tag{42}$$

Points $C_\pm$ describe cases of stiff matter dominated universe, in which the scale factor evolves as $a \sim t^{\frac{1}{3}}$ and the cosmological parameter $q = 2$. Point C_+ ($\Omega_H = 1$) has eigenvalues

$$\{\lambda_i^{C_+}\} = \{4,\, -6\,\alpha\}\,, \tag{43}$$

while C_- ($\Omega_H = -1$) has eigenvalues

$$\{\lambda_i^{C_-}\} = \{-4,\, 6\,\alpha\}\,. \tag{44}$$

Note that points $C_\pm$ lie on the invariant subset $\Omega_{\partial P} = 1$. All the aforementioned critical points along with their stability are summarized in Table I.

In Figs. 3 and 4 we show these critical points for the cases $k \geq 0$ and $k \leq 0$ respectively where the free parameter $\alpha = -0.1$. The variable space for $k \geq 0$, i.e. Fig. 3, is divided into four subregions from the respective separatrices. All four can transiently pass through a static phase in case they approach point B. The right subregion starts from the stiff matter era C_+ expanding exponentially towards the de Sitter point A_+. The left subregion describes cosmologies starting from the contracting Anti-de Sitter point A_- and collapsing to the future stiff matter attractor C_-. The upper subregion describes recollapsing scenarios starting from the expanding stiff point C_+ and ending at the stiff point C_-. The lower subregion is describing bouncing models from the contracting de sitter A_-, to the expanding de Sitter A_+. On the other hand, the variable space for $k \leq 0$ is divided into two subregions since $\frac{1}{2} \leq \Omega_H^2 \leq 1$. The right subregion describes models starting from the stiff matter source C_+, which expand towards the de Sitter point attractor A_+. Whereas, the left subregion describes scenarios starting from contracting de Sitter, point A_-, and eventually collapsing to the stiff mater point attractor C_-. Note that the variable spaces depicted in Figs. 3 and 4 depend only on the free parameter α and they just rescale accordingly. Namely, changing the value of α in the interval $-1 < \alpha < 0$, changes the coordinate $\Omega_{\partial P}$ of points $A_\pm$ in the interval $[-1, 1]$ (alongside with the invariant subset $\Omega_{\partial P} = -(1+2\alpha)$) and B in the interval $[-1/3, 1]$.

The setup $-1 < \alpha < 0$ has also the following consequences:

- For the positive curvature, by combining the limits imposed on $\Omega_{\partial P}$ by the invariant subsets, the Friedmann constraint (13) and the constraint (35), we have

$$-3 \leq \Omega_P \leq 3\,. \tag{45}$$

- For the negative curvature, Friedmann constraint

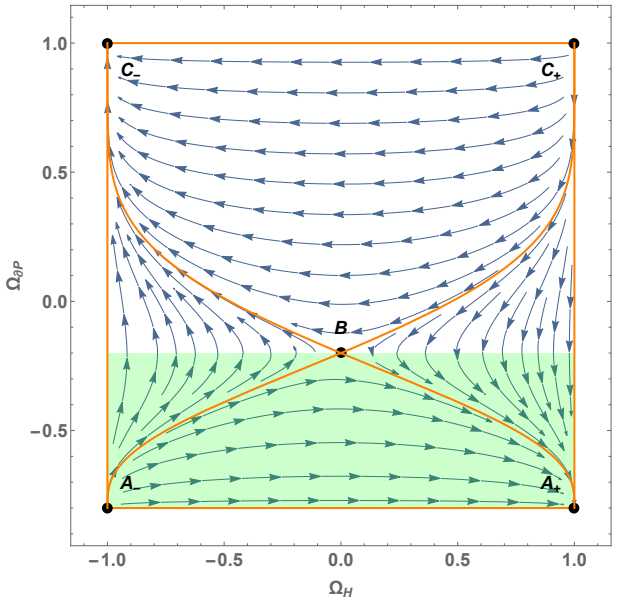

FIG. 3: Invariant subset of the system studied in Sec. 5.1 for non-negative curvature with $\alpha = -0.1$. The green shaded area denotes the phase of accelerated expansion $q < 0$ and the orange thick lines indicate the separatrices.

TABLE I: The critical points of the system described in Sec. 5.1 on the $\{\Omega_H,\ \Omega_{\partial P}\}$ plane and their stability for $-1 < \alpha < 0$ and non-negative curvature.

point	Ω_H	$\Omega_{\partial P}$	stability	curvature
A_+	1	$-(1+2\alpha)$	sink	flat
A_-	-1	$-(1+2\alpha)$	source	flat
B	0	$-\frac{1+4\alpha}{3}$	saddle	positive
C_+	1	1	source	flat
C_-	-1	1	sink	flat
D_+	$\frac{1}{\sqrt{2}}$	1	saddle	negative
D_-	$-\frac{1}{\sqrt{2}}$	1	saddle	negative
E_+	$\frac{1}{\sqrt{2}}$	$-(1+2\alpha)$	saddle	negative
E_-	$-\frac{1}{\sqrt{2}}$	$-(1+2\alpha)$	saddle	negative

together with constraint (35) and the limits imposed on $\Omega_{\partial P}$ by the invariant subsets, lead to

$$\begin{cases} -3\,\Omega_\epsilon \leq \Omega_P \leq 3\,\Omega_\epsilon \\ 0 \leq \Omega_\epsilon \leq 1 \end{cases} \tag{46}$$

By substituting Eq. (33) with $P_\star = 0$ into the continuity equation (3) we can calculate the scale factor in terms of ϵ as follows (taking into account that $-1 < \alpha < 0$)

$$a = a_0 \left(\frac{2 - \left(\frac{\epsilon_\star}{\epsilon_0}\right)^{|\alpha|}}{2 - \left(\frac{\epsilon_\star}{\epsilon}\right)^{|\alpha|}} \right)^{\frac{1}{6|\alpha|}} \left(\frac{\epsilon_0}{\epsilon}\right)^{1/6}\,. \tag{47}$$

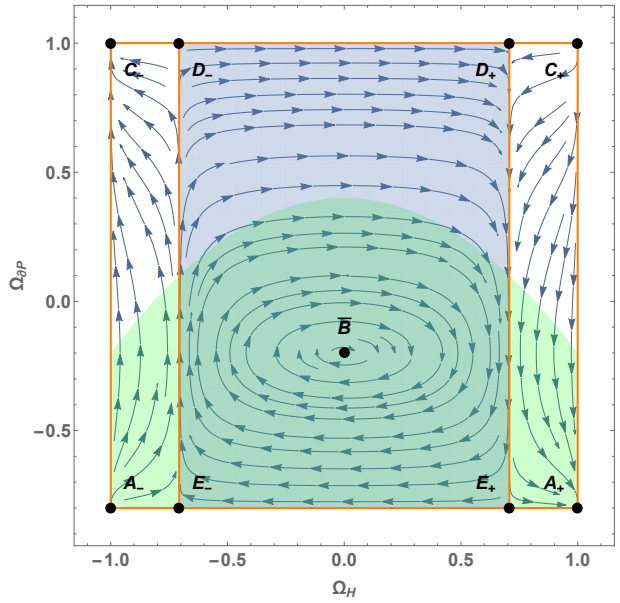

FIG. 4: Invariant subset of the system studied in Sec. 5.1 with $\alpha = -0.1$ for non-positive curvature. The blue shaded area is the region excluded by our assumption that $\Omega_\epsilon > 0$. The green shaded region is the part of the variable space where we have accelerating universe.

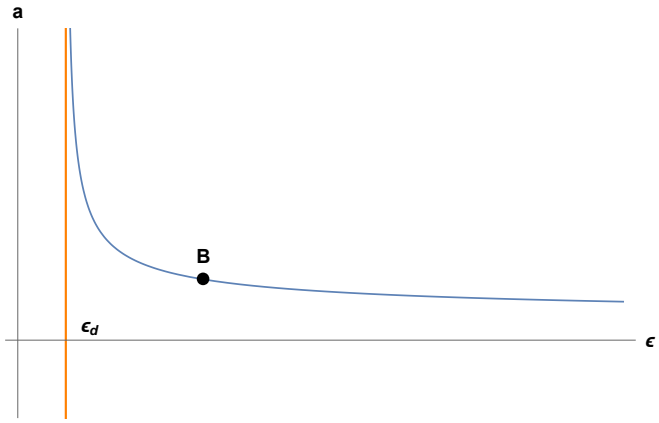

FIG. 5: Behaviour of the scale factor as a function of energy density as given by Eq. (47). The orange line is the value $\epsilon = 2^{-\frac{1}{|\alpha|}}\epsilon_\star$ where the scale factor diverges.

From Eq. (47) and Eq. (31) we can explain the behaviour of the scale factor in the different subregions of Fig. 3 and Fig. 4, with the aid of Fig. 5. Points $C_\pm$ correspond to $\epsilon \to \infty$ where the scale factor $a \to 0$. On the other hand, $A_\pm$ are points in which $\epsilon \to 2^{-\frac{1}{|\alpha|}}\epsilon_\star \equiv \epsilon_d$ and the scale factor diverges. The latter actually happens when the EoS intersects $P = -\epsilon$. Point B corresponds to $\epsilon_B = (3/4)^{\frac{1}{|\alpha|}}\ \epsilon_\star$ which has a finite scale factor value. In the right subregion of Fig. 3 the scale factor evolves from $a = 0$ at $\epsilon = \infty$ to the point $\epsilon = 2^{-\frac{1}{|\alpha|}}\epsilon_\star$ where the scale factor diverges. The left subregion has the opposite behaviour, namely the scale factor starts from infinite value and decreases to zero. In the upper subregion the scale factor starts from zero, increases and then decreases to zero again. The maximum value it can attain is $\epsilon_{\max} > \epsilon_B$. In the lower subregion, the scale factor starts from infinity, decreases and then increases again to infinity. The minimum value it can attain is $\epsilon_{\min} < \epsilon_B$. The behaviour of the scale factor in the left and right subregions of Fig. 4 are analogous to the behaviour in the left and right subregions of Fig. 3 respectively.

When $\alpha > -\frac{1}{2}$, then $\epsilon_d < \epsilon_e$ and $\Omega_{\partial P}$ can attain negative values. For $\alpha = -1/2$ the energy density of the scale factor divergence coincides with the EoS's minimum, i.e $\epsilon_d = \epsilon_e$ and this happens when $\Omega_{\partial P} = 0$. For $\alpha < -\frac{1}{2}$, $\Omega_{\partial P} > 0$.

5.2. The quadratic EoS

In [18–22] the quadratic EoS

$$P = \frac{\delta}{\epsilon_c}\epsilon^2 + \sigma\,\epsilon + P_\star, \tag{48}$$

was studied thoroughly. Here we compare the results of [21] with our formalism, by adopting their reasoning by viewing the EoS (48) as a Taylor expansion of an unknown barotropic EoS around $\epsilon = 0$ without necessarily demanding that $P_\star = 0$. From Eq. (48) we can write

$$\Omega_{\partial P} = 2\frac{\delta}{\epsilon_c}\,\epsilon + \sigma, \tag{49}$$

$$\Omega_P = \frac{3}{2}\,\Omega_\epsilon\,(\Omega_{\partial P} + \sigma) + \Omega_{P_\star} \tag{50}$$

and derive the Γ function in our variables as follows

$$\Gamma = \Omega_{\partial P} - \sigma, \tag{51}$$

which shows that the quadratic EoS brings a Γ which is linear in $\Omega_{\partial P}$. In order to analyze the behaviour of the quadratic EoS we split it into the three cases as done in [21].

a. $\delta = 0$ *the linear EoS.* In this case, since $\Omega_{\partial P} = \sigma$ is a constant, the system is similar to the cases analyzed in Sec. 4.

b. $P_\star = 0$. This amounts to assuming that the pressure tends to zero along with the energy density. Thus, Eq. (50) provides the constraint

$$\Omega_P = \frac{3}{2}\,\Omega_\epsilon\,(\Omega_{\partial P} + \sigma)\,. \tag{52}$$

Similarly to the example given in Sec. 5.1 this constraint reduces the system to two dimensions. Therefore, the critical points $A_\pm$ lie at

$$\{\Omega_H, \Omega_{\partial P}\} = \{\pm 1, -(2+\sigma)\}. \tag{53}$$

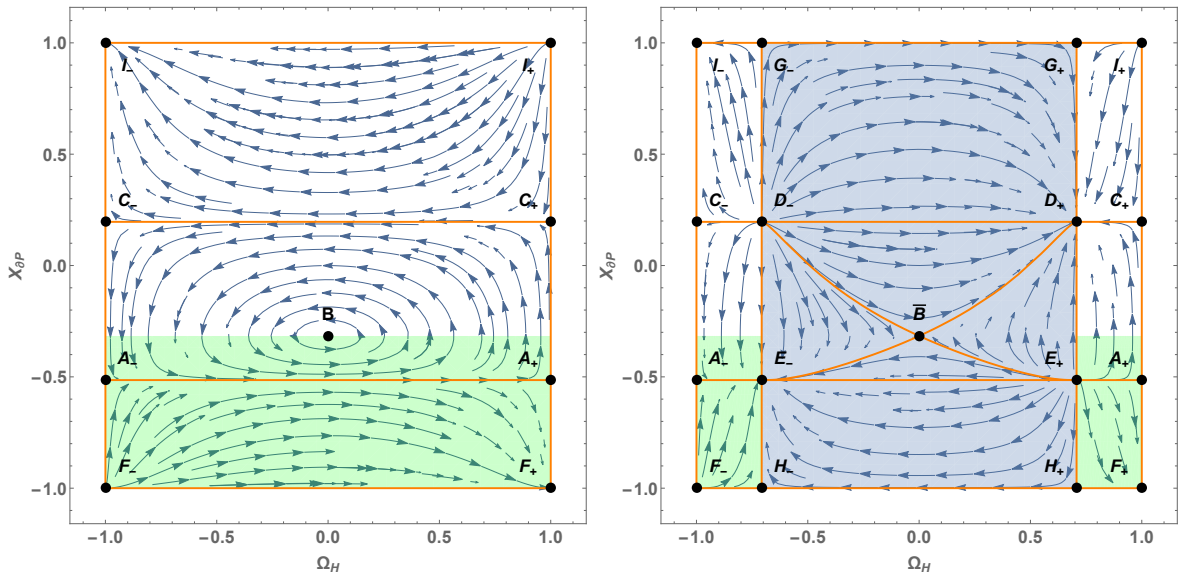

FIG. 6: Invariant subsets $\{\Omega_H, X_{\partial P}\}$ for the quadratic EoS with $P_\star = 0$ in the case of positive spatial curvature (left panel) and negative spatial curvature (right panel) when $\zeta = 0.2$ and $\sigma = 1$. The orange thick lines are the separatrices of the system and the green shaded regions denote the part of the variable space where the universe is accelerating.

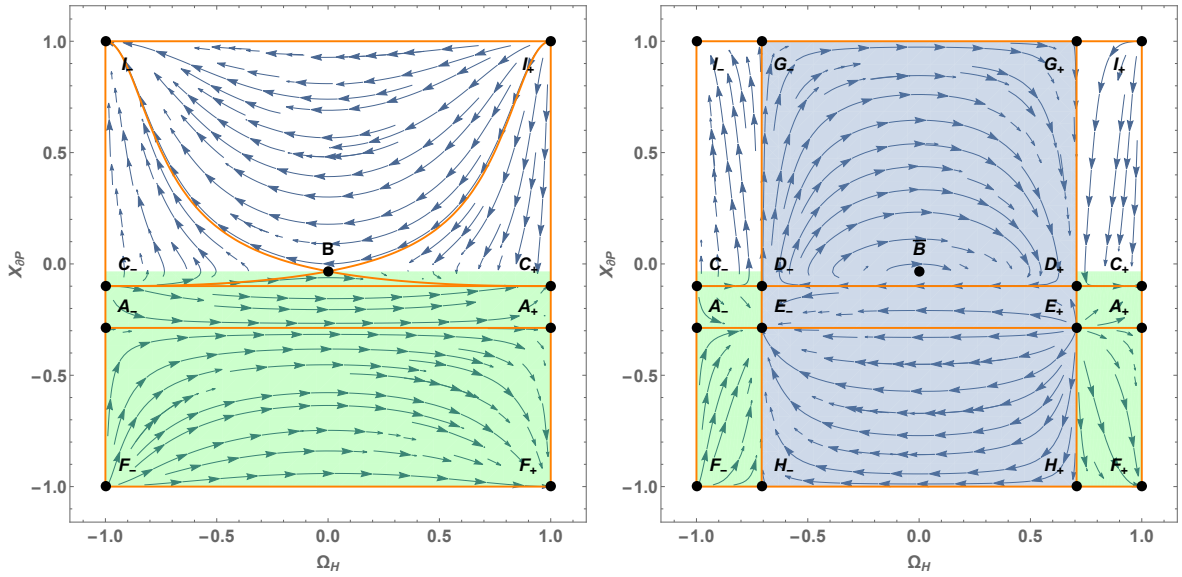

FIG. 7: Invariant subsets $\{\Omega_H, X_{\partial P}\}$ for the quadratic EoS with $P_\star = 0$ in the case of positive spatial curvature (left panel) and negative spatial curvature (right panel) when $\zeta = 0.2$ and $\sigma = -0.5$. The orange thick lines are the separatrices of the system and the green shaded regions denote the part of the variable space where the universe is accelerating.

The critical point B is located at

$$\{\Omega_H, \Omega_{\partial P}\} = \{0, -\left(\frac{2}{3} + \sigma\right)\}. \tag{54}$$

Critical points $C_\pm$ are located at

$$\{\Omega_H, \Omega_{\partial P}\} = \{\pm 1, \sigma\}. \tag{55}$$

Critical lines $D_\pm$ are located at

$$\{\Omega_H, \Omega_{\partial P}\} = \{\pm\frac{1}{\sqrt{2}}, \sigma\}. \tag{56}$$

There is also a pair of Milne-like critical points $E_\pm$ for negative curvature at

$$\{\Omega_H, \Omega_{\partial P}\} = \{\pm\frac{1}{\sqrt{2}}, -(2+\sigma)\}. \tag{57}$$

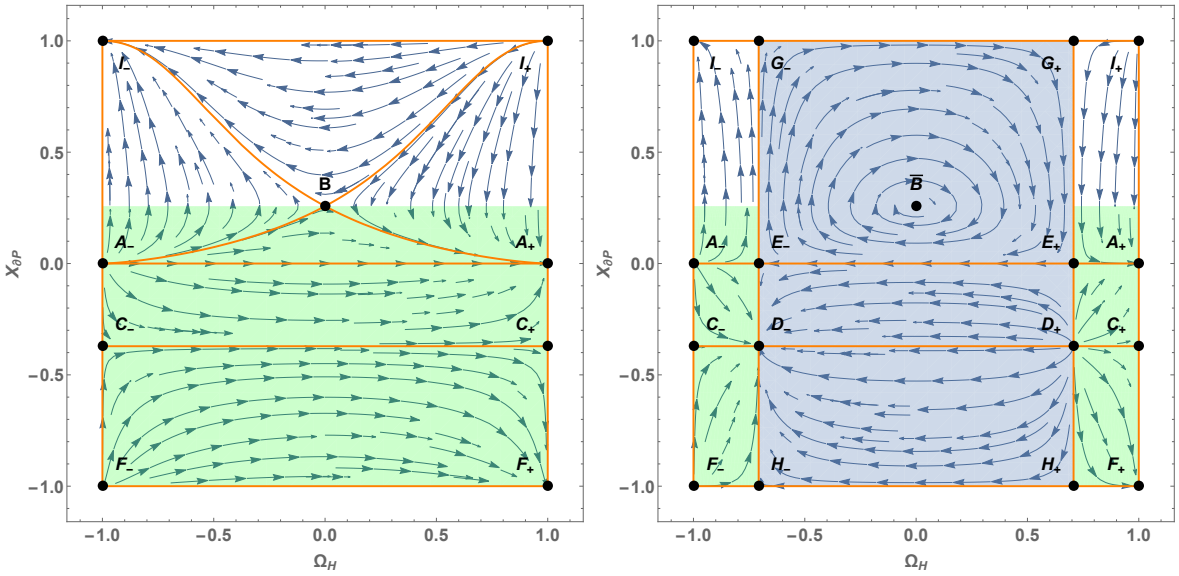

FIG. 8: Invariant subsets $\{\Omega_H, X_{\partial P}\}$ for the quadratic EoS with $P_\star = 0$ in the case of positive spatial curvature (left panel) and negative spatial curvature (right panel) when $\zeta = 0.2$ and $\sigma = -2$. The orange thick lines are the separatrices of the system and the green shaded regions denote the part of the variable space where the universe is accelerating.

As in Sec. 4 in order to compactify the variable space we use the transformation

$$X_{\partial P} = \frac{\zeta \Omega_{\partial P}}{\sqrt{1+\zeta^2 \Omega_{\partial P}^2}} \in [-1, 1]. \tag{58}$$

The evolution equation for $X_{\partial P}$ becomes

$$X'_{\partial P} = \frac{3\,\Omega_H}{2\,\xi}\sqrt{1-X_{\partial P}^2}\times \left(\sigma\,\xi^2\,(\sigma+2)\,(1-X_{\partial P}^2) + X_{\partial P}\left(1+2\,\xi\,\sqrt{1-X_{\partial P}^2}\right)\right) \tag{59}$$

and it holds for both curvatures.

Once we have compactified the variable space two more pairs of critical points appear for the flat case, while two Milne-like pairs of critical points appear for the negative curvature. In particular, $I_\pm$ appear at $\{\Omega_H, \Omega_{\partial P}\} = \{\pm 1, +\infty\}$, $F_\pm$ appear at $\{\Omega_H, \Omega_{\partial P}\} = \{\pm 1, -\infty\}$, $G_\pm$ appear at $\{\Omega_H, \Omega_{\partial P}\} = \{\pm\frac{1}{\sqrt{2}}, +\infty\}$, while $H_\pm$ appear at $\{\Omega_H, \Omega_{\partial P}\} = \{\pm\frac{1}{\sqrt{2}}, -\infty\}$.

In Figs. 6- 8 the variable spaces $\{\Omega_H, X_{\partial P}\}$ for different ranges of σ are plotted. These variable spaces are divided into two main subregions depending on the sign of δ: the subregions above the separatrices connecting points $C_\pm$ correspond to an EoS with $\delta = +1$ and the rest of variable space describes the case $\delta = -1$.

For comparing our analysis to the one in [21] let's denote $\tilde{X}_{\partial P} = X_{\partial P}\,(\Omega_{\partial P} = \sigma)$ by using Eq. (58). Figs. 4 and 7 of [21] correspond to $X_{\partial P} > \tilde{X}_{\partial P}$ and $X_{\partial P} < \tilde{X}_{\partial P}$ in our Fig. 6 respectively. Figs. 3 and 6 of [21] correspond to $X_{\partial P} > \tilde{X}_{\partial P}$ and $X_{\partial P} < \tilde{X}_{\partial P}$ in our Fig. 7 respectively. Figs.1 and 5 of [21] correspond to $X_{\partial P} > \tilde{X}_{\partial P}$ and $X_{\partial P} < \tilde{X}_{\partial P}$ in our Fig. 8 respectively. When $X_{\partial P} = \tilde{X}_{\partial P}$, Eq. (49) implies either $\epsilon = 0$ or $\delta = 0$. However, due to the Friedmann constraint ϵ is in general different from zero; hence we have $\delta = 0$, which is case *a.* above.

TABLE II: Quadratic EoS: number of critical points appearing on the invariant subsets for different ranges of the parameters with $P_\star = 0$. $C_\pm$ exist for any parameter ranges and curvature, while points $D_\pm$ exist for any parameter ranges for negative curvature. The points at infinity are not included.

δ	σ	A_+	A_-	B	E_+	E_-	Figure
$+1$	$-\frac{1}{3} < \sigma$	0	0	0	0	0	Fig.6
	$-1 < \sigma < -\frac{1}{3}$	0	0	1	0	0	Fig.7
	$\sigma < -1$	1	1	1	1	1	Fig.8
-1	$-\frac{1}{3} < \sigma$	1	1	1	1	1	Fig.6
	$-1 < \sigma < -\frac{1}{3}$	1	1	0	1	1	Fig.7
	$\sigma < -1$	0	0	0	0	0	Fig.8

The points $A_\pm$, B, $I_\pm$ and $F_\pm$ were identified also in [21]. Additionally, we find a pair of fluid-dominated models ($C_\pm$) and two pairs of Milne-like solutions for negative curvature ($D_\pm$ and $E_\pm$). Moreover, through compactification we are able to identify the critical points $G_\pm$ and $H_\pm$ at infinity. On the other hand, contrary to [21], in our setting we cannot identify a critical element corresponding to Minkowski spactime.

c. Generic quadratic EoS. We can write $P_\star$ as

$$P_\star = \Delta \frac{\epsilon_c}{4\,\delta}\,(\sigma-\xi)^2, \tag{60}$$

where $\xi \in \{-\infty, +\infty\}$ and $\Delta = -\delta\,\mathrm{sgn}(\sigma-\xi)$. Writing it in terms of our dimensionless variables by using Eq. (49) we get

$$\Omega_{P_\star} = \frac{3}{2}\,\Delta\,\Omega_\epsilon\,\frac{(\sigma-\xi)^2}{\Omega_{\partial P}-\sigma}. \tag{61}$$

By combining Eqs. (60) and (61) along with our assumption $\Omega_\epsilon > 0$, we get the following constraints on the allowed values of $\Omega_{\partial P}$ for $\sigma \neq \xi$:

$$\text{if} \quad \delta > 0 \quad \Rightarrow \quad \Omega_{\partial P} > \sigma \tag{62}$$

$$\text{if} \quad \delta < 0 \quad \Rightarrow \quad \Omega_{\partial P} < \sigma \tag{63}$$

In the case $\sigma = \xi$, then $P_* = 0$ and we reduce to the previous case.

By combining Eqs. (61) and (50) we get the constraint

$$\Omega_P = \frac{3}{2}\,\frac{\Omega_\epsilon}{\Omega_{\partial P}-\sigma}\,\left(\Omega_{\partial P}^2 - \sigma^2 + \Delta\,(\sigma-\xi)^2\right), \tag{64}$$

which together with Friedmann constraints (13) or (15) reduce the system to two dimensions, namely the remaining dynamical variables are $\Omega_{\partial P}$ and Ω_H.

Note that for $\Omega_{\partial P} = \sigma$, Eq. (61) becomes singular: however, this singularity does not affect the evolution equation (12), since the denominator is cancelled by the Γ given by Eq. (51). Actually, $\Omega_{\partial P} = \sigma$ is the intersection line between the plane $\{\Omega_{\partial P}, \Omega_H\}$ and the case *a.* above.

The critical points discussed in Secs. 3 and 4 are now the following:

- the critical points $A_\pm$ are located at

$$\{\Omega_H, \Omega_{\partial P}\} = \{\pm 1, -1 \pm \sqrt{1-\sigma\,(2-\sigma) - \Delta\,(\sigma-\xi)^2}\,\}; \tag{65}$$

- the critical point B is located at

$$\{\Omega_H, \Omega_{\partial P}\} = \{0, -\frac{1}{3} \pm \sqrt{\frac{1}{9} + \sigma\,(\frac{2}{3}+\sigma) - \Delta\,(\sigma-\xi)^2}\,\}; \tag{66}$$

- the critical points $C_\pm$ are located at

$$\{\Omega_H, \Omega_{\partial P}\} = \{\pm 1, \sigma\}; \tag{67}$$

- the critical points $D_\pm$ are located at

$$\{\Omega_H, \Omega_{\partial P}\} = \{\pm\frac{1}{\sqrt{2}}, \sigma\}; \tag{68}$$

The additional Milne-like critical points $E_\pm$ are located at

$$\{\Omega_H, \Omega_{\partial P}\} = \{\pm\frac{1}{\sqrt{2}}, -1 \pm \sqrt{1-\sigma\,(2-\sigma) - \Delta\,(\sigma-\xi)^2}\,\}. \tag{69}$$

In appendix B we show representative cases which are summarized in Table 3. The comparison of the number of critical points between our study and the analysis of [21] for this generic case follows the same lines as in paragraph *b.*

6. CONCLUSIONS

This work introduces a framework to analyze dynamically systems of barotropic fluids with non-negative energy density in spatially curved FRW spacetimes in absence of the cosmological constant. First we have introduced the new variables and the new evolution parametrization of this framework along with the function Γ, which includes all the information about the EoS. In this general setup we have identified three critical lines:

- two de Sitter for spatially flat FRW,
- one static universe for non-negative curvatures,

that are independent of the EoS. The stability of these lines depends on the value of the variable $\Omega_{\partial P}$ along the lines themselves. Then we have discussed general features of the function Γ:

- we have shown that $\Gamma = \Gamma\left(\Omega_{\partial P}, \frac{\Omega_P}{\Omega_\epsilon}\right)$;
- we have shown that the roots of Γ are stationary points in time and in the case $\Gamma = \Gamma(\Omega_{\partial P})$ they define invariant subsets;
- we have studied these invariant subsets in the case that there is a single root $\tilde{\Omega}_{\partial P}$ and have found that:
  - there is a pair of new critical points corresponding to one-fluid flat universe, whose stability depends on $\tilde{\Omega}_{\partial P}$,
  - there is a pair of Milne critical points for non-positive curvature, whose stability depends on $\tilde{\Omega}_{\partial P}$.

In the second part of the work we have provided two examples of how the framework we have introduced can be used.

- In the first example we have taken a function of Γ linear in $\Omega_{\partial P}$ with two free parameters and through physically motivated arguments, like causality, we have trimmed the Γ model to a one parameter model with specific value interval. The resulting EoS represents a linear superposition of an exotic fluid with stiff matter. The stiff matter part of EoS dominates for large energy densities, while for low energy densities the exotic fluid part takes over. In this example apart from the dynamical elements identified in the general setup, a new invariant subset and a new pair of critical points exist. The new pair corresponds to Milne-like models. Regarding the invariant subsets, the one coming from the general analysis confines our model to obey causality, while the new one does not allow the EoS to cross the $P = -\epsilon$ line.
- In the second example we have applied our framework to the quadratic EoS studied in [21] and made the comparison with that study. We have identified

TABLE III: Quadratic EoS: number of critical points appearing on the invariant subsets for different ranges of the parameters with $P_\star \neq 0$. $C_\pm$ exist for any parameter ranges and curvature, while points $D_\pm$ exist for any parameter ranges for negative curvature. The points at infinity are not included.

δ	σ	$P_\star$	ξ	$\Omega_{P_\star}$	A_+	A_-	B	E_+	E_-	Figure
+1	$\sigma<-1$	$\frac{\epsilon_c(1+3\sigma)^2}{36\,\delta}<P_\star$	$-\frac{1}{3}<\xi$	$\frac{1}{6}\Omega_\epsilon\frac{(1+3\,\sigma)^2}{\Omega_{\partial P}-\sigma}<\Omega_{P_\star}$	0	0	0	0	0	Fig.9
		$P_\star=\frac{\epsilon_c(1+3\sigma)^2}{36\,\delta}$	$\xi=-\frac{1}{3}$	$\Omega_{P_\star}=\frac{1}{6}\Omega_\epsilon\frac{(1+3\,\sigma)^2}{\Omega_{\partial P}-\sigma}$	0	0	1	0	0	Fig.10
		$\frac{\epsilon_c(1+\sigma)^2}{4\,\delta}<P_\star<\frac{\epsilon_c(1+3\sigma)^2}{36\,\delta}$	$-1<\xi<-\frac{1}{3}$	$\frac{3}{2}\Omega_\epsilon\frac{(1+\sigma)^2}{\Omega_{\partial P}-\sigma}<\Omega_{P_\star}<\frac{1}{6}\Omega_\epsilon\frac{(1+3\,\sigma)^2}{\Omega_{\partial P}-\sigma}$	0	0	2	0	0	Fig.11
		$P_\star=\frac{\epsilon_c(1+\sigma)^2}{4\,\delta}$	$\xi=-1$	$\Omega_{P_\star}=\frac{3}{2}\Omega_\epsilon\frac{(1+\sigma)^2}{\Omega_{\partial P}-\sigma}$	1	1	2	1	1	Fig.12
		$0<P_\star<\frac{\epsilon_c(1+\sigma)^2}{4\,\delta}$	$\sigma<\xi<-1$	$0<\Omega_{P_\star}<\frac{3}{2}\Omega_\epsilon\frac{(1+\sigma)^2}{\Omega_{\partial P}-\sigma}$	2	2	2	2	2	Fig.13
		$P_\star<0$	$\xi<\sigma$	$\Omega_{P_\star}<0$	1	1	1	1	1	Fig.14
	$-1<\sigma<-\frac{1}{3}$	$\frac{\epsilon_c(1+3\sigma)^2}{36\,\delta}<P_\star$	$-\frac{1}{3}<\xi$	$\frac{1}{6}\Omega_\epsilon\frac{(1+3\,\sigma)^2}{\Omega_{\partial P}-\sigma}<\Omega_{P_\star}$	0	0	0	0	0	Fig.9
		$P_\star=\frac{\epsilon_c(1+3\sigma)^2}{36\,\delta}$	$\xi=-\frac{1}{3}$	$\Omega_{P_\star}=\frac{1}{6}\Omega_\epsilon\frac{(1+3\,\sigma)^2}{\Omega_{\partial P}-\sigma}$	0	0	1	0	0	Fig.10
		$0<P_\star<\frac{\epsilon_c(1+3\sigma)^2}{36\,\delta}$	$\sigma<\xi<-\frac{1}{3}$	$0<\Omega_{P_\star}<\frac{1}{6}\Omega_\epsilon\frac{(1+3\,\sigma)^2}{\Omega_{\partial P}-\sigma}$	0	0	2	0	0	Fig.11
		$P_\star<0$	$\xi<\sigma$	$\Omega_{P_\star}<0$	1	1	1	1	1	Fig.14
	$-\frac{1}{3}<\sigma$	$0<P_\star$	$\sigma<\xi$	$0<\Omega_{P_\star}$	0	0	0	0	0	Fig.9
		$P_\star<0$	$\xi<\sigma$	$\Omega_{P_\star}<0$	1	1	1	1	1	Fig.14
-1	$\sigma<-1$	$0<P_\star$	$\sigma<\xi$	$0<\Omega_{P_\star}$	1	1	1	1	1	Fig.15
		$P_\star<0$	$\xi<\sigma$	$\Omega_{P_\star}<0$	0	0	0	0	0	Fig.20
	$-1<\sigma<-\frac{1}{3}$	$0<P_\star$	$\sigma<\xi$	$0<\Omega_{P_\star}$	1	1	1	1	1	Fig.15
		$\frac{\epsilon_c(1+\sigma)^2}{4\,\delta}<P_\star<0$	$-1<\xi<\sigma$	$\frac{3}{2}\Omega_\epsilon\frac{(1+\sigma)^2}{\Omega_{\partial P}-\sigma}<\Omega_{P_\star}<0$	2	2	0	2	2	Fig.18
		$P_\star=\frac{\epsilon_c(1+\sigma)^2}{4\,\delta}$	$\xi=-1$	$\Omega_{P_\star}=\frac{3}{2}\Omega_\epsilon\frac{(1+\sigma)^2}{\Omega_{\partial P}-\sigma}$	1	1	0	1	1	Fig.19
		$P_\star<\frac{\epsilon_c(1+\sigma)^2}{4\,\delta}$	$\xi<-1$	$\Omega_{P_\star}<\frac{3}{2}\Omega_\epsilon\frac{(1+\sigma)^2}{\Omega_{\partial P}-\sigma}$	0	0	0	0	0	Fig.20
	$-\frac{1}{3}<\sigma$	$0<P_\star$	$\sigma<\xi$	$0<\Omega_{P_\star}$	1	1	1	1	1	Fig.15
		$\frac{\epsilon_c(1+3\sigma)^2}{36\,\delta}<P_\star<0$	$-\frac{1}{3}<\xi<\sigma$	$\frac{1}{6}\Omega_\epsilon\frac{(1+3\,\sigma)^2}{\Omega_{\partial P}-\sigma}<\Omega_{P_\star}<0$	2	2	2	2	2	Fig.16
		$P_\star=\frac{\epsilon_c(1+3\sigma)^2}{36\,\delta}$	$\xi=-\frac{1}{3}$	$\Omega_{P_\star}=\frac{1}{6}\Omega_\epsilon\frac{(1+3\,\sigma)^2}{\Omega_{\partial P}-\sigma}$	2	2	1	2	2	Fig.17
		$\frac{\epsilon_c(1+\sigma)^2}{4\delta}<P_\star<\frac{\epsilon_c(1+3\sigma)^2}{36\,\delta}$	$-1<\xi<-\frac{1}{3}$	$\frac{3}{2}\Omega_\epsilon\frac{(1+\sigma)^2}{\Omega_{\partial P}-\sigma}<\Omega_{P_\star}<\frac{1}{6}\Omega_\epsilon\frac{(1+3\,\sigma)^2}{\Omega_{\partial P}-\sigma}$	2	2	0	2	2	Fig.18
		$P_\star=\frac{\epsilon_c(1+\sigma)^2}{4\delta}$	$\xi=-1$	$\Omega_{P_\star}=\frac{3}{2}\Omega_\epsilon\frac{(1+\sigma)^2}{\Omega_{\partial P}-\sigma}$	1	1	0	1	1	Fig.19
		$P_\star<\frac{\epsilon_c(1+\sigma)^2}{4\delta}$	$\xi<-1$	$\Omega_{P_\star}<\frac{3}{2}\Omega_\epsilon\frac{(1+\sigma)^2}{\Omega_{\partial P}-\sigma}$	0	0	0	0	0	Fig.20

all the critical points found in [21], except from a critical point describing the Minkowski spactime, and additionally we have found

- a pair of fluid-dominated models for the flat case,
- two pairs of Milne-like solutions for negative curvature,
- two pairs of critical points with Milne-like behavior at $\Omega_{\partial P}\to\pm\infty$.

Acknowledgments

The authors would like to thank Sante Carloni and Jiří Bičák for their comments.

Appendix A: Function Γ linear in $\frac{\Omega_P}{\Omega_\epsilon}$.

The linear Γ function Eq. (29) can be written also in terms of the dimensionless combination $\frac{\Omega_P}{\Omega_\epsilon}$. By solving Eq. (32) in term of $\Omega_{\partial P}$

$$\Omega_{\partial P}=\frac{1+\alpha}{3}\frac{\Omega_P-\Omega_{P_\star}}{\Omega_\epsilon}+\beta, \tag{A1}$$

and then substituting it into the Eq. (29) we get

$$\Gamma=\hat{\alpha}\,\frac{\hat{\Omega}_P}{\Omega_\epsilon}+\hat{\beta}, \tag{A2}$$

where $\hat{\alpha}=\dfrac{\alpha\,(\alpha+1)}{3}$, $\hat{\beta}=\beta\,(\alpha+1)$ and

$$\hat{\Omega}_P=\Omega_P-\Omega_{P_\star}=\frac{P-P_\star}{D^2}.$$

In the case that $P_\star=0$, Γ is just a linear function of $\frac{\Omega_P}{\Omega_\epsilon}$.

Appendix B: Invariant subsets for quadratic EoS

In Figs. 9-20 we compare the results of our analysis in different parameter cases with respect to the ones obtained in [21]. Parameter cases that are topologically

analogous are represented by a single figure for each case – see Table III and the captions of the respective figures for details.

[1] N Aghanim, Yashar Akrami, M Ashdown, J Aumont, C Baccigalupi, M Ballardini, AJ Banday, RB Barreiro, N Bartolo, S Basak, et al. Planck 2018 results. vi. cosmological parameters. *arXiv preprint arXiv:1807.06209*, 2018.

[2] Joseph Ryan, Yun Chen, and Bharat Ratra. Baryon acoustic oscillation, hubble parameter, and angular size measurement constraints on the hubble constant, dark energy dynamics, and spatial curvature. *Monthly Notices of the Royal Astronomical Society*, 488(3):3844–3856, 2019.

[3] Eleonora Di Valentino, Alessandro Melchiorri, and Joseph Silk. Planck evidence for a closed Universe and a possible crisis for cosmology. *Nature Astronomy*, 4:196–203, Feb 2020.

[4] MC Bento, Orfeu Bertolami, and Anjan A Sen. Generalized chaplygin gas, accelerated expansion, and dark-energy-matter unification. *Physical Review D*, 66(4):043507, 2002.

[5] Pierre-Henri Chavanis and Suresh Kumar. Comparison between the logotropic and λcdm models at the cosmological scale. *Journal of Cosmology and Astroparticle Physics*, 2017(05):018, 2017.

[6] Eric V Linder and Robert J Scherrer. Aetherizing lambda: Barotropic fluids as dark energy. *Physical Review D*, 80(2):023008, 2009.

[7] Jannis Bielefeld, Robert R Caldwell, and Eric V Linder. Dark energy scaling from dark matter to acceleration. *Physical Review D*, 90(4):043015, 2014.

[8] Rossen I Ivanov and Emil M Prodanov. Dynamical analysis of an n- h- t cosmological quintessence real gas model with a general equation of state. *International Journal of Modern Physics A*, 33(03):1850025, 2018.

[9] Shinichi Nojiri, Sergei D Odintsov, and Shinji Tsujikawa. Properties of singularities in the (phantom) dark energy universe. *Physical Review D*, 71(6):063004, 2005.

[10] Takashi Nakamura and Takeshi Chiba. Determining the equation of state of the expanding universe: Inverse problem in cosmology. *Monthly Notices of the Royal Astronomical Society*, 306(3):696–700, 1999.

[11] Edmund J Copeland, Mohammad Sami, and Shinji Tsujikawa. Dynamics of dark energy. *International Journal of Modern Physics D*, 15(11):1753–1935, 2006.

[12] R. Aldrovandi, J. P. Beltrán Almeida, and J. G. Pereira. Time-Varying Cosmological Term: Emergence and Fate of a FRW Universe. *Gravitation and Cosmology*, 11:277–283, Sep 2005.

[13] Supriya Pan, John D. Barrow, and Andronikos Paliathanasis. Two-fluid solutions of particle-creation cosmologies. *European Physical Journal C*, 79(2):115, Feb 2019.

[14] Weiqiang Yang, Narayan Banerjee, Andronikos Paliathanasis, and Supriya Pan. Reconstructing the dark matter and dark energy interaction scenarios from observations. *Physics of the Dark Universe*, 26:100383, 2019.

[15] Paul J Steinhardt, Limin Wang, and Ivaylo Zlatev. Cosmological tracking solutions. *Physical Review D*, 59(12):123504, 1999.

[16] Adel Awad. Fixed points and flrw cosmologies: Flat case. *Physical Review D*, 87(10):103001, 2013.

[17] Artur Alho, Sante Carloni, and Claes Uggla. On dynamical systems approaches and methods in f (r) cosmology. *Journal of Cosmology and Astroparticle Physics*, 2016(08):064, 2016.

[18] Shin'ichi Nojiri and Sergei D. Odintsov. Final state and thermodynamics of a dark energy universe. *Phys. Rev. D* , 70(10):103522, Nov 2004.

[19] Shin'ichi Nojiri and Sergei D. Odintsov. Inhomogeneous equation of state of the universe: Phantom era, future singularity, and crossing the phantom barrier. *Phys. Rev. D* , 72(2):023003, Jul 2005.

[20] S. Capozziello, V. F. Cardone, E. Elizalde, S. Nojiri, and S. D. Odintsov. Observational constraints on dark energy with generalized equations of state. *Phys. Rev. D* , 73(4):043512, Feb 2006.

[21] Kishore N. Ananda and Marco Bruni. Cosmological dynamics and dark energy with a nonlinear equation of state: A quadratic model. *Physical Review D*, 74(2):023523, Jul 2006.

[22] Kishore N. Ananda and Marco Bruni. Cosmological dynamics and dark energy with a quadratic equation of state: Anisotropic models, large-scale perturbations, and cosmological singularities. *Physical Review D*, 74(2):023524, Jul 2006.

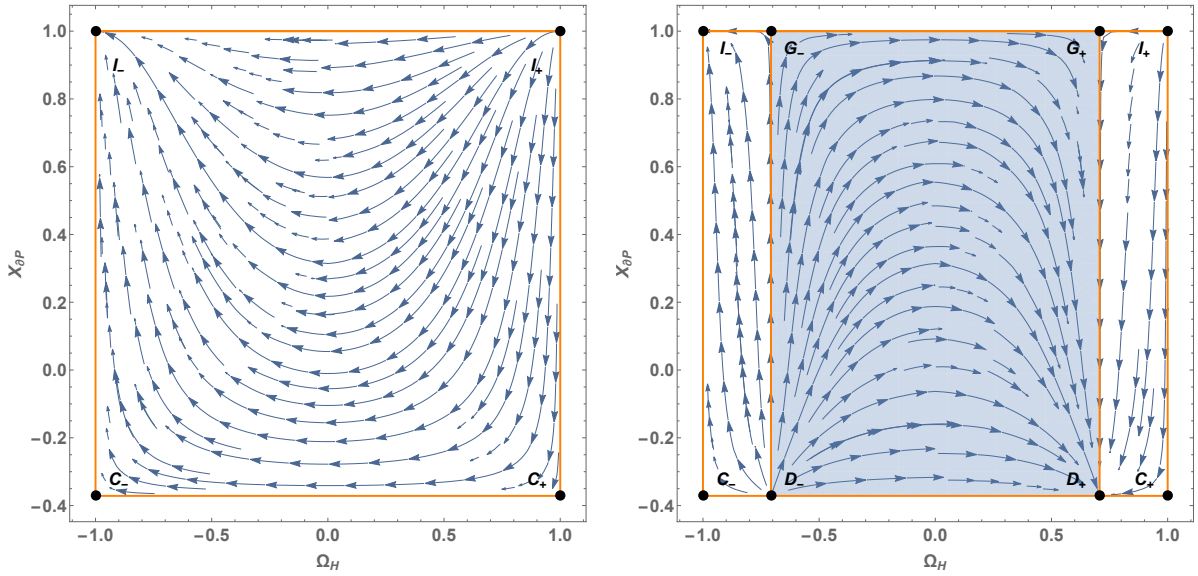

FIG. 9: Invariant subsets $\{\Omega_H, X_{\partial P}\}$ for the quadratic EoS with $P_\star \neq 0$. The right panel corresponds to the positive spatial curvature and the left panel corresponds to the negative spatial curvature case. Invariant subsets are plotted for the parameters $\delta = 1$, $\sigma = -4$, $\xi = 1$ and $\zeta = 0.1$ (these figures are topologically similar to the cases with parameters $\delta = 1$, $-1 < \sigma < -\frac{1}{3}$, $-\frac{1}{3} < \xi$ and also $\delta = 1$, $-\frac{1}{3} < \sigma$, $\sigma < \xi$). The orange thick lines are the separatrices of the system, the blue region corresponds to $\Omega_\epsilon < 0$. This figure corresponds to Fig. 10 in [21].

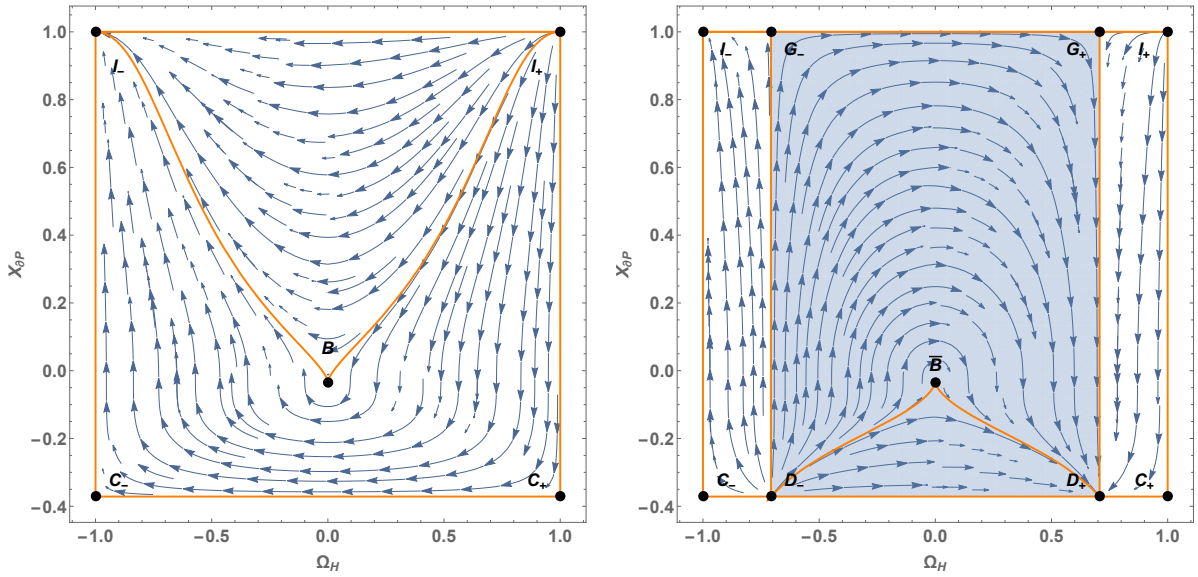

FIG. 10: Invariant subsets $\{\Omega_H, X_{\partial P}\}$ for the quadratic EoS with $P_\star \neq 0$. The right panel corresponds to the positive spatial curvature and the left panel corresponds to the negative spatial curvature case. The invariant subsets are plotted for the parameters $\delta = 1$, $\sigma = -4$, $\xi = -\frac{1}{3}$ and $\zeta = 0.1$ (these figures are topologically similar to the case with parameters $\delta = 1$, $-1 < \sigma < -\frac{1}{3}$ and $\xi = -\frac{1}{3}$). The orange thick lines are the separatrices of the system, the blue region corresponds to $\Omega_\epsilon < 0$. This figure corresponds to Fig. 14 in [21].

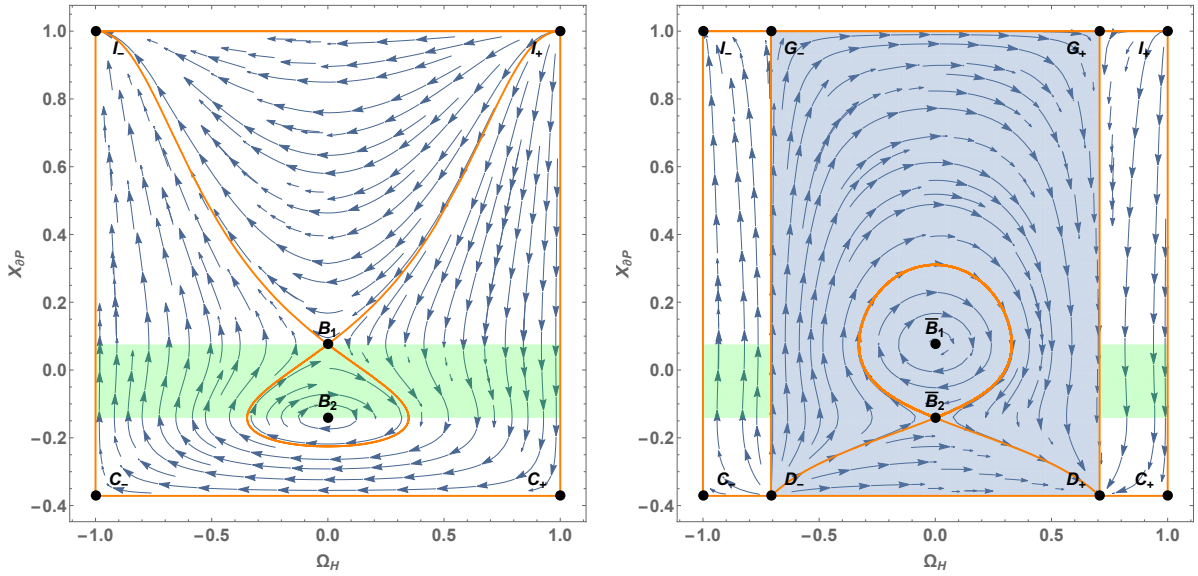

FIG. 11: Invariant subsets $\{\Omega_H, X_{\partial P}\}$ for the quadratic EoS with $P_\star \neq 0$. The right panel corresponds to the positive spatial curvature and the left panel corresponds to the negative spatial curvature case. The invariant subsets are plotted for the parameters $\delta = 1$, $\sigma = -4$, $\xi = -0.5$ and $\zeta = 0.1$ (these figures are topologically similar to the case with parameters $\delta = 1$, $-1 < \sigma < -\frac{1}{3}$, $\sigma < \xi < -\frac{1}{3}$). The orange thick lines are the separatrices of the system, the blue region corresponds to $\Omega_\epsilon < 0$ and the green shaded region corresponds to accelerated dynamics. This figure corresponds to Fig. 15 in [21].

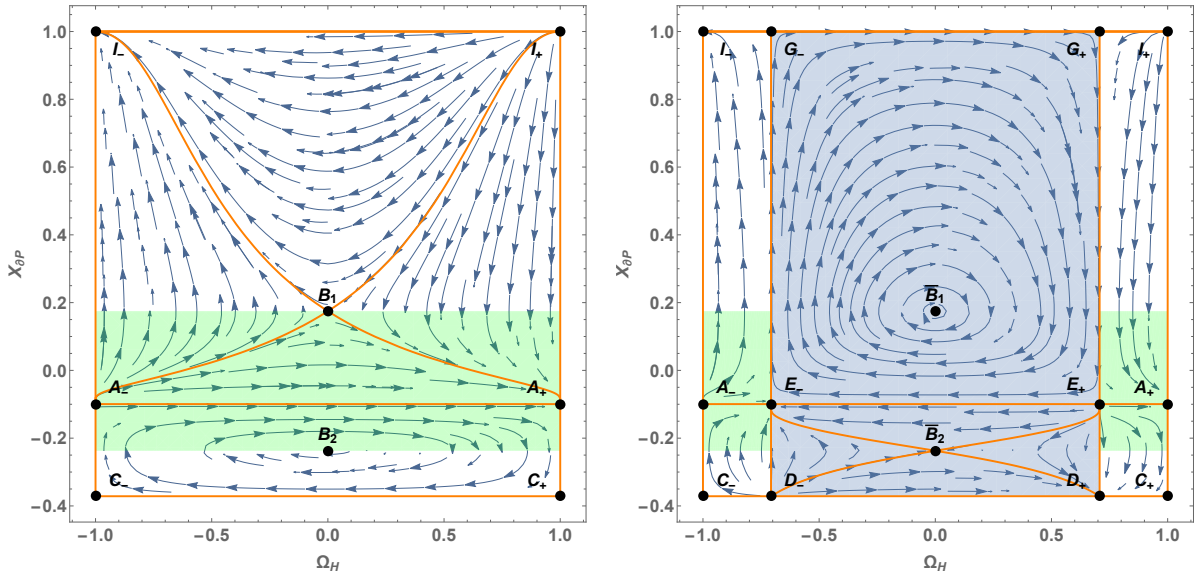

FIG. 12: Invariant subsets $\{\Omega_H, X_{\partial P}\}$ for the quadratic EoS with $P_\star \neq 0$. The right panel corresponds to the positive spatial curvature and the left panel corresponds to the negative spatial curvature case. The invariant subsets are plotted for the parameters $\delta = 1$, $\sigma = -4$, $\xi = -1$ and $\zeta = 0.1$. The orange thick lines are the separatrices of the system, the blue region corresponds to $\Omega_\epsilon < 0$ and the green shaded region corresponds to accelerated dynamics. This figure corresponds to Fig. 16 in [21].

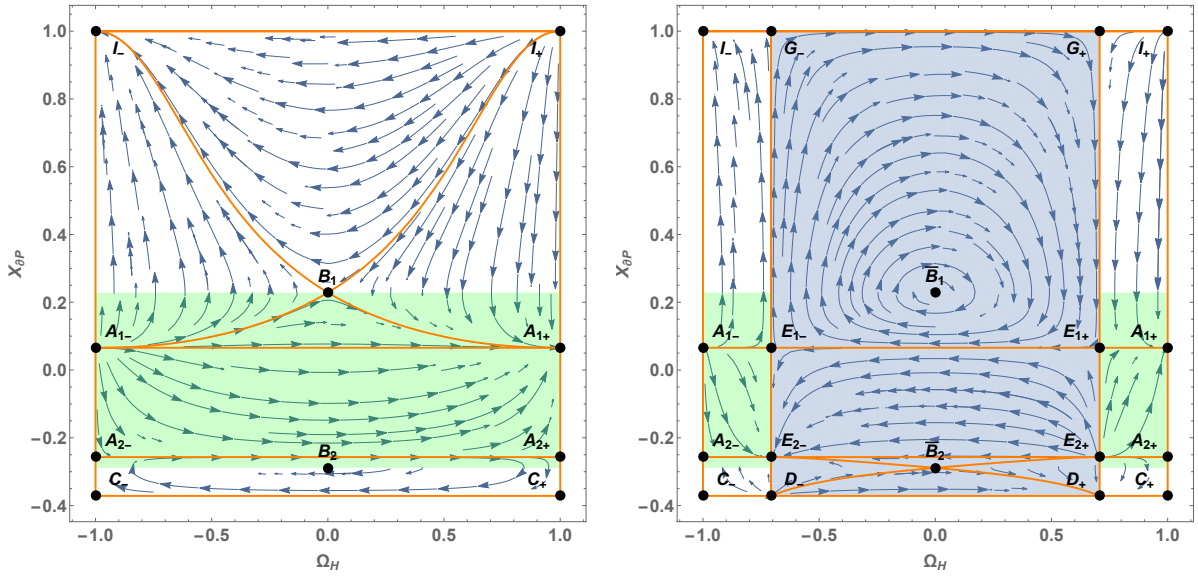

FIG. 13: Invariant subsets $\{\Omega_H, X_{\partial P}\}$ for the quadratic EoS with $P_\star \neq 0$. The right panel corresponds to the positive spatial curvature and the left panel corresponds to the negative spatial curvature case. The invariant subsets are plotted for the parameters $\delta = 1$, $\sigma = -4$, $\xi = -1.5$ and $\zeta = 0.1$. The orange thick lines are the separatrices of the system, the blue region corresponds to $\Omega_\epsilon < 0$ and the green shaded region corresponds to accelerated dynamics. This figure corresponds to Fig. 17 in [21].

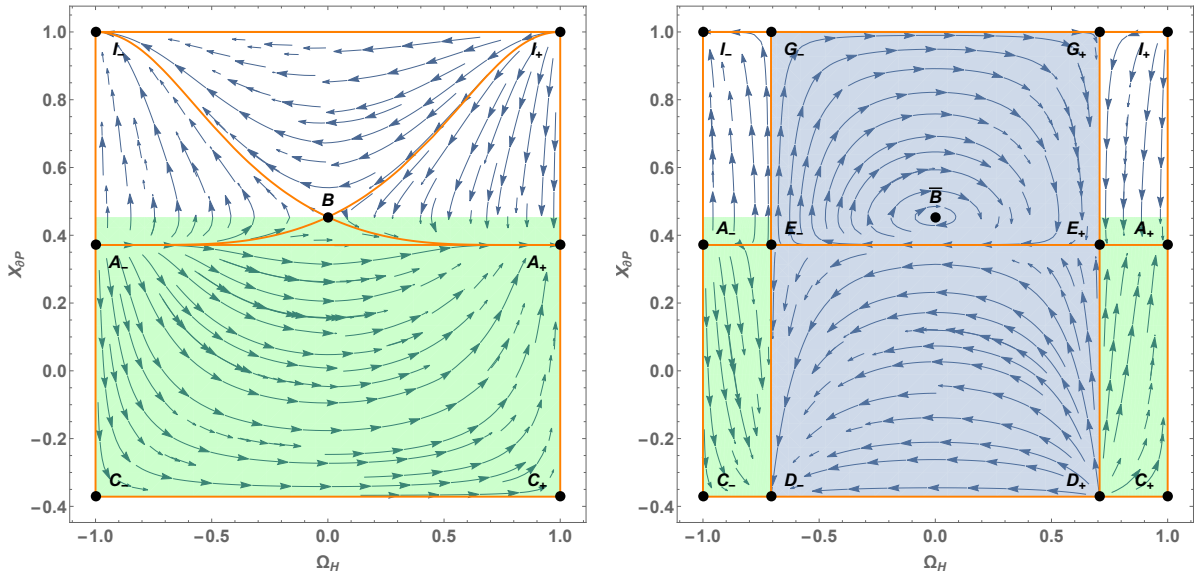

FIG. 14: Invariant subsets $\{\Omega_H, X_{\partial P}\}$ for the quadratic EoS with $P_\star \neq 0$. The right panel corresponds to the positive spatial curvature and the left panel corresponds to the negative spatial curvature case. The invariant subsets are plotted for the parameters $\delta = 1$, $\sigma = -4$, $\xi = -8$ and $\zeta = 0.1$ (these figures are topologically similar to the cases with parameters $\delta = 1$, $-1 < \sigma < -\frac{1}{3}$, $\xi < \sigma$ and also $\delta = 1$, $-\frac{1}{3} < \sigma$, $\xi < \sigma$). The orange thick lines are the separatrices of the system, the blue region corresponds to $\Omega_\epsilon < 0$ and the green shaded region corresponds to accelerated dynamics. This figure corresponds to Fig. 13 in [21].

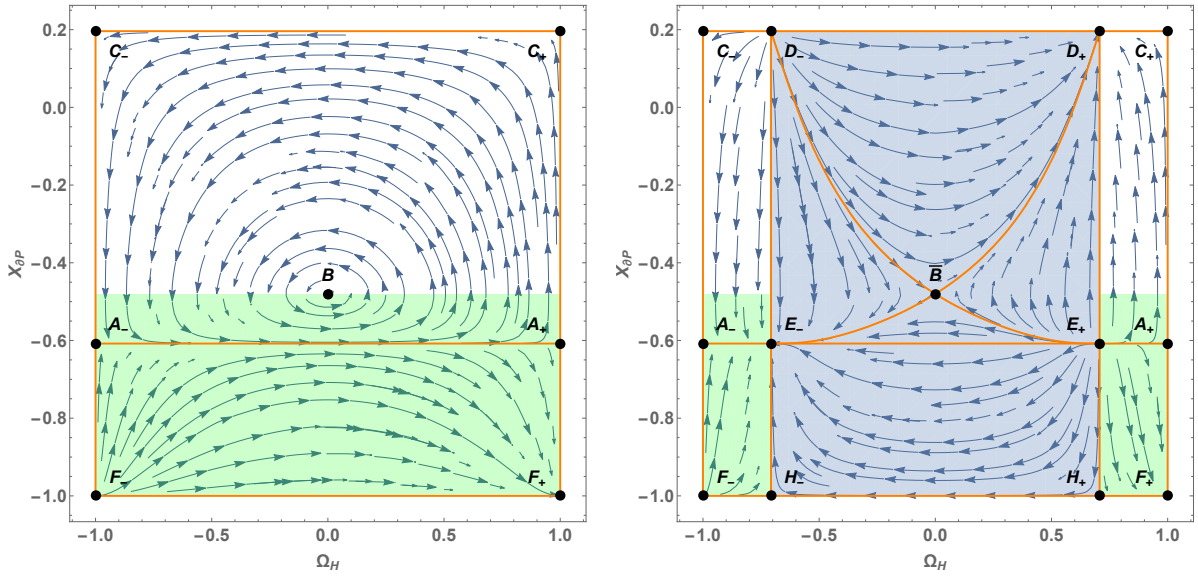

FIG. 15: Invariant subsets $\{\Omega_H, X_{\partial P}\}$ for the quadratic EoS with $P_\star \neq 0$. The right panel corresponds to the positive spatial curvature and the left panel corresponds to the negative spatial curvature case. The invariant subsets are plotted for the parameters $\delta = -1$, $\sigma = 1$, $\xi = 3$ and $\zeta = 0.2$ (these figures are topologically similar to the cases with parameters $\delta = -1$, $\sigma < -1$, $\sigma < \xi$ and also $\delta = -1$, $-1 < \sigma < -\frac{1}{3}$, $\sigma < \xi$). The orange thick lines are the separatrices of the system, the blue region corresponds to $\Omega_\epsilon < 0$ and the green shaded region corresponds to accelerated dynamics. This figure corresponds to Fig. 8 in [21].

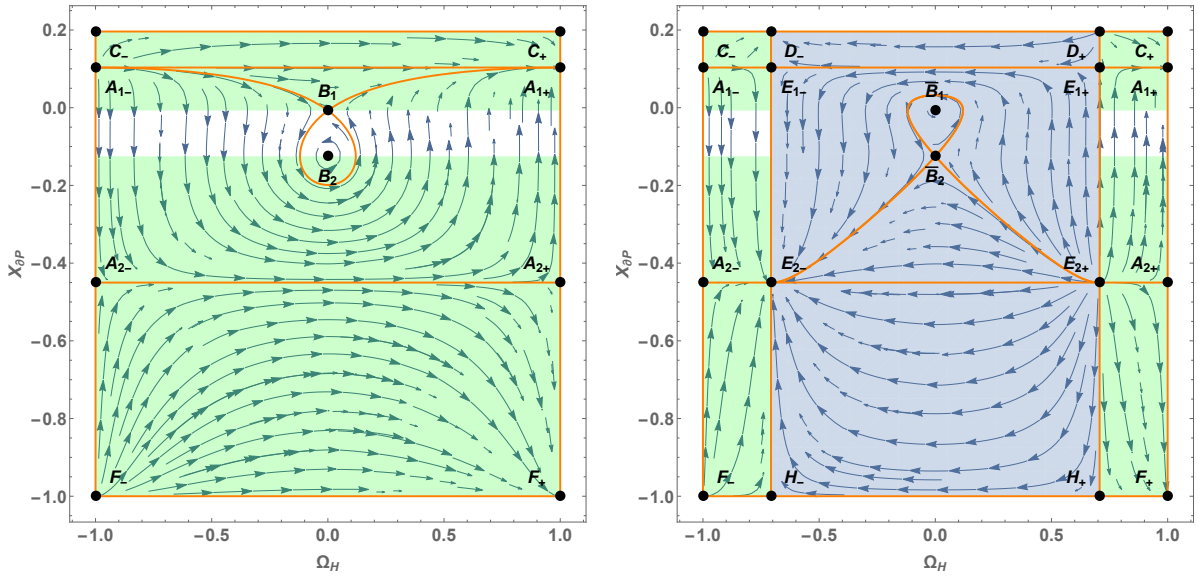

FIG. 16: Invariant subsets $\{\Omega_H, X_{\partial P}\}$ for quadratic EoS with $P_\star \neq 0$. The right panel corresponds to the positive spatial curvature and the left panel corresponds to the negative spatial curvature case. The invariant subsets are plotted for the parameters $\delta = -1$, $\sigma = 1$, $\xi = -0.3$ and $\zeta = 0.2$. The orange thick lines are the separatrices of the system, the blue region corresponds to $\Omega_\epsilon < 0$ and the green shaded region corresponds to accelerated dynamics the blue regions are not covered by the analysis. This figure corresponds to Fig. 18 in [21].

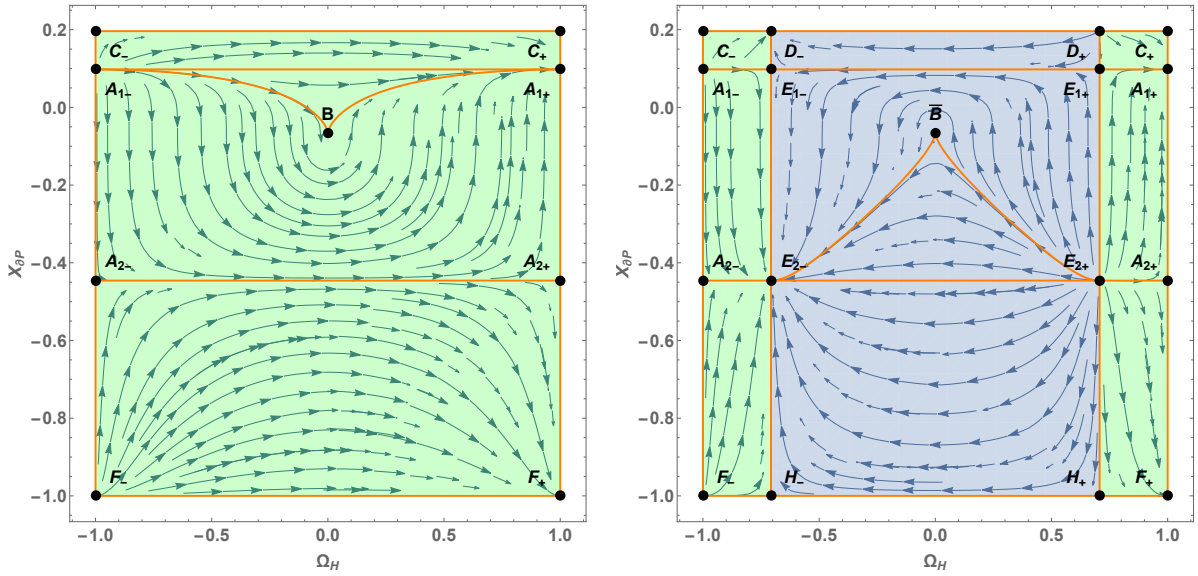

FIG. 17: Invariant subsets $\{\Omega_H, X_{\partial P}\}$ for quadratic EoS with $P_\star \neq 0$. The right panel corresponds to the positive spatial curvature and the left panel corresponds to the negative spatial curvature case. Invariant subsets are plotted for the parameters $\delta = -1$, $\sigma = 1$, $\xi = -\frac{1}{3}$ and $\zeta = 0.2$. The orange thick lines are the separatrices of the system, the blue region corresponds to $\Omega_\epsilon < 0$ and the green shaded region corresponds to accelerated dynamics. This figure corresponds to Fig. 19 in [21].

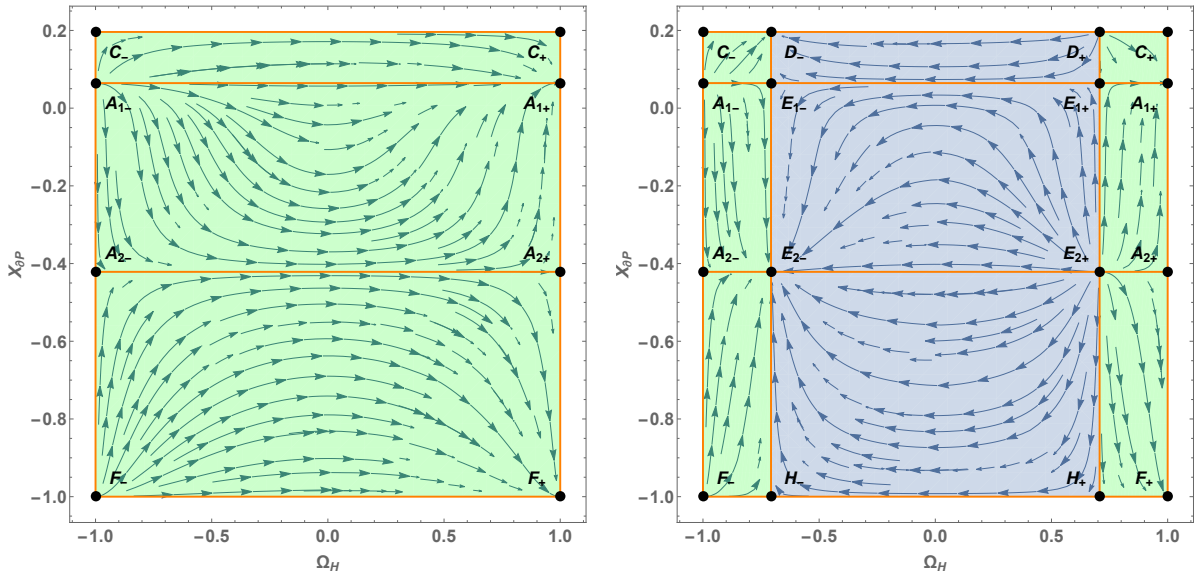

FIG. 18: Invariant subsets $\{\Omega_H, X_{\partial P}\}$ for the quadratic EoS with $P_\star \neq 0$. The right panel corresponds to the positive spatial curvature and the left panel corresponds to the negative spatial curvature case. Invariant subsets are plotted for the parameters $\delta = -1$, $\sigma = 1$, $\xi = -0.5$ and $\zeta = 0.2$ (these figures are topologically similar to the case with parameters $\delta = -1$, $-1 < \sigma < -\frac{1}{3}$, $-1 < \xi < \sigma$). The orange thick lines are the separatrices of the system, the blue region corresponds to $\Omega_\epsilon < 0$ and the green shaded region corresponds to accelerated dynamics. This figure corresponds to Fig. 20 in [21].

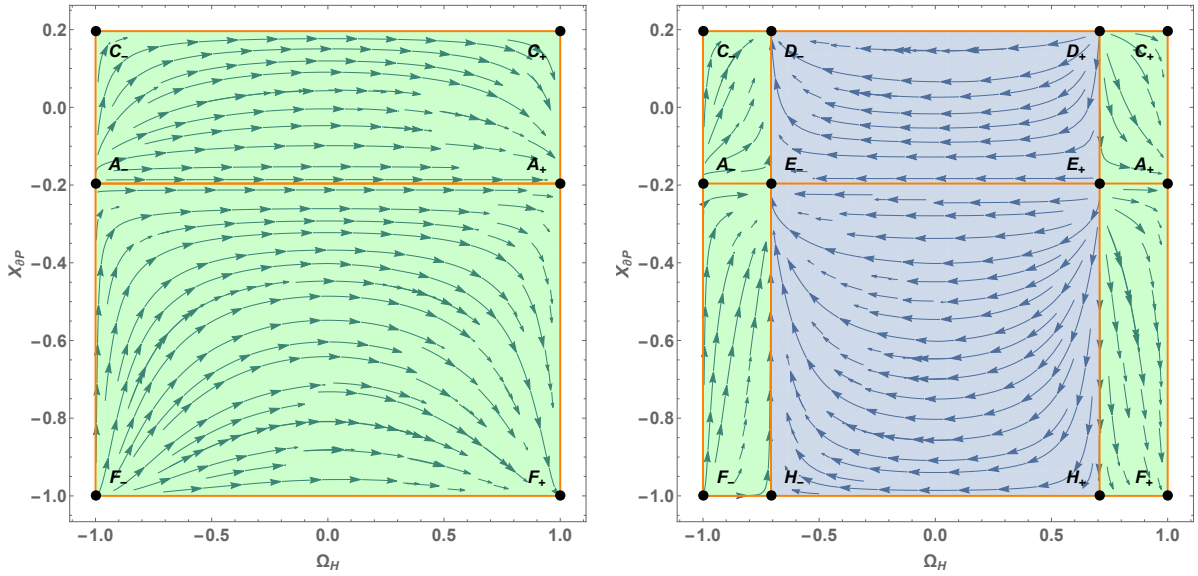

FIG. 19: Invariant subsets $\{\Omega_H, X_{\partial P}\}$ for the quadratic EoS with $P_\star \neq 0$. The right panel corresponds to the positive spatial curvature and the left panel corresponds to the negative spatial curvature case. The invariant subsets are plotted for the parameters $\delta = -1$, $\sigma = 1$, $\xi = -1$ and $\zeta = 0.2$ (these figures are topologically similar to the case with parameters $\delta = -1$, $-1 < \sigma < -\frac{1}{3}$, $\xi = -1$). The orange thick lines are the separatrices of the system, the blue region corresponds to $\Omega_\epsilon < 0$ and the green shaded region corresponds to accelerated dynamics. This figure corresponds to Fig. 21 in [21].

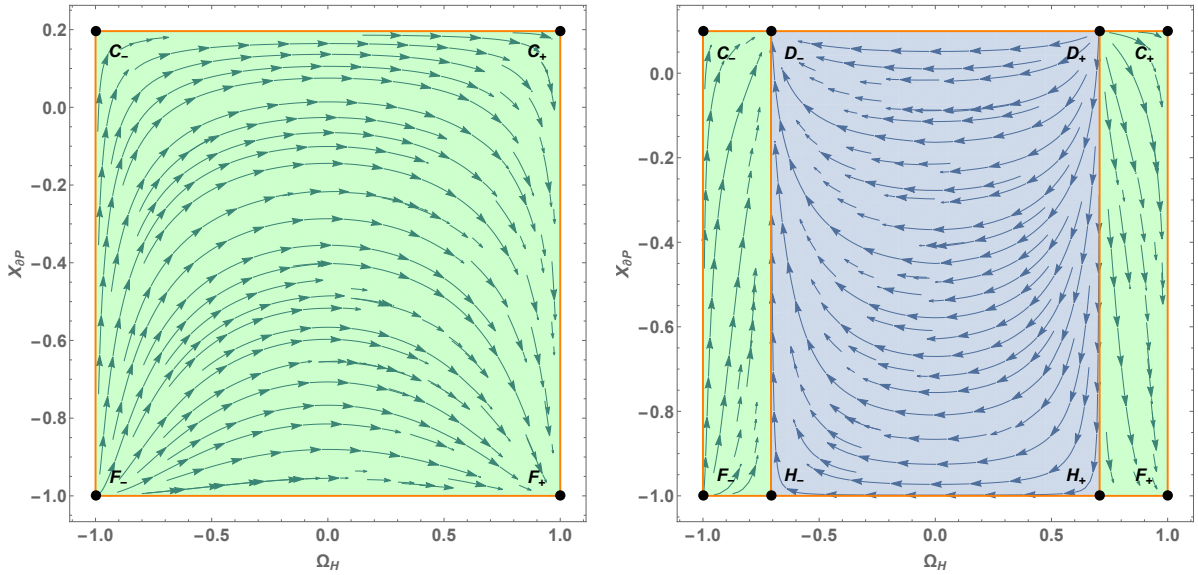

FIG. 20: Invariant subsets $\{\Omega_H, X_{\partial P}\}$ for the quadratic EoS with $P_\star \neq 0$. The right panel corresponds to the positive spatial curvature and the left panel corresponds to the negative spatial curvature case. The invariant subsets are plotted for the parameters $\delta = -1$, $\sigma = 1$, $\xi = -2$ and $\zeta = 0.2$ (these figures are topologically similar to the cases with the parameters $\delta = -1$, $\sigma < -1$, $\xi < \sigma$ and also $\delta = -1$, $-1 < \sigma < -\frac{1}{3}$, $\xi < -1$). The orange thick lines are the separatrices of the system, the blue region corresponds to $\Omega_\epsilon < 0$ and the green shaded region corresponds to accelerated dynamics. This figure corresponds to Fig. 11 in [21].

6. Dynamics of non-minimally coupled scalar field

This chapter is based on the paper Kerachian et al. [2019] " Classes of non-minimally coupled scalar fields in spatially curved FRW spacetimes", published in Physical Review D. Here, we presented the version from arXiv.

In the first part of this paper, we analyzed the dynamics of a non-minimal coupled scalar field, with an unspecified positive potential, in spatially curved FRW spacetime. As we have seen from previous chapters, the first step to start analyzing the dynamics of a cosmological model is to determine the dimensionless variables. However, defining the dimensionless variables for complicated cases, such as non-minimal coupling scalar field, requires more attention than the previous cases studied in Chapters 4 and 5.

In Sec. 1.7, we derived the Friedmann equation for a non-minimal coupling scalar field in Eq.(1.78). This equation together with equation (1.81), will be

$$3\left(H^2+\frac{k}{a^2}\right)\left(1-\xi\,\psi^2\right)=6\,\xi\,H\,\psi\,\dot{\psi}+\frac{1}{2}\,\dot{\psi}^{\,2}+V(\psi). \tag{6.1}$$

In the previous cases, we divide the Friedmann equation by $3H^2$ for the minimal coupling, and $3(H^2+\mid k\mid/a^2)$ for barotropic the fluid; however, here if we divide the Friedmann equation by $3(H^2+\mid k\mid/a^2)(1-\xi\psi^2)$, we would not get the suitable dimensionless variables. The problem comes from the fact that, by doing this, we came to the dimensionless variables which are mixture of spacetime elements and scalar field. Therefore, we transformed the Friedmann equation (6.1) for positive spatial curvature into the form

$$3\left(H^2+\frac{k}{a^2}\right)\left(1+\xi\,\psi^2\right)=6\,\xi\,\psi^2\,\frac{k}{a^2}+3\,\xi\left[2\,\psi^2\,H^2+2\,H\,\psi\,\dot{\psi}+\frac{1}{2}\,\dot{\psi}^{\,2}\right]+\frac{1}{2}\,(1-3\,\xi)\,\dot{\psi}^{\,2}+V(\psi), \tag{6.2}$$

at this point, we can divide both sides by $3\left(H^2+\frac{k}{a^2}\right)(1+\xi\,\psi^2)$ to get

$$\begin{aligned}1=&\,2\xi\,(\frac{\psi}{\sqrt{1+\xi\,\psi^2}})^2\,\frac{k/a^2}{D^2}\\&+3\,\xi\,\left[\frac{2}{3}\,(\frac{\psi}{\sqrt{1+\xi\,\psi^2}})^2(\frac{H}{D})^2+2\sqrt{\frac{2}{3}}\,\frac{\psi}{\sqrt{1+\xi\,\psi^2}}\,\frac{H}{D}+(\frac{\dot{\psi}}{\sqrt{6}D\sqrt{1+\xi\,\psi^2}})^2\right]\\&+(1-3\,\xi)\,\frac{\dot{\psi}}{6\,D^2\,(1+\xi\,\psi^2)}+\frac{V}{3\,D^2\,(1+\xi\,\psi^2)},\end{aligned} \tag{6.3}$$

where $D=\sqrt{H^2+\mid k\mid/a^2}$. Thus, from the former equation, it is easy to determine the well-defined dimensionless variables (see Kerachian et al. [2019]). By substituting those variables into the Friedmann equation (6.3), after some

manipulations we obtain

$$1 = 2\,\xi\,\Omega^2\,\left(1-\Omega_H^2\right) + 3\,\xi\,\left(\sqrt{\frac{2}{3}}\,\Omega_H\,\Omega + \Omega_\psi\,\sqrt{1-\xi\,\Omega^2}\right)^2 + (1-3\,\xi)\,\Omega_\psi^2\,\left(1-\xi\,\Omega^2\right) + \Omega_V^2\,\left(1-\xi\,\Omega^2\right). \tag{6.4}$$

In a similar way, one can determine the Friedmann equation for the negative spatial curvature.

From this procedure, one can define the well-defined dimensionless variables, namely all the dimensionless variables are only a function of either spacetime elements or scalar field divided by the normalization $f(D)$.

From the dynamical variables we determined the autonomous system and from that, the critical points of this systems were derived together with their cosmological interpretation. For this general setup, we identified the following critical points/ lines/ planes of the system:

- two de Sitter critical points for the case $k = 0$,
- two de Sitter critical lines for the case $k = 0$,
- two radiation-like critical lines for the case $k = 0$,
- two Milne-like critical planes for the case $k < 0$.

In the second part of this work, we analyzed the specific potentials, namely the exponential potentials, the runaway potentials, and potentials with positive powers of the field.

Classes of non-minimally coupled scalar fields in spatially curved FRW spacetimes

Morteza Kerachian,[1,*] Giovanni Acquaviva,[1,†] and Georgios Lukes-Gerakopoulos[2,‡]

[1] *Institute of Theoretical Physics, Faculty of Mathematics and Physics, Charles University, CZ-180 00 Prague, Czech Republic*

[2] *Astronomical Institute of the Academy of Sciences of the Czech Republic, Boční II 1401/1a, CZ-141 00 Prague, Czech Republic*

In this work we perform a dynamical analysis of a broad class of non-minimally coupled real scalar fields in the Friedmann-Robertson-Walker (FRW) spacetime framework. The first part of our study concerns the dynamics of an unspecified positive potential in a spatially curved FRW spacetime, for which we define a new set of dimensionless variables and a new evolution parameter. In the framework of this general setup we have recognized several general features of the system, like symmetries, invariant subsets and critical points, and provide their cosmological interpretation. The second part of our work focuses on flat FRW cases for which the tracker parameter is constant, i.e. we examine specific classes of potentials. After analyzing these cases dynamically, we discuss their physical interpretation.

PACS numbers:
Keywords: Gravitation, Cosmology; Dynamical systems

1. INTRODUCTION

The importance of scalar fields in cosmological frameworks is manifold. In the context of inflation [1–4], for instance, field theories have been proposed which could appropriately explain the observational evidence of large-scale homogeneity and flatness of the Universe, together with several other features (the graceful exit from inflation itself [5] and the subsequent reheating [6]). While the specific mechanism giving rise to such *inflaton field* is still debated, several forms of potentials that are able to trigger a transient phase of exponential expansion of the Universe have been proposed, see *e.g.* [7, 8]. Scalar fields play a major role as well in the description of the present-day accelerated expansion of the Universe [9]: the simplest and most effective model available, the ΛCDM, considers a constant potential, but the origin of such *cosmological constant* is purely phenomenological and cannot be physically motivated in the context of GR and quantum field theory yet; however, other potential forms [10, 11] are also able to provide the necessary slow-rolling dynamic of the field, which is necessary for achieving a sufficiently negative pressure and consequently an acceleration of the scale factor's expansion.

In a Lagrangian formulation of a gravitating scalar field, the simplest choice is to ignore any direct coupling between the field and the Ricci curvature, *i.e.* to consider the so-called *minimal coupling*. However, the inclusion of coupling terms involving products of the Ricci scalar with the field (or its derivatives [12–14]) can be motivated in different contexts: they can arise from quantum corrections to the field in curved metrics [15, 16] or as low-energy limits of superstring theories or in induced gravity [17, 18]; moreover, a non-minimal coupling can render the Higgs field a good candidate for inflation [19], hence giving a cosmological status to the recently-discovered particle [20]. On a more fundamental level, requiring a non-minimal coupling is actually necessary in order to avoid causal pathologies in the propagation of the fields in generic curved backgrounds [21]. Several authors have analysed the repercussions of non-minimal couplings on the cosmological dynamics [22–31],

In the present paper we perform a global analysis of models in which a curved Friedmann-Robertson-Walker background is non-minimally coupled to a scalar field with generic potential. A similar analysis in the context of dynamical systems has been performed in [28] with the additional presence of matter. Our goal here is to present an alternative formulation which allows for several improvements in the aforementioned analysis. Namely we consider a generic spatially curved FRW model and we include in the analysis the collapsing scenarios as well. In Sec. 2 we provide definitions of dimensionless variables that render the invariant subsets compact in a physically relevant range of the coupling parameter ξ, without the need of further compactification through an additional change of variables. In Sec.3 we perform an initial analysis keeping the potential of the field completely unspecified (apart from its positivity): this approach covers a class of potentials broader than the ones in [28]. Under our general assumptions we derive the existence, stability and cosmological meaning of the critical points of the system. It is known that the system cannot be closed without specifying the functional form of the potential: in Sec.4 we briefly review the case of exponential potentials and then introduce the analysis of the wide class of potentials characterised by a constant tracker parameter Γ. In the latter case, we show that the models with $\Gamma \geq \text{const} > 1$ and constant always posses de Sitter attractors, irrespective of the value of the other parameters

*Electronic address: kerachian.morteza@gmail.com
†Electronic address: gioacqua@gmail.com
‡Electronic address: gglukes@gmail.com

involved.

We start by considering the effective Lagrangian describing a scalar field ψ with generic potential $V(\psi)$ and non-minimally coupled to a FRW background spacetime:

$$L = 6\,\left(\dot{a}^2 - k\right)\,a\,U(\psi) + 6\,\dot{a}\,a^2\,\dot{\psi}\,U'(\psi) - \frac{1}{2}\,a^3\,\dot{\psi}^2 + a^3\,V(\psi), \tag{1}$$

where dot and prime denote derivatives w.r.t. the cosmic time and the scalar field respectively. The function $U(\psi)$ specifies the type of coupling considered: minimal coupling corresponds to a constant $U = 1/2$, while in the following we will consider the quadratic form

$$U = \frac{1}{2}\,\left(1 - \xi\,\psi^2\right)\,, \tag{2}$$

with $\xi \geq 0$. The case $\xi = 1/6$ corresponds to the conformal coupling. With the choice Eq. (2), we can explicitly calculate the momenta conjugate to the generalized coordinates $\{a, \psi\}$, namely

$$p_a \equiv \frac{\partial L}{\partial \dot{a}} = 6\,\dot{a}\,a\,\left(1 - \xi\,\psi^2\right) - 6\,\xi\,a^2\,\psi\,\dot{\psi} \tag{3}$$

$$p_\psi \equiv \frac{\partial L}{\partial \dot{\psi}} = -6\,\xi\,a^2\,\dot{a}\,\psi - a^3\,\dot{\psi}\,, \tag{4}$$

and hence the Hamiltonian function

$$\mathcal{H} \equiv p_a\,\dot{a} + p_\psi\,\dot{\psi} - L \tag{5}$$

The Hamiltonian constraint is expressed by the condition $\mathcal{H} = 0$ and it corresponds to Friedmann equation

$$3\,\left(H^2 + \frac{k}{a^2}\right)\,\left(1 - \xi\,\psi^2\right) = 6\,\xi\,H\,\psi\,\dot{\psi} + \frac{1}{2}\,\dot{\psi}^2 + V(\psi)\,, \tag{6}$$

where $H = \dot{a}/a$ is the FRW Hubble expansion. The Hamilton-Jacobi equations,

$$\dot{p}_a = \frac{\partial L}{\partial a} \quad , \quad \dot{p}_\psi = \frac{\partial L}{\partial \psi}\,, \tag{7}$$

correspond, respectively, to Raychaudhuri and Klein-Gordon equations:

$$\left(2\,\dot{H} + 3\,H^2 + \frac{k}{a^2}\right)\,\left(1 - \xi\,\psi^2\right) - 4\,\xi\,H\,\psi\,\dot{\psi} - 2\,\xi\,\psi\,\ddot{\psi} = -\,\left(1 - 4\,\xi\right)\,\frac{1}{2}\,\dot{\psi}^2 + V(\psi) \tag{8}$$

$$\ddot{\psi} + 3\,H\,\dot{\psi} + \partial_\psi V + 6\,\xi\,\psi\,\left(\dot{H} + 2\,H^2 + \frac{k}{a^2}\right) = 0\,. \tag{9}$$

2. THE SYSTEM IN A NEW SET OF VARIABLES

In the minimally coupled case one can clearly distinguish two behaviours of the dynamics depending on the sign of the spatial curvature: specifically, if $k > 0$ the expansion scalar can change sign during the evolution, leading to bounces or recollapses, while if $k \leq 0$ the solutions are either always expanding or always contracting. For this reason, in order to construct well-defined dimensionless variables in the case of positive curvature, one usually employs the normalization $\sqrt{H^2 + k/a^2}$ which is positive definite and does not vanish at the turning points of the scale factor. Introducing a nonminimal coupling renders the former distinction meaningless, due to the modifications of the Raychaudhuri equation which allow for sign changes of H during the evolution irrespective of the sign of k. Since now the evolution of the scale factor can present turning points in either curvature cases, we define a set of dimensionless variables which is well-defined for both:

$$\Omega = \frac{\psi}{\sqrt{1 + \xi\,\psi^2}} \quad , \quad \Omega_H = \frac{H}{D} \tag{10}$$

$$\Omega_\psi = \frac{\dot{\psi}}{\sqrt{6}\,D} \quad , \quad \Omega_V = \frac{\sqrt{V}}{\sqrt{3}\,D} \tag{11}$$

$$\Omega_{\partial V} = \frac{\partial_\psi V}{V} \quad , \quad \Gamma = \frac{V \cdot \partial_\psi^2 V}{(\partial_\psi V)^2} \tag{12}$$

where

$$D^2 = H^2 + \frac{|k|}{a^2}\,. \tag{13}$$

A useful relation is the time evolution of D in terms of the dimensionless variables:

$$\frac{\dot{D}}{D^2} = \Omega_H\,\left(\frac{\dot{H}}{D^2} + \Omega_H^2 - 1\right)\,. \tag{14}$$

The Friedmann, Raychaudhuri and Klein-Gordon equations in terms of the normalized variables will take a different form depending on the sign of the spatial curvature (see next subsections). It is however possible to derive a common autonomous system of equations for the variables, with evolution parameter defined by $d\tau = D\,dt$, by taking derivatives of the definitions with respect to such parameter and using Eq. (14):

$$\Omega' = \sqrt{6}\,\Omega_\psi\,\left(1 - \xi\,\Omega^2\right)^{3/2} \tag{15}$$

$$\Omega_H' = \left(1 - \Omega_H^2\right)\,\left(\frac{\dot{H}}{D^2} + \Omega_H^2\right) \tag{16}$$

$$\Omega_\psi' = \frac{\ddot{\psi}}{\sqrt{6}\,D^2} - \Omega_\psi\,\Omega_H\,\left(\frac{\dot{H}}{D^2} + \Omega_H^2 - 1\right) \tag{17}$$

$$\Omega_V' = \Omega_V\,\left[\sqrt{\frac{3}{2}}\,\Omega_{\partial V}\,\Omega_\psi - \Omega_H\,\left(\frac{\dot{H}}{D^2} + \Omega_H^2 - 1\right)\right] \tag{18}$$

$$\Omega_{\partial V}' = \sqrt{6}\,\Omega_{\partial V}^2\,\Omega_\psi\,\left(\Gamma - 1\right)\,, \tag{19}$$

where $\Gamma = V\,\cdot\,\partial_\psi^2 V/\left(\partial_\psi V\right)^2$ is the so-called tracker parameter. The quantities $\dot{H}$ and $\ddot{\psi}$ are obtained by decoupling Eq. (8) and Eq. (9) and they determine different dynamics for the two curvature cases. For the

generic non-minimally coupled cases the decoupling of the Eqs. (8), (9) can be achieved by diagonalizing the following linear system:

$$\begin{bmatrix} 2(1-\xi\psi^2) & -2\xi\psi \\ 6\xi\psi & 1 \end{bmatrix} \begin{bmatrix} \dot{H} \\ \ddot{\psi} \end{bmatrix} = \begin{bmatrix} f_1(\Omega_i) \\ f_2(\Omega_i) \end{bmatrix}, \qquad (20)$$

where $f_1(\Omega_i)$ and $f_2(\Omega_i)$ include the terms which are not linear in $\dot{H}$ and $\ddot{\psi}$ in Raychaudhuri and Klein-Gordon equations respectively, with Ω_i representing the set of dimensionless variables. In order to diagonalize the matrix in Eq. (20) its determinant should be non-zero, i.e. $\psi^2\,\xi\,(1-6\xi) \neq 1$. The case $\xi = 0$ is trivial, while the conformal coupling case $\xi = 1/6$, as we will see, leads to a generic unboundedness of the invariant subsets of the system. We will be mostly interested in the range $\xi \in (0, 1/6)$ for two reasons: first of all, the invariant subsets of the system in this range of the parameter are compact; moreover, in [32] the value of the coupling constant has been constrained using observational data from the *Union2.1+H(z)+Alcock-Paczyński* data set and found to be in good accord with values around the conformally coupled case. In this sense we will scan the behaviour of the system inside the intersection between the physically motivated and the mathematically convenient range. The vanishing of the determinant for specific values of the field implies the appearance of singularities in the system. Such anomalies are independent of the definition adopted for the dimensionless variables: different definitions would simply move the singularities in different parts of the parameter space. We point out that our choice of dimensionless variables is particularly suitable for the analysis of the late-time behaviour of the system and for situations in which the scalar field diverges $\psi \to \pm\infty$, because the new variable Ω remains finite.

2.1. Positive curvature

When $k > 0$, the Friedmann equation can be expressed in terms of the variables Eqs. (10)-(12) in the following form:

$$1 = 2\,\xi\,\Omega^2\,\left(1-\Omega_H^2\right) + 3\,\xi\,\left(\sqrt{\frac{2}{3}}\,\Omega_H\,\Omega + \Omega_\psi\,\sqrt{1-\xi\,\Omega^2}\right)^2 + (1-3\,\xi)\,\Omega_\psi^2\,\left(1-\xi\,\Omega^2\right) + \Omega_V^2\,\left(1-\xi\,\Omega^2\right) \qquad (21)$$

Since from the definitions we have that $\Omega \in \left(-1/\sqrt{\xi}, 1/\sqrt{\xi}\right)$ and $\Omega_H \in (-1,1)$, the constraint Eq. (21) defines a compact parameter space if $\xi \in (0, 1/6)$ (see discussion in Sec. 2.3 paragraph b). From Klein-Gordon and Raychaudhuri equations we get

$$\frac{\ddot{\psi}}{\sqrt{6}\;D^2} = -3\;\Omega_H\;\Omega_\psi - \sqrt{\frac{3}{2}}\;\Omega_{\partial V}\;\Omega_V^2 - \frac{\sqrt{6}\;\xi\;\Omega}{\sqrt{1-\xi\;\Omega^2}}\left(\frac{\dot{H}}{D^2} + \Omega_H^2 + 1\right), \qquad (22)$$

$$\frac{\dot{H}}{D^2} + \Omega_H^2 + 1 = -\frac{1}{1-2\;\xi\;(1-3\,\xi)\;\Omega^2}\left\{-\frac{1}{2}\left(1-2\,\xi\,\Omega^2\right) + \xi\,\Omega\,\sqrt{1-\xi\,\Omega^2}\left(\sqrt{6}\,\Omega_H\,\Omega_\psi + 3\,\Omega_{\partial V}\,\Omega_V^2\right) + \frac{3}{2}\left(1-\xi\,\Omega^2\right)\left[(1-4\,\xi)\,\Omega_\psi^2 - \Omega_V^2\right]\right\} \qquad (23)$$

2.2. Non-positive curvature

Applying the same definitions given by Eqs. (10)-(12) to the case of non-positive spatial curvature $k \leq 0$, one can express the Friedmann constraint in the following form:

$$1 = 2\;\left(1-\xi\,\Omega^2\right)\;\left(1-\Omega_H^2\right) + 3\,\xi\,\left(\sqrt{\frac{2}{3}}\,\Omega_H\,\Omega + \Omega_\psi\,\sqrt{1-\xi\,\Omega^2}\right)^2 + (1-3\,\xi)\,\Omega_\psi^2\,\left(1-\xi\,\Omega^2\right) + \Omega_V^2\,\left(1-\xi\,\Omega^2\right). \qquad (24)$$

In this case the parameter space spanned by such variables is not compact, because Ω_ψ diverges as $\Omega \to \pm 1/\sqrt{\xi}$. Eqs. (8)-(9) give

$$\frac{\ddot{\psi}}{\sqrt{6}\;D^2} = -\,3\;\Omega_H\;\Omega_\psi - \sqrt{\frac{3}{2}}\;\Omega_{\partial V}\;\Omega_V^2 + \frac{\sqrt{6}\;\xi\;\Omega}{\sqrt{1-\xi\;\Omega^2}}\left(1 - \frac{\dot{H}}{D^2} - 3\,\Omega_H^2\right), \qquad (25)$$

$$\frac{\dot{H}}{D^2} + \Omega_H^2 = \frac{1}{2} - \Omega_H^2 + \frac{1}{1-2\;\xi\;(1-3\,\xi)\;\Omega^2}\left\{3\,\xi^2\,\Omega^2\;\left(1-2\,\Omega_H^2\right) - \xi\,\Omega\,\sqrt{1-\xi\,\Omega^2}\left(\sqrt{6}\,\Omega_H\,\Omega_\psi + 3\,\Omega_{\partial V}\,\Omega_V^2\right) - \frac{3}{2}\left(1-\xi\,\Omega^2\right)\left[(1-4\,\xi)\,\Omega_\psi^2 - \Omega_V^2\right]\right\}. \qquad (26)$$

2.3. General features of the system

a. Symmetries. The dynamical system (15)-(19) remains invariant under the simultaneous transformation $\{\Omega, \Omega_H, \Omega_\psi, \Omega_V, \Omega_{\partial V}\} \to \{-\Omega, \Omega_H, -\Omega_\psi, \Omega_V, -\Omega_{\partial V}\}$. Physically such symmetry is equivalent to the invariance

under the transformation $\psi \to -\psi$. Having assumed the positivity of the potential, we have that $V(-\psi)$ is still positive and hence Ω_V is not affected by this transformation.

b. Singularities. As we have discussed before, the decoupling of Raychaudhuri and Klein-Gordon equations cannot be carried out if the determinant of Eq. (20) vanishes: the points where this is the case appear as singularities in the autonomous system. In terms of dimensionless variables these singularities correspond to the vanishing of the denominators in Eqs. (23) and (26), namely

$$\Omega = \pm \frac{1}{\sqrt{2\xi(1-3\xi)}}. \tag{27}$$

By plugging Eq. (27) into the Friedmann constraints and solving for Ω_ψ we get

$$\Omega_\psi = \frac{\sqrt{6\xi}\Omega_H + \sqrt{(\Omega_H^2 \mp \Omega_V^2 - 1)6\xi \pm \Omega_V^2}}{\sqrt{1-6\xi}}, \tag{28}$$

where the upper/lower sign corresponds to negative/positive curvature. In either cases the coordinates (Ω, Ω_ψ) of the singularity remain finite in the range $\xi \in (0, 1/6)$. For $\xi > 1/6$, Ω_ψ is complex. In the case of a flat spacetime $\Omega_H = \pm 1$ we call these singularities $S_\pm$ respectively. Comparing with [28], we note that for $\Omega_H^2 = 1$ and $\Omega_V = 0$ this corresponds to their critical point 1., which was identified as a finite scale factor singularity. Such critical point was identified thanks to a time reparametrization (see eq. (2.14) of [28]), which, however, we are not considering here as it is ill-defined in the point (27).

c. Invariant subsets. Invariant submanifolds are very useful tools in studying a dynamical system, as they allow to characterize and understand some global features of the phase space. One can identify some invariant subsets of the system Eqs. (15)-(19), namely $\Omega_H = \pm 1$ (flat spacetime) and $\Omega_V = 0$ (free scalar field). For the latter case we plot in the left and right panels of Fig. 1 the Friedmann constraints (21) and (24) respectively; in the middle panel of Fig. 1 we plot the Friedmann constraint in the spatially flat expanding case $\Omega_H = 1$ (the collapsing case can be obtained by transforming $\Omega_\psi \to -\Omega_\psi$). Notice that our definitions of variables allow to have compact invariant subsets for the positive and zero curvature cases, but not for the negative curvature case.

Although from the system of equations $\Omega = \pm 1/\sqrt{\xi}$ looks like an invariant subset, it is actually outside of the Friedmann constraint in the case of positive and zero spatial curvature; for negative curvature, instead, the Friedmann constraint in that locus reduces to $\Omega_H^2 = 1/2$.

The condition $\Omega_{\partial V} = $ const., which is equivalent to $\Gamma = 1$ (including the $\Omega_{\partial V} = 0$ case), looks also like an invariant subset due to Eq. (19), but this is a more subtle case, since choosing a constant value of $\Omega_{\partial V}$ actually constraints the form of the potential to the exponential form $V = V_0\, e^{\Omega_{\partial V}\,\psi}$ (see, e.g., [33] and references therein). We will discuss these kind of potentials in Sec 4. However, being the potential V a function of the field ψ only, in order to allow for the most general forms of the potential, $\Omega_{\partial V}$ has to be left as a general function of Ω.

3. CRITICAL POINTS AND THEIR INTERPRETATION

To study the behaviour of the dynamical system Eqs. (15)-(19), we need to derive the equilibrium points of the system. The equilibrium points (or critical points) of the system $\boldsymbol{\Omega}' = \boldsymbol{f}(\boldsymbol{\Omega})$ correspond to those points $\boldsymbol{\Omega_c}$ that satisfy $\boldsymbol{\Omega}'(\boldsymbol{\Omega_c}) = 0$, which means that the system is at rest. The stability of the critical points can be investigated by inspecting the eigenvalues of the Jacobian matrix of the linearized system evaluated at each critical point: if the real part of all eigenvalues is positive (resp. negative), then the point is an unstable source (resp. stable sink); mixed signs of the eigenvalues signal the presence of a saddle point; the presence of vanishing eigenvalues means that the critical point is non-hyperbolic and one would need to implement further method in order to ascertain the stability unambiguously – or resort to numerical and visual approaches.

One can interpret the critical points in terms of cosmological models thanks to several physical quantities, such as the *deceleration parameter*

$$q = -1 - \Omega_H^{-2}\,\frac{\dot{H}}{D^2}\,, \tag{29}$$

and the *effective equation of state parameter*, which stems from considering the scalar field as a barotropic fluid sourcing the unmodified Einstein's equations with equation of state

$$w_e = \frac{p_e}{\epsilon_e}, \tag{30}$$

where from Eqs. (6), (8) we define the *effective energy density* and *pressure*, respectively:

$$\epsilon_e := 3\left(H^2 + \frac{k}{a^2}\right), \tag{31}$$

$$p_e := -2\dot{H} - 3H^2 - \frac{k}{a^2}. \tag{32}$$

3.1. Two de Sitter critical points

The coordinates of these two critical points are $\{\Omega, \Omega_H, \Omega_\psi, \Omega_V, \Omega_{\partial V}\} = \{0, \pm 1, 0, 1, 0\}$. One of these points (called A_+) has $\Omega_H = 1$ and it describes an exponentially expanding model, i.e $a \sim e^{H_0 t}$, with the typical cosmological constant behaviour given by $q = -1$ and $w_e = -1$. The corresponding eigenvalues are

$$\{\lambda_i^{A_+}\} = \{-3, -2, 0, -\frac{\sqrt{3}}{2}\Big(\sqrt{3} + \sqrt{3 - 16\xi}\Big),$$
$$\frac{\sqrt{3}}{2}\Big(-\sqrt{3} + \sqrt{3 - 16\xi}\Big)\}, \tag{33}$$

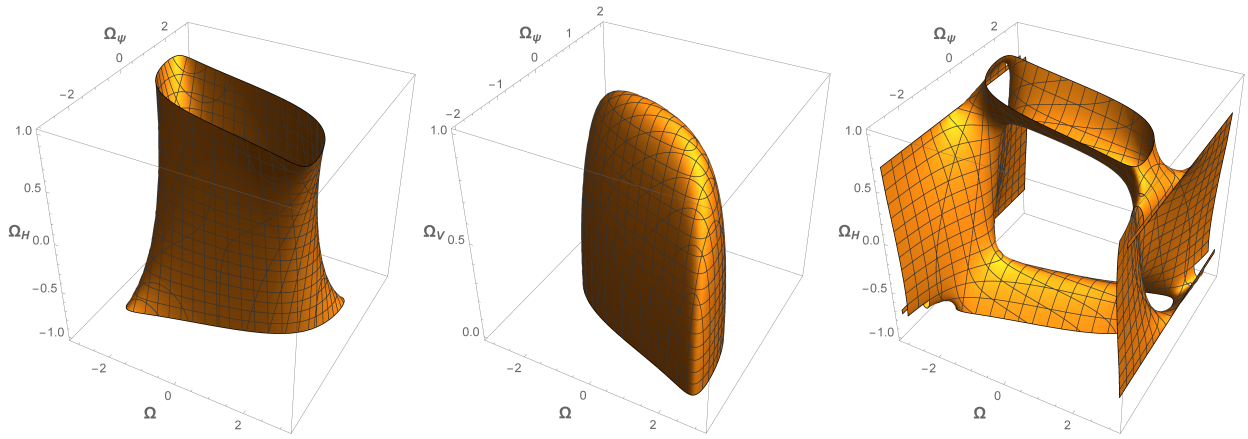

FIG. 1: Invariant subsets constrained by the Friedmann equations for $\xi = 1/10$. *Left Panel:* Positive curvature Eq. (21) for $\Omega_V = 0$. *Middle Panel:* Spatially flat Eqs. (21) and (24) for $\Omega_H = 1$. *Right Panel:* Non-positive curvature Eq. (24) for $\Omega_V = 0$.

TABLE I: The critical elements of the system and their stability in the range $0 \leq \xi \leq 1/6$.

	Ω_ψ	Ω_H	Ω	Ω_V	$\Omega_{\partial V}$	Curvature	q	w_e	stability
A_+	0	1	0	1	0	flat	-1	-1	sink
A_-	0	-1	0	1	0	flat	-1	-1	source
B_+	0	1	$0 < \Omega^2 < \frac{1}{2\xi}$	$\sqrt{\frac{1-2\xi\Omega^2}{1-\xi\Omega^2}}$	$-\frac{4\xi\Omega\sqrt{1-\xi\Omega^2}}{1-2\xi\Omega^2}$	flat	-1	-1	sink
B_-	0	-1	$0 < \Omega^2 < \frac{1}{2\xi}$	$\sqrt{\frac{1-2\xi\Omega^2}{1-\xi\Omega^2}}$	$-\frac{4\xi\Omega\sqrt{1-\xi\Omega^2}}{1-2\xi\Omega^2}$	flat	-1	-1	source
$C_\pm$	0	± 1	$\pm\frac{1}{\sqrt{2\xi}}$	0	$\forall$	flat	1	$\frac{1}{3}$	saddle
$D_\pm$	0	$\pm\frac{1}{\sqrt{2}}$	$\forall$	0	$\forall$	negative	0	-	saddle

where the $i = 1, ..., 5$. The real parts of all the non-vanishing eigenvalues is always negative.

The critical point with $\Omega_H = -1$ (called A_-) describes an exponentially collapsing model, i.e. $a \sim e^{-H_0 t}$ with $q = -1$ and $w_e = -1$. The eigenvalues in this case are

$$\{\lambda_i^{A_-}\} = \{3, 2, 0, \frac{\sqrt{3}}{2}\Big(\sqrt{3} - \sqrt{3 - 16\xi}\Big), \frac{\sqrt{3}}{2}\Big(\sqrt{3} + \sqrt{3 - 16\xi}\Big)\}, \tag{34}$$

The real part of all the non-vanishing eigenvalues is always positive.

For both points, the eigenvalues are complex in the range $\xi > 3/16$: this signals a transition of the character of the critical points from node to focus and it is in accord with the findings of [34]. Since $\Omega_{\partial V} = 0$, then in a neighborhood of the critical points $V = V_0 > 0$: this eliminates the relevance of the $\Omega'_{\partial V}$ equation in such neighborhood. Using the remaining 4×4 system of equations with $\Omega_{\partial V} = 0$, one recovers exactly the above sets of eigenvalues (33), (34) where the $\lambda_3^{A_\pm} = 0$ are missing. This indicates that indeed the A_+ and A_- are a sink and a source respectively.

3.2. Two de Sitter critical lines

These critical points lie along the segments $0 < \Omega^2 < \frac{1}{2\xi}$ for the cases $\Omega_H = \pm 1$ with $\Omega_\psi = 0$, $\Omega_V^2 = \frac{1-2\xi\Omega^2}{1-\xi\Omega^2}$ and[1]

$$\Omega_{\partial V} = -\frac{4\xi\Omega\sqrt{1-\xi\Omega^2}}{1-2\xi\Omega^2}\,. \tag{35}$$

In this case one can derive a form of the potential in a neighbourhood of the critical lines by integrating the definition of $\Omega_{\partial V}$ as a function of Ω given above: transforming back to the variable ψ one obtains

$$V = V_0(1 - \xi\psi^2)^2, \tag{36}$$

as well as $H = \pm\sqrt{V_0(1 - \xi\psi^2)/3}$. Potential (36) has a Higgs-like form which can provide a symmetry breaking Goldstone mechanism. One can see that $\Omega = 0$ corresponds to the local maximum of the potential, while $\Omega = \pm 1/\sqrt{2\xi}$ correspond to the global minima.

[1] Note that the since $\Omega_V > 0$ by definition, the only acceptable solution is $\Omega_V = \sqrt{\frac{1-2\xi\Omega^2}{1-\xi\Omega^2}}$ (Table I). Similarly, in Sec. 3.1 from $\Omega_V = \pm 1$ we accept only $\Omega_V = 1$.

Exactly on the critical lines, both the potential V and the Hubble parameter H are constant, thus describing exponentially expanding and collapsing models with $a \sim e^{\pm Ht}$ respectively. For calculating the eigenvalues below, we need to specify Γ. To do this, we use the local expression of the potential (36). These points for $\Omega_H = 1$ (called B_+) describe sources, since they have eigenvalues

$$\{\lambda_i^{B_+}\} = \{0, -2, 0, -3, -3\}, \tag{37}$$

which holds in the allowed ranges of ξ and Ω.

The critical points for $\Omega_H = -1$ (called B_-) have eigenvalues

$$\{\lambda_i^{B^-}\} = \{0, 2, 3, 3, 0\}, \tag{38}$$

thus, we can interpret B_- as source points.

Critical points A_+ and B_+ agree with the critical points 5 of [28], in our analysis there are additionally the A_- and B_- sources describing collapsing models. As it is stressed in [28] the evolution of the system is independent of the form of the potential, but we find that in the neighborhood of $B_\pm$ the potential has to acquire the form (36).

One would expect that in the limit $\Omega \to 0$ one should recover the eigenvalues of the previous critical point, *i.e.* $\{\lambda_i^{B_\pm}\} \to \{\lambda_i^{A_\pm}\}$, which however is not the case, since potential (36) is just an approximation holding in the neighbourhood of the critical line. However, the feature that matters for the local stability is the sign of the $\{\lambda_i^{B_\pm}\}$. Just like in Sec. 3.1, specifying the local form of the potential makes one equation of motion redundant and thus reduces the dimensionality of the system.

3.3. Two radiation-like critical lines

There exist other sets of critical points arranged as critical lines with coordinates

$$\{\Omega, \Omega_H, \Omega_\psi, \Omega_V, \Omega_{\partial V}\} = \{\pm\frac{1}{\sqrt{2\xi}}, \pm 1, 0, 0, \forall\}. \tag{39}$$

The cosmological parameters at these points are $q = 1$ and $w_e = \frac{1}{3}$, being in agreement with the model describing a radiation dominated universe in which the scale factor evolves like $a \sim \sqrt{t}$. The corresponding eigenvalues are

$$\{\lambda_i^{C_+}\} = \{2, 2, -1, 1, 0\}, \tag{40}$$

for $\Omega_H = 1$ (called C_+), and

$$\{\lambda_i^{C_-}\} = \{-2, -2, -1, 1, 0\}, \tag{41}$$

for $\Omega_H = -1$ (called C_-).

To investigate the exact form of scale factor, from Raychaudhuri equation we get

$$H = \frac{1}{2(t - t_0) + \frac{1}{H_0}}, \tag{42}$$

where H_0 is the Hubble parameter value at time t_0 with $a_0 = 1$. For expanding models ($\dot{a} > 0$) $a = \sqrt{2H_0(t - t_0) + 1}$ with $t > t_0 - \frac{1}{2H_0}$, while for collapsing ($\dot{a} < 0$) $a = \sqrt{-(2H_0(t - t_0) + 1)}$ with $t < t_0 - \frac{1}{2H_0}$. Since the eigenvalues of both critical lines have real parts with mixed signs, they correspond to saddle points. The set of points B_+ agrees with the critical point 3.b of [28].

3.4. Two Milne-like critical planes

These critical points lie on planes defined by $\{\Omega, \Omega_H, \Omega_\psi, \Omega_V, \Omega_{\partial V}\} = \{\forall, \pm\frac{1}{\sqrt{2}}, 0, 0, \forall\}$.[2] All points in this case describe vacuum FLRW space-time with negative spatial curvature. This model is known as the Milne universe with the scale factor $a = c_2(t + c_1)$ and Hubble function $H = \frac{1}{t+c_1}$. Given that $\Omega_H^2 = 1/2$, one finds that $c_2^2 = |k|$. From the definitions of the effective energy and pressure (31), (32) we get that $\epsilon_e = 0$ and $p_e = 0$. This implies that we have a vacuum universe dominated by negative curvature and the effective equation of state parameter (30) is undefined. Furthermore, this implies that $D \to 0$ for $t \to \infty$. Since $\Omega_V = 0$ and $\Omega_\psi = 0$ in the critical point, we necessarily have that $\dot{\psi} \to 0$ and $V \to 0$, both faster than D approaches zero. Since we do not have a specific form for the potential, the limiting value of $\Omega_{\partial V}$ remains unspecified.

For the line with $\Omega_H = \frac{1}{\sqrt{2}}$, which we call D_+, we get the eigenvalues

$$\{\lambda_i^{D_+}\} = \{0, 0, \frac{1}{\sqrt{2}}, -\sqrt{2}, -\frac{1}{\sqrt{2}}\}, \tag{43}$$

and for $\Omega_H = -\frac{1}{\sqrt{2}}$, which we call D_- , we get

$$\{\lambda_i^{D^-}\} = \{0, 0, -\frac{1}{\sqrt{2}}, \frac{1}{\sqrt{2}}, \sqrt{2}\}. \tag{44}$$

The mixed character of the eigenvalues identify these critical planes as saddles.

4. SPECIFIC POTENTIAL CASES

Once a form of potential is chosen, the system is completely specified and the variable $\Omega_{\partial V}$ becomes redundant. In the most general case $\Omega_{\partial V}$ has to be a function of Ω only, because $V = V(\psi)$. This fact allows to rewrite $\Omega'_{\partial V}$ as

$$\Omega'_{\partial V} = \frac{\partial \Omega_{\partial V}}{\partial \Omega}\, \Omega' \,. \tag{45}$$

---

[2] Note that $\forall$ means any Ω satisfying the Friedmann constraint. In our case $\Omega^2 \leq \frac{1}{2\xi(1-3\xi)}$.

Using now eqs. (15) and (19) we obtain the following differential equation (for $\Omega_\psi \neq 0$):

$$\frac{\partial \Omega_{\partial V}}{\partial \Omega}\,\left(1-\xi\,\Omega^2\right)^{3/2} = \Omega_{\partial V}^2\,\left(\Gamma(\Omega)-1\right). \qquad (46)$$

To consider $\Omega_{\partial V} = \Omega_{\partial V}(\Omega)$ has been our assumption up to here. One can however make a different, less general assumption, like in [28] where it is assumed that $\Omega = \Omega(\Omega_{\partial V})$ and $\Gamma = \Gamma(\Omega_{\partial V})$: this implies that $\Omega_{\partial V} = \Omega_{\partial V}(\Omega)$ has to be an invertible function, which might not always be the case. In the cases in which this is true, it holds that

$$\psi = \int \frac{d\Omega_{\partial V}}{\Omega_{\partial V}^2(\Gamma(\Omega_{\partial V})-1)}, \qquad (47)$$

cfr. eq. (2.16) in the reference above.

Dropping the discussion of general potential forms, in this section we are going to focus our study on specific classes of potentials and further restrict our analysis on spatially flat spacetime, which corresponds to an invariant subset of the system. In particular, once the form of potential is chosen, the system reduces to 4 dimensions; further, by assuming $\Omega_H = \pm 1$ and by employing the Friedmann constraint the system effectively reduces to 2-dimensions, evolving on the (Ω, Ω_ψ) plane. Thus, the critical points discussed in Sec. 3 and singularities of the system (see Sec. 2.3) will be depicted in the invariant subsets.

Some of these points are independent of the form of potentials and hence will be present in every specific case that we will discuss below. These points are

1. *Big Bang and Big Crunch:*
   There are two points S_+ on the invariant subsets $\Omega_H = 1$ at $\{\Omega, \Omega_\psi\} \to \{\pm\sqrt{\frac{1}{2\xi(1-3\xi)}}, \mp\sqrt{\frac{6\xi}{1-6\xi}}\}$, which are the singular points of the system and act like Big Bang sources. Moreover, there are two points S_- on the invariant subset $\Omega_H = -1$ at $\{\Omega, \Omega_\psi\} \to \{\pm\sqrt{\frac{1}{2\xi(1-3\xi)}}, \pm\sqrt{\frac{6\xi}{1-6\xi}}\}$: these are also singular points of the system and act like Big Crunch sinks. In order to recognize the cosmological character of such points, recall the definition of the evolution parameter of system $\tau = \pm \ln a$, where plus/minus applies to the expanding/collapsing dynamics: as the critical points are approached along the trajectories we have that the parameter $\tau \to \mp\infty$ and hence in both cases $a \to 0$.
2. *Radiation-like transient phase:*
   One can find saddle points C_+ or C_- with coordinates $\{\Omega, \Omega_\psi\} \to \{\pm\frac{1}{\sqrt{2\xi}}, 0\}$ in each invariant subset. These points describe a radiation-like universe since $w_e = 1/3$ (see Table I), and evolution flows around them define a possible radiation-like transition phase of the universe.

In order to find the locations of the *de-Sitter points* $B_\pm$ in the invariant subsets, one needs instead to specify the form of the potential.

4.1. $\Gamma = 1$: exponential potentials

For the special cases when $\Gamma = 1$ it holds that $\Omega_{\partial V} =$ const., thus in this case the potentials are of the form

$$V = V_0 e^{\Omega_{\partial V}\psi}.$$

Each system with $\Omega_H = 1$ has one sink at the coordinate:

- $\{\Omega, \Omega_\psi\} \to \{\sqrt{\frac{1}{2\xi} - \frac{1}{\sqrt{\Omega_{\partial V}^2\xi+4\xi^2}}}, 0\}$ for $\Omega_{\partial V} < 0$,
- $\{\Omega, \Omega_\psi\} \to \{-\sqrt{\frac{1}{2\xi} - \frac{1}{\sqrt{\Omega_{\partial V}^2\xi+4\xi^2}}}, 0\}$ for $\Omega_{\partial V} > 0$,
- $\{\Omega, \Omega_\psi\} \to \{0, 0\}$ for $\Omega_{\partial V} = 0$.

These three cases correspond to the points B_+ depicted on the right column of Fig. 2, from top to bottom. With $\Omega_H = -1$ instead the system has a source at the coordinate:

- $\{\Omega, \Omega_\psi\} \to \{\sqrt{\frac{1}{2\xi} - \frac{1}{\sqrt{\Omega_{\partial V}^2\xi+4\xi^2}}}, 0\}$ for $\Omega_{\partial V} < 0$,
- $\{\Omega, \Omega_\psi\} \to \{-\sqrt{\frac{1}{2\xi} - \frac{1}{\sqrt{\Omega_{\partial V}^2\xi+4\xi^2}}}, 0\}$ for $\Omega_{\partial V} > 0$,
- $\{\Omega, \Omega_\psi\} \to \{0, 0\}$ for $\Omega_{\partial V} = 0$.

These cases correspond to the points B_- depicted in the left column of Fig. 2, from top to bottom. For a global view see Fig. 3: horizontal slicings correspond to different constant values of $\Omega_{\partial V}$.

4.2. Constant $\Gamma \neq 1$

Assuming $\Gamma \neq 1$ and constant we can integrate Eq. (46) and obtain

$$\Omega_{\partial V} = \frac{\sqrt{1-\xi\,\Omega^2}}{(1-\Gamma)\Omega - c_1\sqrt{1-\xi\,\Omega^2}}\,. \qquad (48)$$

Using the definition of $\Omega_{\partial V}$, this expression can be integrated again, resulting in the following family of potentials:

$$V = V_0\left((1-\Gamma)\psi - c_1\right)^{\frac{1}{1-\Gamma}} \qquad (49)$$

The denominator of Eq. (48) introduces a singular line when

$$c_1 - \frac{(1-\Gamma)\Omega}{\sqrt{1-\xi\,\Omega^2}} = 0 \qquad (50)$$

and the location of the singular line is at

$$\Omega_s^2 = \frac{c_1^2}{(1-\Gamma)^2 + \xi\,c_1^2} < \frac{1}{2\xi\,(1-3\,\xi)} \qquad (51)$$

for $\forall\,\Omega_\psi$ inside the Friedmann constraint apart the Friedmann constraint's outer edge ($\Omega_V = 0$). The inequality in Eq. (51) comes from the restrictions of Ω_s between the singularities (27) discussed in Sec. 2.3, also shown in Figs. 2, 3. Further, Eq. (50) indicates that:

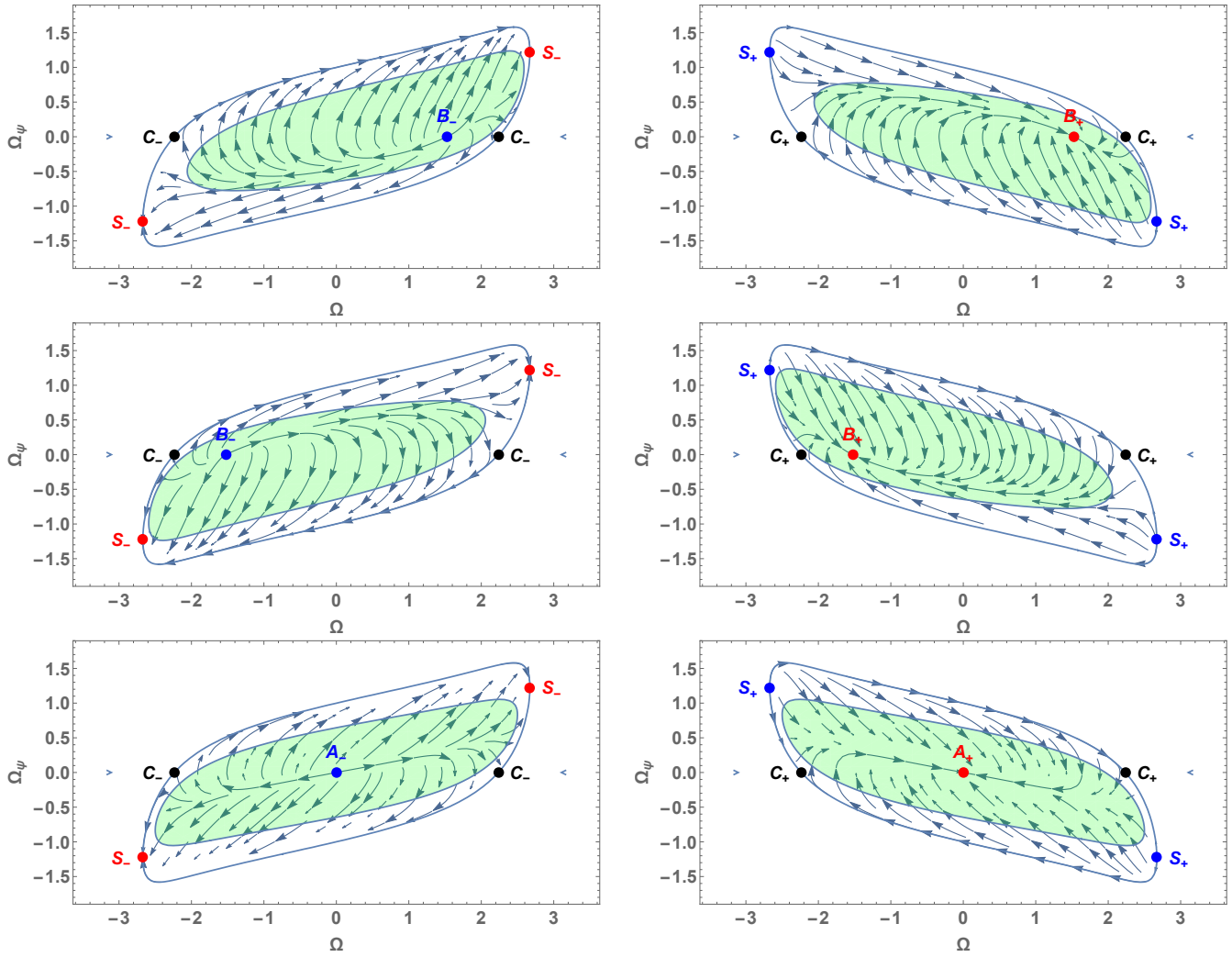

FIG. 2: Some invariant subsets $\Omega_{\partial V}$ = const. for $\xi = \frac{1}{10}$. The left column of panels shows $\Omega_H = -1$ cases, while the right column shows the $\Omega_H = 1$ cases. Upper panels show $\Omega_{\partial V} = -1$, the middle ones $\Omega_{\partial V} = 1$ and the Lower ones $\Omega_{\partial V} = 0$. Blue dots identify sources, red dots are sinks and black ones are saddle points. The green areas denote the phase of accelerated expansion $q < 0$.

- when $\Gamma < 1$ then the sign of Ω (Eq. (51)) has to be the same as of c_1,

- while when $\Gamma > 1$, then the sign of Ω (Eq. (51)) has to be the opposite of c_1.

In order to find the critical points $B_\pm$ for the potential (49) we equate Eq. (48) with the value of $\Omega_{\partial V}$ (Eq. (35)) presented in Sec. 3.2. Note that by doing this we select a particular case of the general treatment. This provides the following relation that will be helpful in order to determine which critical points are inside the Friedmann constraint:

$$c_1\Omega = \frac{1 + 2\,\xi\,\Omega^2\,(1 - 2\Gamma)}{4\,\xi\,\sqrt{1 - \xi\,\Omega^2}} \tag{52}$$

Solving the equation above provides four solutions for Ω:

$$\Omega_{\pm,\pm} = \pm\frac{1}{\sqrt{2\xi}}\sqrt{\frac{(4c_1^2\xi + 2\Gamma - 1) \pm 2\sqrt{c_1^2\xi(4c_1^2\xi + 4\Gamma - 3)}}{4(c_1^2\xi + \Gamma(\Gamma - 1)) + 1}}\,, \tag{53}$$

where the first set of signs in the definition refers to the global sign, while the second one refers to the sign under square-root. [3] The existence of such critical points depends on the relative sign of c_1 and Ω as expressed in Eq. (52); then, if a root exists, we need additionally a condition for it to satisfy the Friedmann constraint. In

[3] One can easily check that these 4 roots appear as critical points of the general dynamical system when $\Omega_{\partial V}$ is given by Eq.(48).

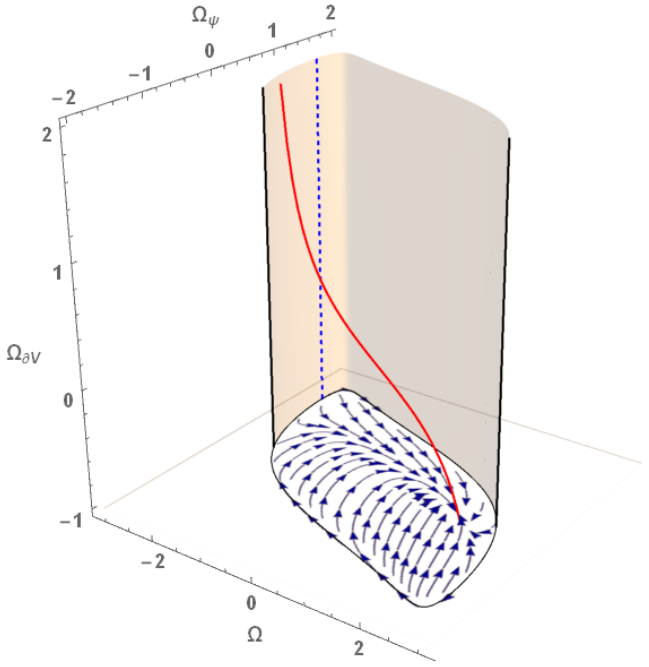

FIG. 3: Global view of the parameter space for the system with $\Gamma = 1$, $\Omega_H = 1$ and $\xi = 1/10$. The dynamics takes place inside every horizontal plane with constant $\Omega_{\partial V}$; the case $\Omega_{\partial V} = -1$ is shown as representative. For a better view, the closed boundary surface corresponding to $\Omega_V = 0$ is cut along the plane $\Omega_\psi = 0$. The blue dashed line is one set of sources, the black lines are the saddles and the red line is the set of future attractors.

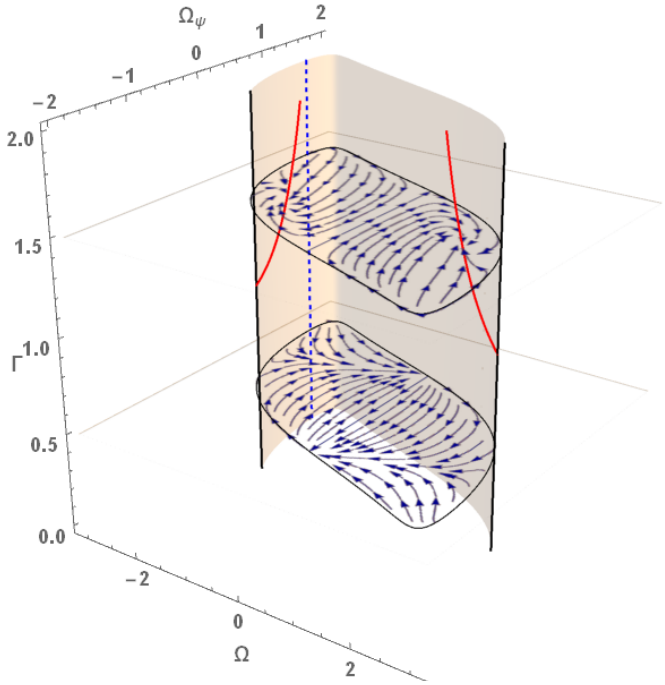

FIG. 4: Global view of the parameter space for the system with $\Gamma \neq 1$ and constant, $\Omega_H = 1$, $\xi = 1/10$ and $c_1 = 0$. The dynamics takes place inside every horizontal plane with constant Γ; the cases $\Gamma = 1/2$ and $\Gamma = 3/2$ are shown as representative. For a better view, the closed boundary surface corresponding to $\Omega_V = 0$ is cut along the plane $\Omega_\psi = 0$. The blue dashed line is the set of sources, the black lines are the saddles and the red lines are the sets of future attractors.

Tables II–IV we give the exact ranges of parameters in which the roots (53) exist. In particular:

1. if $\Gamma \leq 1/2$, then the numerator of Eq. (52) is positive and hence c_1 and Ω should have the same sign, *i.e.* $c_1 \cdot \Omega > 0$. This implies that only the two roots among those in Eq. (53) with the same global sign as c_1 will be allowed. Additionally, the Friedmann constraint and the combination of parameters will define whether these two roots will appear or not, as shown in Table II. When both roots exist, they appear on the same side of the singular line Ω_s: if $c_1 > 0$, then Ω_{+-} is a sink (source) while Ω_{++} is a saddle; if $c_1 < 0$, then Ω_{--} is a sink (source) while Ω_{-+} is a saddle.

2. if $1/2 < \Gamma < 1$, then

$$1 + 2\,\xi\,\Omega^2\,(1 - 2\,\Gamma) > 1 - 2\,\xi\,\Omega^2 > 0\,, \qquad (54)$$

where the last inequality comes from the Friedmann constraint. This has the same implication as the case above about the relative signs of c_1 and Ω. In this case there is at most one root, see Table III for the details.

3. if $\Gamma > 1$, the numerator of Eq. (52) has two roots $\Omega = \pm\,(2\,\xi\,|1 - 2\Gamma|)^{-1/2}$: between these roots the numerator is positive, while outside it is negative. The sign of $c_1 \cdot \Omega$ has to be the same as the one of the numerator, thus determining which of the roots in Eq. (53) are present, see Table IV. When both roots exist, the singular line Ω_s lies between them; in this case B_+ (B_-) retain their sink (source) nature.

It is worth stressing that the critical points $\Omega_{\pm\pm}$, denoted as $B_\pm$ in Figs.5-7, move inside the Friedmann constraint along the line $\Omega = 0$ when the parameters change in the ranges allowed by Tables II,III and IV. In cases 1. and 3. above, when $\xi\,c_1^2 \to (1 - \Gamma)^2$, then $\Omega_{\pm+}$ approaches the position of the radiation-like saddle points $C_\pm$; in case 2., the same happens for $\Omega_{\pm-}$. However, the cosmological interpretation of points $B_\pm$ is preserved as they move and Table 1 excludes the case $\Omega^2 = 1/2\xi$ for the de Sitter sinks/sources: hence the de Sitter character which is preserved as the points move is not in contradiction with the radiation character on the boundary in the above-mentioned limit.

In Fig. 5 we show the case $\Gamma = -1$, corresponding to a potential $V \propto \sqrt{\psi}$ which has some interesting dynamical property but is otherwise physically questionable. From top to bottom, we change gradually the parameter c_1 in order to show how one of the de Sitter points B_+

appears inside the Friedmann constraint and changes its character from sink to saddle. In the top panel such point is outside the constraint; in the middle panel, it coincides with the radiation-like saddle C_+; and in the bottom panel, it appears as a saddle on the right-hand side of the singular segment. The dynamical setup of the bottom panel is quite intriguing, as it presents de Sitter phases both as a transient and as an asymptotic attractor; note however that the potential is complex on the left-hand side of the singular segment, so one cannot give a physical interpretation to such dynamics. In the next subsection instead we will present some physically meaningful cases.

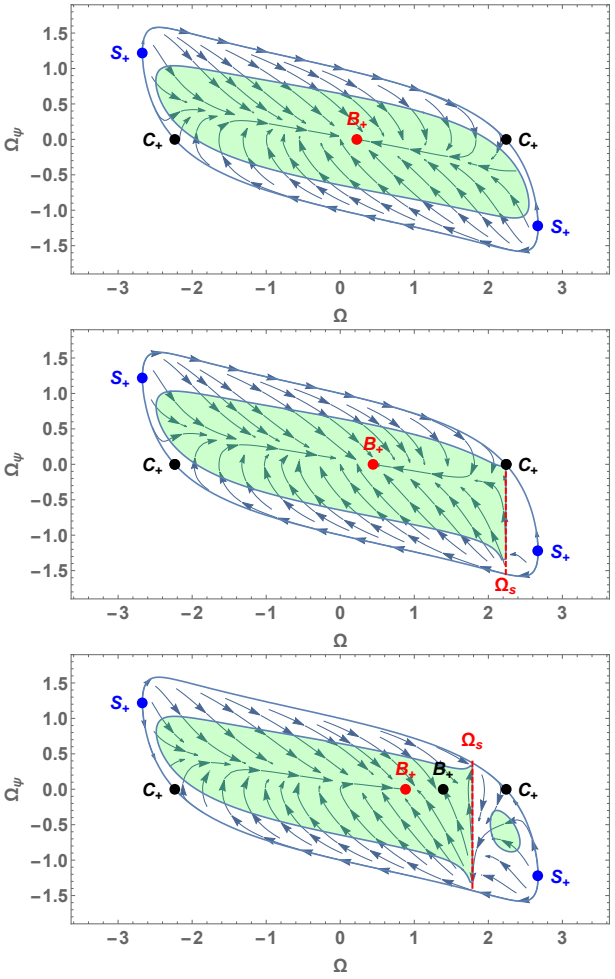

FIG. 5: For the case $\xi = \frac{1}{10}$ invariant subsets for $\Gamma = -1$. The upper panel shows $c_1 = \sqrt{\frac{(1-\Gamma)^2}{\xi}} + 5$, the middle panel $c_1 = \sqrt{\frac{(1-\Gamma)^2}{\xi}}$ and the bottom panel $c_1 = \sqrt{\frac{(1-\Gamma)^2}{\xi}} - 2$. The green areas denote the phase of accelerated expansion $q < 0$.

	$c_1 < 0$	$c_1 = 0$	$c_1 > 0$
Ω_{++}	–	–	$\frac{3}{4} - \Gamma \leq \xi\, c_1^2 < (1-\Gamma)^2$
Ω_{+-}	–	–	$\xi\, c_1^2 > \frac{3}{4} - \Gamma$
Ω_{-+}	$\frac{3}{4} - \Gamma \leq \xi\, c_1^2 < (1-\Gamma)^2$	–	–
Ω_{--}	$\xi\, c_1^2 > \frac{3}{4} - \Gamma$	–	–

TABLE II: Existence of the roots Eq. (53) for $\Gamma \leq 1/2$.

	$c_1 < 0$	$c_1 = 0$	$c_1 > 0$
Ω_{++}	–	–	–
Ω_{+-}	–	–	$\xi\, c_1^2 > (1-\Gamma)^2$
Ω_{-+}	–	–	–
Ω_{--}	$\xi\, c_1^2 > (1-\Gamma)^2$	–	–

TABLE III: Existence of the roots Eq. (53) for $1/2 < \Gamma < 1$.

4.3. Physical interpretation

In this section we focus on the cases with $\Gamma \neq 1$ that could have physical interest. Our discussion will be constrained to $\Omega_H = 1$ and we will keep $\xi = 1/10$ for our examples.

First of all, our initial requirement of positivity of the potential translates into the choice $\Gamma = \frac{2n+1}{2n}$ for $n \in \mathbb{Z}$: the set of potentials characterized by such exponents are positively defined on the real axis. Depending on the sign of the integer n one can identify the following classes:

1. if $n \in \mathbb{N}^-$, then $\Gamma > 1$ and the potentials have the so-called *runaway* form:

$$V = V_0 \left(\frac{\psi}{2|n|} + c_1 \right)^{-2|n|} \tag{55}$$

2. if $n \in \mathbb{N}^+$, then $1/2 \leq \Gamma < 1$ and the potentials are positive even powers of the (shifted) field:

$$V = V_0 \left(\frac{\psi}{2n} - c_1 \right)^{2n} \tag{56}$$

As one usually considers only potentials with even powers of the field, the cases $\Gamma < 1/2$ are excluded. Note that potentials Eq. (56) can be considered as truncated Taylor expansions of more general potentials.

One can check whether a potential defines a mass for the scalar field by analysing the second derivative $\partial_\psi^2 V$ in

	$c_1 < 0$	$c_1 = 0$	$c_1 > 0$
Ω_{++}	$0 < \xi\, c_1^2 < (1-\Gamma)^2$	$\forall\xi$	–
Ω_{+-}	–	$\forall\xi$	$\forall\xi$
Ω_{-+}	–	$\forall\xi$	$0 < \xi\, c_1^2 < (1-\Gamma)^2$
Ω_{--}	$\forall\xi$	$\forall\xi$	–

TABLE IV: Existence of the roots Eq. (53) for $\Gamma > 1$.

a local minimum $\bar{\psi}$ of V itself. While in the class 1. there is no such minimum for finite values of the field, in the class 2. we can distinguish

- $n = 1 \Rightarrow \Gamma = 1/2$ and $(\partial^2_\psi V)_{\bar{\psi}} = V_0/2 > 0$, massive scalar field;

- $n \geq 2 \Rightarrow (\partial^2_\psi V)_{\bar{\psi}} = 0$, massless scalar field.

Hence, in the class of positive definite potentials, only the ones with $\Gamma = 1/2$ have non-zero mass. This case corresponds to the simple quadratic potential.

On the other hand, one could relax the requirement of positivity and well-definedness of the potential on the whole real axis and accept also potentials which are defined only for some ranges of ψ. Potentials of class 1. diverge in $\psi_0 = 2|n|c_1$ and the field is expected to roll down the slope only on one side of ψ_0: this translates into a dynamics which is confined only on one side of the singular line (51) in the parameter space. Hence, in the case of runaway potentials one could in principle allow for any real value in the range $\Gamma > 1$ and be careful to consider only the dynamics in the appropriate side of the parameter space. For instance, in Fig. 6 we represent the case $\Gamma = 3/2$, for which the runaway-type potential is real and positively defined on the whole real axis except for the singular point ψ_0: hence the field can in principle roll down on both sides of the singularity, depending on the initial conditions, and both sides of the parameter space are physically admissible. For $c_1 < \sqrt{(1-\Gamma)^2/\xi}$, the model evolves towards an asymptotic de Sitter attractor on both sides.

For the massless case $\Gamma = 3/4$ we give a couple of examples in Fig. 7. In the top panel we show a case where the Ω_s splits the invariant subset in two parts. The flow of the stream plot indicates that the trajectories oscillate around the Ω_s segment. However, this interpretation is ambiguous since the flow has to reach the invariant subset $\Omega_V = 0$ to pass from one side to the other. The problem stems from our choice of variables which makes the system singular around the minimum of the potential. Thus, the cases we can interpret clearly in the range $1/2 < \Gamma < 1$ are the ones for which Ω_s lies outside the Friedman constraint: such a case is shown in the middle panel of Fig. 7. For one of the trajectories of the middle panel (dashed black line) we provide also the evolution of the effective equation of state, which starts from ultrastiff close to S_+ and ends up at the de Sitter sink.

5. CONCLUSIONS

We have started our study in a very general setup of non-minimally coupled real scalar fields in a FRW spacetime in the absence of regular matter. Namely, in a spatially curved FRW we have specified only the coupling term and not the potential of the scalar field, which we have just demanded to be positive. Transforming properly the variables of the system we have achieved to end up with a new set of dimensionless variables, which are bounded for most of the parameter ranges we consider and are well–defined even for recollapsing scenarios. In this general setup, we have investigated the general features of the system, some of which we recall below:

- There are singularities lying on the the boundaries of the Friedmann constraint. In the case of the flat spacetime $\Omega_H = \pm 1$ we have named them $S_\pm$ respectively, S_+ singularities act as sources and S_- as sinks.

- For the positive curvature and the flat FRW cases the invariant subsets are compact in our new variables in the range $\xi \in (0, 1/6)$.

- The critical points, we have found, can be separated into three categories: de Sitter points, radiation–like points and Milne–like points. The critical points of the first two categories exist for the spatially flat FRW, while the Milne–like points exist for the FRW with negative curvature. The critical points found for the spatially flat case are in agreement with those found in [28]. Note, however, that our analysis covers a broader family of potentials than the one in [28] and takes into account also collapsing scenarios. The critical points found for the negative curvature were analysed in this context for the first time.

We start the second part with the reasonable assumption assumption that $\Omega_{\partial V}$ depends only on Ω (because $V = V(\psi)$) and derive the general Eq. (46), which can be integrated in order to obtain classes of potentials. We further specialize our investigation for spatially flat cases and constant tracking parameter Γ: on one hand, the case $\Gamma = 1$ corresponds to the well-known exponential potential; on the other hand, $\Gamma \neq 1$ provides the broad class of potentials given in Eq. (49). The latter case is further divided into two main subclasses: $\Gamma > 1$ corresponds to runaway potentials, while $\Gamma < 1$ corresponds to potentials with positive powers of the field. The free parameters of the model are ξ, Γ and the integration constant c_1: we analyse in detail the ranges of values for which the de Sitter critical points exist inside the Friedmann constraint. We find that, while the $\Gamma > 1$ cases are easily interpreted as transitions from an early-time ultrastiff era towards a late-time de Sitter expansion (possibly passing through an intermediate radiation epoch), the cases $1/2 < \Gamma < 1$ might present a singular behaviour introduced by our choice of coordinates; if $\Gamma < 1/2$, the potentials might be real and positive only in some ranges of the field, which implies that only some portions of the parameter space can have physical interpretation.

Acknowledgments

G.A. is supported by Grant No. GAČR-17-16260Y of the Czech Science Foundation. G.L-G is supported

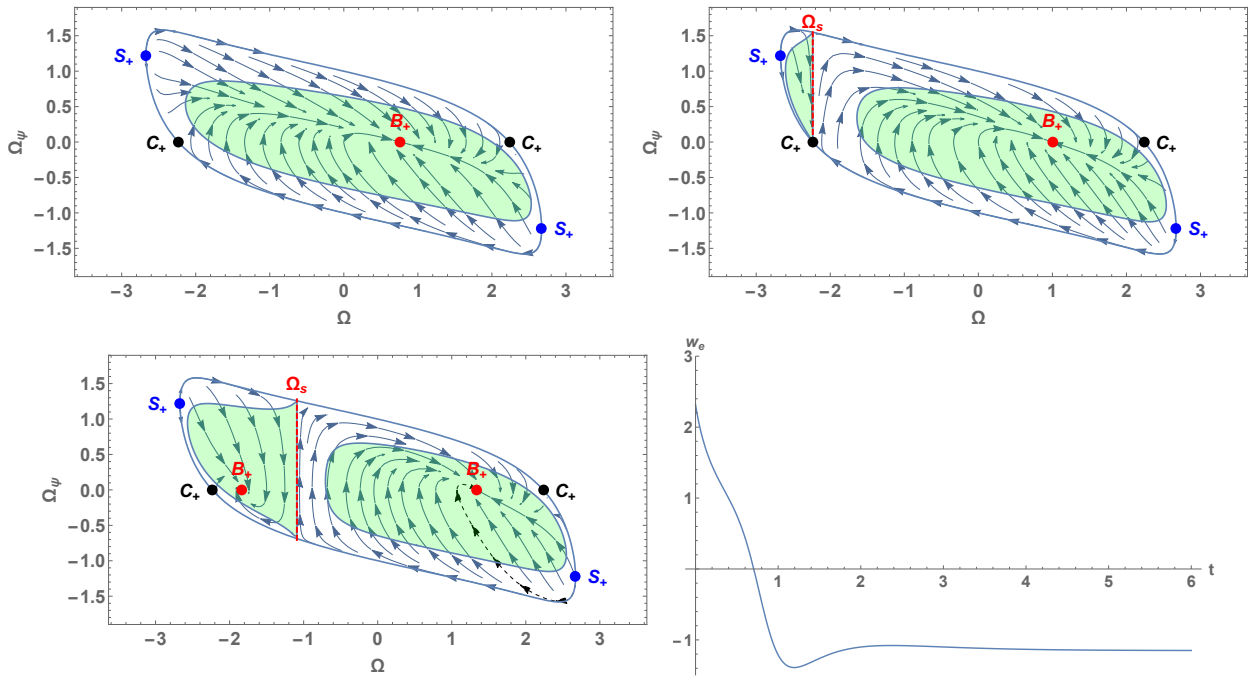

FIG. 6: For the case $\xi = \frac{1}{10}$ invariant subsets for $\Gamma = 3/2$. The upper left panel shows $c_1 = \sqrt{\frac{(1-\Gamma)^2}{\xi}} + 1$, the upper right panel $c_1 = \sqrt{\frac{(1-\Gamma)^2}{\xi}}$ and the bottom ones $c_1 = \sqrt{\frac{(1-\Gamma)^2}{\xi}} - 1$. The green areas denote the phase of accelerated expansion $q < 0$. The bottom right panel shows the effective EOS parameter corresponding to the black-dashed trajectory in the left bottom panel, with initial conditions given by $\{\Omega = 5/2, \Omega_\psi = -1 - 1/\sqrt{3}\}$.

by Grant No. GAČR-17-06962Y of the Czech Science Foundation. We would like to thank Sante Carloni and Jiří Bičák for his advises and remarks.

[1] AA Starobinsky. Aa starobinsky, jetp lett. 30, 682 (1979). *JETP Lett.*, 30:682, 1979.
[2] AH Guth. Ah guth, phys. rev. d 23, 347 (1981). *Phys. Rev. D*, 23:347, 1981.
[3] Andrei D Linde. A new inflationary universe scenario: a possible solution of the horizon, flatness, homogeneity, isotropy and primordial monopole problems. *Phys. Lett. B*, 108(6):389–393, 1982.
[4] Y Akrami, F Arroja, M Ashdown, J Aumont, C Baccigalupi, M Ballardini, AJ Banday, RB Barreiro, N Bartolo, S Basak, et al. Planck 2018 results. x. constraints on inflation. *arXiv preprint arXiv:1807.06211*, 2018.
[5] A Albrecht. A. albrecht and pj steinhardt, phys. rev. lett. 48, 1220 (1982). *Phys. Rev. Lett.*, 48:1220, 1982.
[6] Lev Kofman, Andrei Linde, and Alexei A. Starobinsky. Reheating after inflation. *Phys. Rev. Lett.*, 73:3195–3198, Dec 1994.
[7] Edward W Kolb and Michael S Turner. The early universe. *Front. Phys.*, 69:1–547, 1990.
[8] Mario Galante, Renata Kallosh, Andrei Linde, and Diederik Roest. Unity of cosmological inflation attractors. *Phys. Rev. Lett.*, 114(14):141302, 2015.
[9] N Aghanim, Y Akrami, M Ashdown, J Aumont, C Baccigalupi, M Ballardini, AJ Banday, RB Barreiro, N Bartolo, S Basak, et al. Planck 2018 results. vi. cosmological parameters. *arXiv preprint arXiv:1807.06209*, 2018.
[10] Ivaylo Zlatev, Limin Wang, and Paul J Steinhardt. Quintessence, cosmic coincidence, and the cosmological constant. *Phys. Rev. Lett.*, 82(5):896, 1999.
[11] Edmund J Copeland, Mohammad Sami, and Shinji Tsujikawa. Dynamics of dark energy. *Int. J. Mod. Phys. D*, 15(11):1753–1935, 2006.
[12] Luca Amendola. Cosmology with nonminimal derivative couplings. *Phys. Lett. B*, 301(2-3):175–182, 1993.
[13] Sergey V Sushkov. Exact cosmological solutions with nonminimal derivative coupling. *Phys. Rev. D*, 80(10):103505, 2009.
[14] Emmanuel N Saridakis and Sergey V Sushkov. Quintessence and phantom cosmology with nonminimal derivative coupling. *Phys. Rev. D*, 81(8):083510, 2010.
[15] Bruce Allen. Phase transitions in de sitter space. *Nucl. Phys. B*, 226(1):228–252, 1983.
[16] ND Birrel and P Davies. Quantum fields in curved space 1982.
[17] Kei-ichi Maeda. Stability and attractor in a higher-dimensional cosmology. i. *Classical Quant. Grav.*, 3(2):233, 1986.
[18] Frank S Accetta, David J Zoller, and Michael S Turner. Induced-gravity inflation. *Phys. Rev. D*, 31(12):3046, 1985.

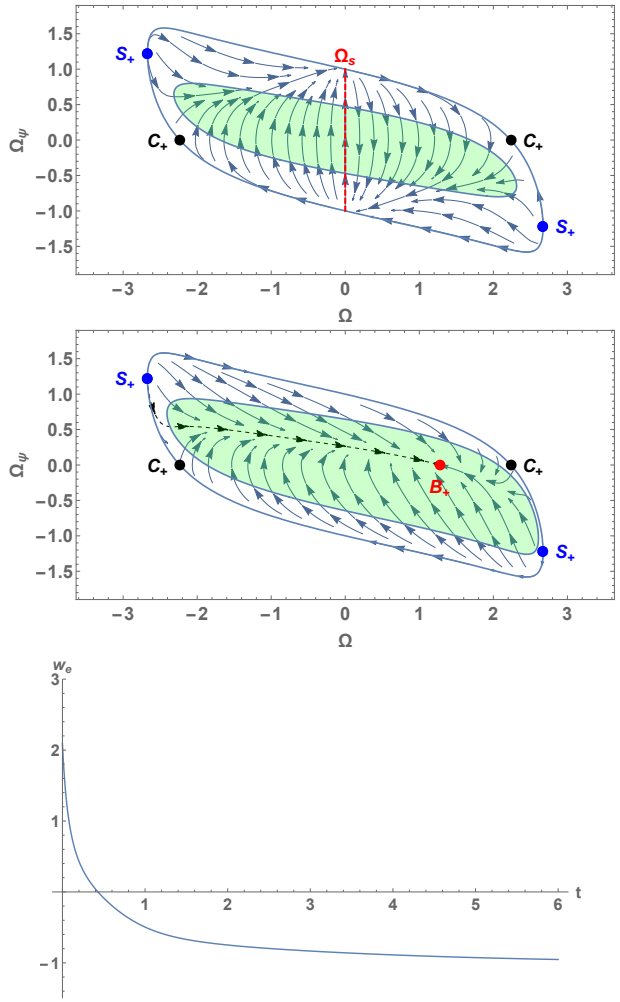

FIG. 7: *Top panel:* invariant subset $\Omega_H = 1$ for $\Gamma = 3/4$ ($V \propto \psi^4$), $c_1 = 0$ and $\xi = 1/10$. *Middle panel:* invariant subset $\Omega_H = 1$ for $\Gamma = 3/4$, $c_1 = \sqrt{\frac{(1-\Gamma)^2}{\xi}} + 1$ and $\xi = 1/10$. *Bottom panel:* evolution of the effective equation of state parameter for the black-dashed trajectory showed in the middle panel, with initial conditions $\{\Omega = -2.63, \Omega_\psi = 0.9\}$.

[19] Fedor Bezrukov and Mikhail Shaposhnikov. The standard model higgs boson as the inflaton. *Phys. Lett. B*, 659(3):703–706, 2008.

[20] Georges Aad. G. aad et al.(atlas collaboration), phys. lett. b 716, 1 (2012). *Phys. Lett. B*, 716:1, 2012.

[21] Valerio Faraoni. Conformally coupled inflation. *Galaxies*, 1(2):96–106, 2013.

[22] A Barroso, J Casasayas, P Crawford, P Moniz, and A Nunes. Inflation in the presence of a non-minimal coupling. *Phys. Lett. B*, 275(3-4):264–272, 1992.

[23] Jean-Philippe Uzan. Cosmological scaling solutions of nonminimally coupled scalar fields. *Phys. Rev. D*, 59(12):123510, 1999.

[24] Edgard Gunzig, Valerio Faraoni, Annibal Figueiredo, TM Rocha Filho, and Léon Brenig. The dynamical system approach to scalar field cosmology. *Classical Quant. Grav.*, 17(8):1783, 2000.

[25] Orfeu Bertolami and PJ Martins. Nonminimal coupling and quintessence. *Phys. Rev. D*, 61(6):064007, 2000.

[26] Ruggiero de Ritis, Alma A Marino, Claudio Rubano, and Paolo Scudellaro. Tracker fields from nonminimally coupled theory. *Phys. Rev. D*, 62(4):043506, 2000.

[27] Alain Riazuelo and Jean-Philippe Uzan. Cosmological observations in scalar-tensor quintessence. *Phys. Rev. D*, 66(2):023525, 2002.

[28] O. Hrycyna and M. Szydłowski. Uniting cosmological epochs through the twister solution in cosmology with non-minimal coupling. *J. Cosmol. Astropart. Phys.*, 12:016, December 2010.

[29] M Sami, M Shahalam, M Skugoreva, and A Toporensky. Cosmological dynamics of a nonminimally coupled scalar field system and its late time cosmic relevance. *Phys. Rev. D*, 86(10):103532, 2012.

[30] Alexander Yu Kamenshchik, Ekaterina O Pozdeeva, Alessandro Tronconi, Giovanni Venturi, and Sergey Yu Vernov. Integrable cosmological models with nonminimally coupled scalar fields. *Classical Quant. Grav.*, 31(10):105003, 2014.

[31] Maria A Skugoreva, Alexey V Toporensky, and Sergey Yu Vernov. Global stability analysis for cosmological models with nonminimally coupled scalar fields. *Phys. Rev. D*, 90(6):064044, 2014.

[32] Orest Hrycyna. What ξ? cosmological constraints on the non-minimal coupling constant. *Phys. Lett. B*, 768:218–227, 2017.

[33] S. Bahamonde, C. G. Böhmer, S. Carloni, E. J. Copeland, W. Fang, and N. Tamanini. Dynamical systems applied to cosmology: Dark energy and modified gravity. *Phys. Rep.*, 775:1–122, November 2018.

[34] Orest Hrycyna and Marek Szydłowski. Cosmological dynamics with non-minimally coupled scalar field and a constant potential function. *J. Cosmol. Astropart. Phys.*, 2015(11):013, 2015.

Summary

This thesis was devoted to analyzing three problems in the isotropic and homogeneous universe. On one hand, we studied the accelerated observers in the expanding universe. One the another hand, we analyzed the dynamics of two cosmological models in the FRW spacetime.

In Chapter 1, we introduced the fundamental elements of modern cosmology. We started from the cosmological principle to introduce the FRW spacetime. Since we assume that our universe is isotropic and homogeneous, we presented the energy-momentum tensor for a suitable matter inside the universe. The Friedmann equation and the Raychaudhuri equation were introduced since they are the most important equations in the modern cosmology. From this step, we provided the form of the scale factor for positive, negative, and zero spatial curvatures. Later on, we introduced the definitions of the geodesics and uniformly accelerated motion in the FRW spacetime. Although the Einstein static universe is not an actual cosmological model, we mentioned it in this chapter because the causal structure of other spacetimes can be simply studied from the static universe. Subsequently, the conformal structures and the Penrose diagrams for spatially curved FRW spacetimes were introduced. However, these aspects of modern cosmology are mainly based on the theoretical considerations; observations raise more fundamental questions about our universe. The observations tell us that our knowledge about the universe is only a small portion of the whole universe. Namely, our knowledge covers approximately 5% of the actual universe. What is the rest is the main question of contemporary cosmology. So far, observations admitted that the hidden side of the universe consists of a dark matter and dark energy. Since this part of modern cosmology is the most challenging one, we provided a succinct introduction to the dark sector. There exist three main areas that have been suggested in the context of cosmology in order to find out the physics behind the dark energy. These areas are the cosmological constant, scalar fields, and the extended gravity. In the rest of this chapter, we introduced the first two areas. The ΛCDM model is introduced as a standard model for the dark energy. However, this model suffers from some problems, which were discussed. Finally, we introduced the scalar field cosmology. Namely, the minimal coupling and the non-minimal coupling were discussed at the end of this chapter.

In Chapter 2, we analyzed the dynamics of a test particle in the FRW spacetime. Although in the previous chapter we introduced the definition of the uniformly accelerated motion and geodesic motion in FRW spacetime, solving respective equations of motion for a given cosmological model is not an easy task. Therefore, we presented a framework in which the uniformly accelerated trajectory and the geodesic can be calculated if for a given cosmological model, the expansion factor is given as a function of coordinate time. To derive this formalism we did the following steps: we started from the spatially curved FRW metric. Then, the conformal time transformation was applied. Since, the transformed metric share a common coefficient $a(\eta)$, i.e. the scale factor in the transformed coordinates, this allowed us to derive the trajectory for an accelerated radial motion. Moreover, from this formalism, we studied the return journey of a rocketeer in the expanding universe. Although it was suggested that having the uniform

deceleration is enough to have a return journey Rindler [1960], we proved that this condition is necessary but not sufficient for all spacetimes. Finally, in this work, we presented a formalism to derive the accelerated trajectory and geodesic in the anti-de Sitter spacetime.

Chapter 3 is dedicated to the dynamical system theory. In this chapter, we provided the necessary theorems and definitions in dynamical system analysis. We introduced the linear stability theorem to analyse the stability of hyperbolic critical points along with the Lyapunov and centre manifold theories to study the stability of the non-hyperbolic critical points. Since our interest lies in the applications of dynamical systems in cosmology, we did not present the proof of the theorems. This chapter ends with an explicit example to show how the stability of a non-hyperbolic critical point can be determined from the Lyapunov and the centre manifold stability.

In the first part of Chapter 4, we provided useful information about the procedures that one should follow in order to implement the dynamical systems analysis to a cosmological model. Namely, we explained why we can not directly use the governing cosmological equations to do dynamical systems analysis. Afterwards, we introduced the normalization parameter and the dynamical variables. Then, by introducing the evolution parameter we presented autonomous dynamical system. In the second part of this chapter we provided a pedagogical example on how a cosmological model can be studied as a dynamical system. We started from the governing equations, i.e. the Friedmann, Raychaudhuri, and Klein-Gordon equations, of a minimally coupled scalar field with an unspecified potential in the FRW spacetime background. Then, we introduced the dimensionless variables from the Friedmann equation. Subsequently, the autonomous system was determined from the dimensionless variables. Additionally, we analyzed the general features of this system, such as global critical points, invariant subsets, and symmetries of the system. Later on, we defined the scalar field potential, i.e. exponential potentials, in which three dimensional dynamical system reduced into the two dimensional dynamical systems. Therefore, at this point, we calculated the critical points of this system, which are

- one matter dominated critical point,
- two stiff fluid like critical points,
- one scaling solution critical point,
- one scalar field dominated critical point.

Finally, the stability of the critical points, their interpretations, and the portraits of the parameter space was derived and discussed. This showed the procedures needed to analyse a cosmological model by implementing the dynamical system analysis.

Chapter 5 presents the content of Kerachian et al. [2020], in which we studied the dynamics of a broad class of barotropic fluids in spatially curved FRW spacetime. Namely, we started from a cosmological model for which the EoS of the barotropic fluid is not determined. For this system, we introduced the dimensionless variables that are well-defined and valid for all spatial curvatures. Then, the autonomous system for these variables were presented. We defined a

function Γ which tells us all the necessary information about the EoS. For this general setup, the critical lines were identified:

- two de Sitter critical lines for spatially flat FRW.
- one static critical line for positive spatially curved FRW.

These critical lines are valid for all barotropic fluids since they are independent of the choice of EoS. Furthermore, we investigated the general features of the function Γ. We showed that, for the specific forms of Γ, we found more critical points. Up to this point, we presented the general investigation for an unknown barotropic fluids. In the second part of this work, two examples were studied to show how this general setup can be used.

Chapter 6 covers the dynamics of classes of non-minimally coupled scalar fields in spatially curved FRW spacetime; this chapter is based on our work Kerachian et al. [2019]. Similar to the previous chapter, where we analyzed the dynamics of barotropic fluids with an unspecified EoS; here, we studied dynamics of a non-minimal coupling scalar field for a generic unspecified positive potential. As we have seen in Chapters 4 and 5, the first step to study a dynamical cosmology is to define the dynamical variables. However, for the non-minimally coupled case, determining these variables is more subtle than in the other cases. The first part of this chapter is dedicated to this issue; we fully explained what procedures should be followed in order to derive well-defined dimensionless variables. Similar to the previous chapter, also here the dimensionless variables are valid for positive and non-positive curvatures. Then, from these variables, the autonomous systems were obtained together with the critical points/ lines/ planes of the system, which are

- two de Sitter critical points for the case $k = 0$,
- two de Sitter critical lines for the case $k = 0$,
- two radiation-like critical lines for the case $k = 0$,
- two Milne-like critical planes for the case $k < 0$.

These critical points/ lines/ planes are independent of the choice of the potentials. Apart from these, we found that, there are two singular points in this general setup; these singular points can be identified as a finite scale factor singularity. This chapter ends with two examples where we examine specific classes of potentials in this framework.

Bibliography

A. Alho, S. Carloni, and C. Uggla. On dynamical systems approaches and methods in f (r) cosmology. *Journal of Cosmology and Astroparticle Physics*, 2016 (08):064, 2016.

K. N. Ananda and M. Bruni. Cosmological dynamics and dark energy with a nonlinear equation of state: A quadratic model. *Physical Review D*, 74(2): 023523, 2006.

K. N. Ananda and M. Bruni. Cosmological dynamics and dark energy with a nonlinear equation of state: A quadratic model. *Physical Review D*, 74(2): 023523, 2006.

M. Azreg-Aïnou. Phase-space analysis of the cosmological 3-fluid problem: families of attractors and repellers. *Classical and Quantum Gravity*, 30(20):205001, 2013.

S. Bahamonde, C. G. Böhmer, S. Carloni, E. J Copeland, W. Fang, and N. Tamanini. Dynamical systems applied to cosmology: dark energy and modified gravity. *Physics Reports*, 775:1–122, 2018.

N. D. Birrell and P. C. W. Davies. *Quantum Fields in Curved Space*. Cambridge University Press, 1982.

Jr. Callan, C. G., S. Coleman, and R. Jackiw. A new improved energy-momentum tensor. *Annals of Physics*, 59(1):42–73, 1970.

S. M. Carroll. The cosmological constant. *Living reviews in relativity*, 4(1):1, 2001.

N. A. Chernikov and E. A. Tagirov. Quantum theory of scalar field in de sitter space-time. *In Annales de l'IHP Physique théorique*, 9:109–141, 1968.

A. A Coley. *Dynamical systems and cosmology*. Springer Science & Business Media, 2013.

E. J. Copeland, A. R. Liddle, and D. Wands. Exponential potentials and cosmological scaling solutions. *Physical Review D*, 57(8):4686–4690, 1998.

A. De La Macorra and G. Piccinelli. Cosmological evolution of general scalar fields and quintessence. *Physical Review D*, 61(12):123503, 2000.

W. de Sitter. On einstein's theory of gravitation and its astronomical consequences. third paper. *Monthly Notices of the Royal Astronomical Society*, 78 (1):3–28, 1917.

C. DeWitt and B. DeWitt. *Relativity, Groups and Topology*. 1964.

V. Faraoni. *Cosmology in scalar-tensor gravity*, volume 139. Springer Science & Business Media, 2004.

J. B. Griffiths and J. Podolský. *Exact space-times in Einstein's general relativity*. Cambridge University Press, 2009.

I. PC Heard and D. Wands. Cosmology with positive and negative exponential potentials. *Classical and Quantum Gravity*, 19(21):5435, 2002.

M. Kerachian. Uniformly accelerated traveler in an flrw universe. *Physical Review D*, 101(8):083536, 2020.

M. Kerachian, G. Acquaviva, and G. Lukes-Gerakopoulos. Classes of nonminimally coupled scalar fields in spatially curved frw spacetimes. *Physical Review D*, 99(12):123516, 2019.

M. Kerachian, G. Acquaviva, and G. Lukes-Gerakopoulos. Dynamics of classes of barotropic fluids in spatially curved frw spacetimes. *Physical Review D*, 101 (4):043535, 2020.

L. Perko. *Differential equations and dynamical systems*. Springer Science & Business Media, 2013.

S. Perlmutter, G. Aldering, G. Goldhaber, R. A. Knop, P. Nugent, P. G. Castro, S. Deustua, S. Fabbro, A. Goobar, D. E. Groom, et al. Measurements of ω and λ from 42 high-redshift supernovae. *The Astrophysical Journal*, 517(2): 565, 1999.

Planck Collaboration, Aghanim, N., Akrami, Y., Ashdown, M., Aumont, J., Baccigalupi, C., Ballardini, M., et al. Planck 2018 results - vi. cosmological parameters. *Astronomy & Astrophysics*, 641:A6, 2020.

E. Poisson. *A relativist's toolkit: the mathematics of black-hole mechanics*. Cambridge university press, 2004.

A. G Riess, A. V. Filippenko, P. Challis, A. Clocchiatti, A. Diercks, P. M. Garnavich, R. L. Gilliland, C. J. Hogan, S. Jha, R. P. Kirshner, et al. Observational evidence from supernovae for an accelerating universe and a cosmological constant. *The Astronomical Journal*, 116(3):1009, 1998.

W. Rindler. Hyperbolic motion in curved space time. *Physical Review*, 119(6): 2082, 1960.

W. Rindler. *Essential relativity: special, general, and cosmological*. Springer Science & Business Media, 2012.

F. Rohrlich. *Classical charged particles*. CRC Press, 2020.

M. Sami, M. Shahalam, M. Skugoreva, and A. Toporensky. Cosmological dynamics of a nonminimally coupled scalar field system and its late time cosmic relevance. *Physical Review D*, 86(10):103532, 2012.

P. J. Steinhardt, L. Wang, and I. Zlatev. Cosmological tracking solutions. *Physical Review D*, 59(12):123504, 1999.

M. Szydłowski, O. Hrycyna, and A. Stachowski. Scalar field cosmology—geometry of dynamics. *International Journal of Geometric Methods in Modern Physics*, 11(02):1460012, 2014.

N. Tamanini. *Dynamical systems in dark energy models*. PhD thesis, UCL (University College London), 2014.

J. Wainwright and G. F. R. Ellis. *Dynamical systems in cosmology*. Cambridge University Press, 2005.

J. Wainwright and W. C. Lim. Cosmological models from a dynamical systems perspective. *Journal of Hyperbolic Differential Equations*, 2(02):437–469, 2005.

S. Weinberg. *Cosmology*. Oxford university press, 2008.

C. Wetterich. Cosmology and the fate of dilatation symmetry. *Nuclear Physics B*, 302(4):668–696, 1988.

S. Wiggins. *Introduction to applied nonlinear dynamical systems and chaos*. Springer Science & Business Media, 2003.

S. Y. Zhou. A new approach to quintessence and a solution of multiple attractors. *Physics Letters B*, 660(1-2):7–12, 2008.

List of Figures

List of Tables

List of publications

- M. Kerachian, G. Acquaviva, and G. Lukes-Gerakopoulos. Classes of non-minimally coupled scalar fields in spatially curved FRW spacetimes. *Physical Review D*, 99(12):123516, 2019.
- M. Kerachian, G. Acquaviva, and G. Lukes-Gerakopoulos. Dynamics of classes of barotropic fluids in spatially curved FRW spacetimes. *Physical Review D*, 101(4):043535, 2020.
- M. Kerachian. Uniformly accelerated traveler in an FLRW universe. *Physical Review D*, 101(8):083536, 2020.